Czech Geological Survey

Geology, Soil Environment and Hydrogeology of the Gedeo Zone, Ethiopia

David Buriánek and Karel Martínek (eds)

Geology, Soil Environment and Hydrogeology of the Gedeo Zone, Ethiopia

Explanatory notes to the thematic geoscientific maps at a 1:100,000 scale

Czech Geological Survey
Geological Survey of Ethiopia
Ministry of Water and Energy of Ethiopia
Charles University in Prague
All for Soil
Aquatest

David Buriánek and Karel Martínek (eds)

with co-authors
Jiří Šíma, Jana Janderková, Kryštof Verner, Leta Megerssa, Tomáš Hroch, Petra Pacherová, Getie Balke, Samuel Getaneh, Melaku Abuye, Jan Jelének, Tadege Arefayne, Niguse Berhanu, Tarekegn Dure, Petra Hejtmánková, Josef Laštovička, Bezuneh Melka, Přemysl Štych, Melese Tute, Jan Valenta, Dominika Čermáková, Kateřina Zelenková, Michaela Hrabalíková, Jan Ureš, Daniela Valchářová, Vilém Spálovský, Tsehay Amare, Muhudin Abdela, Yonas Wubishet, Ondřej Nol, Lukáš Vaverka.

Czech Geological Survey
2022

Reviewed by Bedřich Mlčoch (Czech Geological Survey, Prague, Czech Republic),
Tarekegn Tadesse (Addis Ababa Science and Technology University, Ethiopia)
and Benjamin van Wyk de Vries (Université Clermont Auvergne, France)

Funded by the Czech Development Agency, Czech Republic in frame
of Development Aid Cooperation between the Czech Republic and F.D.R. Ethiopia

ISBN 978-80-7075-948-6

ACKNOWLEDGEMENT

The fieldwork and primary compilation of the map and explanatory notes were jointly done by a team of geologists from the Czech Geological Survey and the Geological Survey of Ethiopia within the framework of the Czech Official Development Assistance Program supported by the Czech Government through the Czech Development Agency. The South Nations, Nationalities and People's Region of FDRE (SNNP Region) President's Office and SNNP Region Mines and Energy Agency are thanked for their welcoming and cooperative engagement. The work also benefited from the undivided support and facilitation by the management of the Geological Survey of Ethiopia, particularly Mrs. Enatfanta Melaku (Director General), Dr. Dejene Hailemariam (Deputy Director), Mr. Hundie Melka and Mr. Muhuddin Abela (head of the Directorate of Hydrogeology). The team is also grateful to drivers from the Geological Survey of Ethiopia: Mulugeta Simegn, Mekonen Hailu, Mulisa Legese and Getachew Tegene and others who were responsible for the demanding task of getting us around the remote and rough terrain at different stages of the field work. Last but not least, the authors would like to express many thanks for the excellent cooperation and support from the Czech Development Agency, the Czech Embassy in Ethiopia and the management of the Czech Geological Survey. Finally, the team would like to acknowledge the untiring support of the local people who assisted the team by all means possible and facilitated the data collection and all those who helped us in various ways.

Buriánek D., **Martínek K**., Šíma J., Janderková J.,Verner K., Megerssa L.A., Hroch T., Pacherová P., Getie B., Samuel G., Melaku A., Jelének J., Tadege A., Niguse B., Tarekegn D., Hejtmánková P., Laštovička J., Bezuneh M., Štych P., Melese T., Valenta J., Valchářová D., Spálovský V., Tsehay A., Muhudin A., Yonas W., Nol O., Vaverka L. (2022). Geology, Soil Environment and Hydrogeology of the Gedeo Zone, Ethiopia. Explanatory notes to the thematic geoscientific maps at a 1:100,000 scale. 106 pages, 2 annexes, 3 maps. ISBN 978-80-7673-045-8. Czech Geological Survey, Prague, Czech Republic.

CZECH REPUBLIC DEVELOPMENT COOPERATION

ALL FOR SOIL

LIST OF ABBREVIATIONS

apfu:	Atoms per formula units
CES:	Code of Ethiopian Standard
CGS:	Czech Geological Survey
CZDA:	Czech Development Agency
DEM:	Digital Elevation Model
EARS:	East African Rift System
EMA:	Ethiopian Mapping Agency
FAO:	Food Aid Organization
FDRE:	Federal Democratic Republic of Ethiopia
GPS:	Global Positioning System
GSE:	Geological Survey of Ethiopia
IUSS:	International Union of Soil Sciences
JICA:	Japan International Cooperation Agency
Ma:	Million years
MER:	Main Ethiopian Rift
MoWIE:	Ministry of Water Resources, Irrigation and Energy
MoWR:	Ministry of Water Resources
NMA:	National Meteorological Agency of Ethiopia
RSG:	Reference Soil Group
RVLB:	Rift Valley Lakes Basin
SNNP Region:	South Nations, Nationalities and People Region of FDRE
TDS:	Total Dissolved Solid
UNDP:	United Nations Development Program
WFB:	World Food Program
WRB:	world Reference Base (for Soil Resources)
WWDSE:	Water Works Design and Supervision Enterprise

CONTENT

LIST OF FIGURES

LIST OF TABLES

SUMMARY

Multidisciplinary geoscientific information accompanied by thematic maps at a scale of 1:100,000 focused on geology, groundwater and soils of the Gedeo Zone is presented. The maps as well as this booklet are intended to provide vital spatial information on natural resources distribution which can help in making informed and objective decisions in the management of the resources.

Three distinct Cenozoic volcanic events took place within the Gedeo Zone (southern Main Ethiopian Rift – MER): pre-rift (Eocene to Oligocene), syn-rift (Miocene), and post-rift stage (Pliocene–Pleistocene). Pre-rift volcanic sequences of the Amaro–Gamo basalts and Shole ignimbrites reach a minimum thickness of ~1700 m. They are the dominant lithological unit in the Gedeo Zone and consist mainly of tholeiitic basalt to trachybasalt with minor basaltic pyroclastic deposits. Mainly in the upper part of the sequence, the Amaro–Gamo basalts are interbedded with strongly welded to partly welded Shole ignimbrites, which have a rhyolitic composition. A subsequent eruptive event consisted of trachydacite to trachybasalt lavas which outcrop mainly east of the town of Dila. The syn-rift Miocene rhyolite volcanic sequence comprises rhyolitic lava to volcanic breccia and minor glassy-rich ignimbrite. The post-rift volcanic sequence consists of Pliocene ignimbrites, partially covered by massive basalt lava flows and basaltic pyroclastic deposits.

Extensional joints, faults and fault zones with normal or oblique-slip kinematics were observed across the mapped area. The faults modified the entire geological pattern forming typical fault-dominated rift morphology. The prevailing rift-related faults dip steeply to ~W, with fewer dipping slightly to ~E, having a prominent ~N–S strike. These faults are often associated with fault lineation (slickensides) plunging steeply to W(SW), bearing evidence of normal kinematics. The most prominent fault zone trends N–S, the main subordinate normal faults are subvertical ~W(SW)–E(NE) trending; they are perpendicular to the prevailing series of normal faults parallel to the southern Main Ethiopian Rift.

The major Reference Soil Groups mapped in the Gedeo Zone comprise Technosols, Regosols, Luvisols, Cambisols, Leptosols, Fluvisols and Nitisols. Their properties and geochemistry are described in detail. Soil erosion is a major threat to the soil resource, soil fertility and productivity in the Gedeo Zone. The susceptibility to land degradation differs within the main agricultural soil types of the study area. They are discussed in detail, e.g. on steep slopes, soils are generally shallower and their nutrient and water storage capacities are limited. Thus, when exposed to soil eroding agents, soils in these areas face greater degradation consequences compared to soils in flat areas.

The Gedeo area receives an average of 1,200 mm of rainfall, which is a relatively good volume for direct infiltration to aquifers. The majority of the area has fissured aquifers that developed in various volcanic rocks and have a large volume of groundwater storage. A small area is covered by alluvial sediments forming a porous aquifer. A relatively large shallow groundwater resource is present in the regolith and can be used particularly for household irrigation.

Groundwater is of good quality for drinking water. It is recommended to explore groundwater in deeper fissured aquifers by drilling wells and to use them particularly for drinking purposes. Shallow groundwater in regolith can be exploited by cheaply dug wells.

Geohazard mapping revealed falls and topplings, landslides, surface water erosion and floods as the main geodynamic risk processes in the Gedeo Zone. Prevention of the negative impact of geological hazards should take place at two levels: 1) long-term strategy studies predicting area vulnerability and the mitigation of impact of natural hazards to humans, 2) response to and solution of current problems, which includes proposing remedial and security measures to reduce damage caused by current hazardous natural processes. Specific preventive and mitigation measures for rehabilitation after natural disasters are suggested.

SUMMARY IN AMHARIC

የፕሮጅክቱ ይዘት

ይህ የጥናት ሪፖርት በ 1፡100,000 መስፈርት በደቡብ ብሔር ብሔረሰቦች እና ህዝቦች ክልል የጌዲኦ ዞንን በማካለል ዘርፈብዙ ማለትም የሥነ-ምድር (የጂኦሎጂ) ፤ የአፈር ዓይነት ስርጭት እና የከርሰ-ምድር ውሃ አለኝታ ካርታዎች ላይ ተመስርቶ የተዘጋጀ ነው። እነዚህ ካርታዎች እና ይህ አስረጂ የጥናት ሪፖርት በዞኑ ያለውን የተፈጥሮ ሃብት ይዘትና ስርጭት ቦታዊ መረጃ በመስጠት የተፈጥሮ ሃብት አስተዳደርን ለማገዝ ወሳኝ ሚና እንዲኖረው ታልሞ የተዘጋጀ ነው። በተዘጋጀው የ1፡100,000 መስፈርት የጂኦሎጂ፤የአፈር እና የከርሰ-ምድር ውሃ አለኝታ ካርታዎች ላይ የተመለከቱት አካላት እና በተፈጥሮ ሃብት ብዝሃነት ላይ ያለው አንድምታ በዚህ አስረጂ ሪፖርት ተብራርቶዋል። ይህ ጥናት በቼክ ሪፐብሊክ አለም አቀፍ ልማት ትብብር (CZDA) የቴክኒክ እና የገንዘብ ድጋፍ በቼክ ጂኦሎጂካል ሰርቬይ እና በኢትዮጵያ ጂኦሎጂካል ኢኒስቲትዩት (የቀድሞው የኢትዮጵያ ጂኦሎጂካል ሰርቬይ) አከናዋኝነት በጋራ ቅንጅት እ.ኤ.አ. ከ2019 አስከ 2022 ዓ.ም. የተከናወነ ነው።

የሥነ-ምድር ካርታውን ለማዘጋጀት እ.ኤ.አ. ከ2019-2021 ዓ.ም. ተከታታይ ዝርዝር የመስክ ቅኝት ፤ በላቦራቶሪ የናሙና ምርመራ (የአለቶቹ የማእድን እና ንጥረ ነገር ይዘት (major and trace elements) እና የቀደምት ጥናቶች ዝርዝር ክለሳ የተካሄደ ሲሆን ዝርዝር መረጃዎቹ በዚህ ገላጭ ሪፖርት በእንግሊዝኛ ቋንቋ ተካተዋል። የተዘጋጀውም የሥነ-ምድ ካርታ ለተከታይ የአፈር እና የከርሰ-ምድር ውሃ አለኝታ ካርታዎች ዝግጅት በግብአትነት አገልግሎት ላይ የዋለ ሲሆን፤ በቀጣይ ለልዩ ልዩ የተፈጥሮ ሃብት አስተዳደርና አጠቃቀም አይነተኛ ሚና ይኖረዋል። በዚህም መሰረት በጌዲኦ ዞን የሚገኙት አለቶች የሚያካልሉት ከፓሌዮጊን እና ከኢዮሲን-ኦሊጎሲን ጊዜያት “ቅድመ ስምጥ ሸለቆ” ፤ ከማዮሲን-ፕሊዮሲን ዘመን “በስምጥ ሸለቆ ጅማሮ” እና ከፕሌይስቶሲን እስከ ሆሎሲን ዘመን ደግሞ “ድህረ-ስምጥ ሸለቆ” ተብለው ሊከፈሉ በሚችሉ የእሳተ-ጎሞራ ቅልጥ አለቶች የተዋቀረ ነው። የ“ቅድመ ስምጥ ሸለቆ” ቅልጤ አለቶች አብዛኛውን የዞኑን ክፍል የሚሸፍኑ ሲሆን በዋናነት የአማሮ-ጋሞ ጥቁር ድንጋይ (ቀዝቅዞ ከጠጠረ የእሳተ-ጎሞራ ቅልጤ ጥቁር አለት - Amaro–Gamo basalts) እና ሾሌ ኢግኒምብራይትን (ከእሳተ-ጎሞራ ፍንዳታ ፍንጥቅጣቂ ተጠባብቆ የቀዘቀዘ አለት - Shole ignimbrites) የሚያካትት ነው። የ“በስምጥ ሸለቆ ጅማሮ” ወቅት የተፈጠሩት አለቶች በሌላ መልኩ ቀዝቅዞ ከጠጠረ የእሳተ-ጎሞራ ቅልጤ ነጣ ያሉ አለቶችን እና ከእሳተ-ጎሞራ ፍንዳታ ፍንጥቅጣቂ ተጠባብቆ የተፈጠሩ አለቶች ናቸው። የ“ድህረ-ስምጥ ሸለቆ” እሳተ-ጎሞራ ወቅት የተፈጠሩት አለቶች በተነባበሩ ከእሳተ-ጎሞራ ፍንዳታ ፍንጥቅጣቂ አለቶች እና ከቀዘቀዘ የእሳተ-ጎሞራ ቅልጤ ጥቁር አለት ያካተተ ነው። በአጠቃላይ በሥፍራው የሚገኙት የሥነ-ምድር መዋቅሮች (tectonic pattern) ተሰባሪ መዋቅሮች (brittle deformation) ሲሆኑ የመልከአ ምድሩን አቀማመጥ ላይ ያሳደሩት ተጽእኖ በግልጠጽ ይታያል። እነዚህ ዘግይተው የተፈጠሩት ተሰባሪ የአለት መዋቅሮች ከሰሜን ወደ ደቡብ (N-S) እና ከምሥራቅ ወደ ምዕራብ (E-W) አቅጣጫዎች በአካባቢው የሚገኙትን አለቶች በስፋት በመሰነጣጠቅ የሚገኙ ናቸው። የነዚህ መዋቅሮች አሰዳደር የከርሰ-ምድር ውሃን ጨምሮ ለልዩ ልዩ የተፈጥሮ ሃብት መገኛነት አመላካች በመሆን ከፍተኛ ጠቀሜታ አላቸው።

በሲዳማ ክልል የሚገኙ ዋና ዋና የአፈር አሃዶች በተዘጋጀው የ1፡100,000 መስፈርት የአፈር ካርታ ተለይተው የተመላከቱ ሲሆን ያላቸው ልዩ ልዩ ባህሪያትም በዚህ አስረጂ የጥናት ሪፖርት ተካቶ ቀርቧል። የአፈር አሃዶቹን ለመለየት ቀደም ብሎ የተዘጋጀው ሥነ-ምድር (የጂኦሎጂ) ካርታ ፤ በመስክ ማመሳከሪያ መረጃዎች ታግዘው ASTER እና Sentinel-2 በሚባሉ የሳተላይት ምስሎችና መረጃዎች ተመስርቶ በተዘጋጀ የገፀ-ምድር ሽፋን ካርታ እንዲሁም በመስክ እና ላቦራቶሪ የአፈር ቅኝትና ምርመራ ጥቅም ላይ ውሏል። በዚህም መሰረት የተለዩት ዋና ዋና የአፈር አውዶች ባላቸው ባህሪት አካያ

በመሬት መራቆትና መቦርቦር እንዲሁም ለልዩ ልዩ ተፈጥሮ አደጋዎች ተጋላጭነት ያላቸው እንደምታ ተተንትኗል። በተዘጋጀው ካርታ መስረት ቴክኖሶል ፣ ሬጎሶል ፣ ሉቪሶል ፣ ካምቢሶል ፣ ሌፕቶሶል ፣ ፍሉቪሶል እና ኒቲሶል ዋና ዋና የአፈር አውዶች መለየት ተችሏል። በዞኑ የአፈር መሸርሸር ለምርታማነት ማሽቆልቆል እና ከፍተኛ የአፈር መራቆት ዋና ምክንያት ነው። መረፊ ጥቁር የአፈር አይነት (ቨርቲሶል) አብዛኛውን ዝቅተኛ ስፍራ የሚሸፍኑ ሲሆን ሉቪሶል እና ኒቲሶለ የአፈር አይነቶች ደግሞ በአብዛኛው ዳገታማ ስፍራዎች ላይ የሚገኙ ናቸው። በጌዲኦ ዞን በአብዛኛው የሚስተዋሉት የአፈር አይነቶች ከተዳፋታማ የመሬት አቀማመጥ አንፃር ያላቸው ስብጥር (soil catena) ሲታይ በላይኛው ደልዳላ የተዳፋት ክፍል ቀይ እና ጥልቀት ሌላቸው የሉቪሶል እና የኒቲሶል አፈር አይነቶች የሚገኙ ሲሆን መጠነኛ ጥልቀት ያላቸው ቀይ የአፈር አይነቶች ማለትም ሌፕቶሶል እና ካምቢሶል በጣም ዳገታማ በሆነው ተዳፋት መሬት ላይ ይፈጠራሉ። እነዚህ የአፈር አይነቶች አሸዋማ እና ውሃን በውስጣቸው የማስተላለፍ ባህሪ ያላቸው ናቸው። በታችኛው ደልዳላ የዳገታማ ስፍራ በአመዛኙ ውሃን በማቆር የሚታወቀው ጥቁር መረፊ የአፈር አይነት ወይም ቨርቲሶል ይገኛል። ኮረታማ ወይም ሬጎሶል ተብሎ የሚታወቀው የአፈር አይነት በአብዛኛው በከፍተኛ አፋፎች ስር በሚገኙ ስፍራዎች በሰፊው ይገኛል። ከመስክ ከተሰበሰቡ የአፈር ናሙናዎች ላይ ኬሚካላዊ ባህሪያት ምርመራ የተደረገ ሲሆን በዚህም መሰረት የአፈር አሲዳማነት መጠን በአብዛኛው የአፈር አይነቶች ከፍተኛ ሲሆን ካታዮን ኤክስቼንጅ ካፓሲቲ (CEC) በሚባለው የአፈር ፖሰቲቭ ቻርጅ ያላቸውን ንጥረ ነገሮች የመያዝ አቅም አንጻር ደግሞ በሁሉም የአፈር አይነቶች ከመካከለኛ እስከ ከፍተኛ ሆኖ ተገኝቶዋል። ይህ ባህሪ ባጠቃላይ ከምርታማነት አንፃር ክፍተኛ ቢሆን የሚመረጥ ሲሆን በአፈር ውስጥ ያለውን የፍግ መጠንና የሸክላ አፈር መጠን ክፍተኛነት የሚያንፀባርቅ ነው። ቤዝ ሳቹሬሽን በሚባለው የካልሲየም፣ የፖታሲየም፣ የማግኒዚየም እና የሶዲየም አዮኖችን ከካታዮን ኤክስቼንጅ ካፓሲቲ (CEC) አንፃር የመያዝ አቅም ኬሚካላዊ ባህሪ እንደሚያሳየው በስፍው የሚገኙት የአፈር አይነቶች እጅግ በጣም አነስተኛ እስከ ከፍተኛ ይዘት አላቸው። የአፈር የፍግ (ሶይል ኦርጋኒክ ካርቦን) ይዘት በአጠቃላይ ዝቅተኛ መሆኑ ታይቷል።

በጌዲኦ ዞን የከርሰ-ምድር ውሃ አለኝታ ካርታ በ1፡100,000 መስፈርት የተዘጋጀ ሲሆን የከርሰ-ምድር ውሃ ቋት ተፈጥሮአዊ አሞላል እና አወጣጥ በምስላዊ ሞዴሎች በደጋፊነት በክርታው ላይ ተካቷል። በተጨማሪም የከርሰ-ምድር ውሃውን አቅፎ የሚይዘው አለት የሚያሳድርበት የንጥረ-ነገር ይዘት በከርሰ-ምድር ውሃ ኬሚካላዊ ባሪያት አመላካች ካርታ ተካቷል። በዚህ ገላጭ ሪፖርት ላይ አጠቃላይ የከርሰ-ምድር ውሃ ሃብት መጠንና ጥራት ከሜትዮሮሎጂያዊ መረጃዎች ጋር በተያያዙ ሞዴሎች አማካኝነት ተገምግሞ ቀርቧል። የከርሰ-ምድር ውሃ አለኝታ ከተለየባቸው የውሃ አዘል አካላት (አኩዊፈር aquifers) የመጀመሪውና በቀላሉ ጥቅም ላይ ሊውል የሚችለው ባልተጠቀጠቁ የአለትና የአፈር ውስጥ ክፍተቶች ሰርጎ የሚገኝ ውሃ ሲሆን በቀላሉ በሰው ኃይል ተቆፍሮ ሊደረስበት የሚችል የአለኝታ ቦታ ነው። በሌላ መልኩ በጠጣር አለቶች ስንጥቅ እና አለቶች ውስጥ ባሉ ክፍተቶች የተጠራቀሙ የከርሰ-ምድር ውሃ ሃብት በስፋት የሚገኝበት ሲሆን በማሽን እገዛ በሚቆፈሩ ጥልቅ ጉድጓዶች (100 ሜትር ወይም በላይ ጥልቀት ያላቸው) ውስጥ ፓምፕ በመግጠም ውሃውን ማውጣት የሚቻልበት የከርሰ-ምድር ውሃ አለኝታ ሲሆን ለማልማት ከፍተኛ መዋዕለ-ንዋይ የሚጠይቅ ነው። በአጠቃላይ በአመት በ2278 ሚሊዮን ሜትር ኪዩብ የሚገመት የከርሰ-ምድር ውሃ በዞኑ ማግኘት እንደሚቻል ጥናቱ የሚያመላክት ሲሆን ለንጹህ ውሃ አቅርቦትም ሆነ ለመስኖ ልማት ጥቅም ላይ ለማዋል የሚያሳስብ የጥራት ይዘት የሌለው መሆኑም የተከናወኑት የናሙና ምርመራዎች እና ቀደምት ጥናቶች ያመለክታሉ።

በዚህም መሰረት ዋና ዋናዎቹ የከርሰ-ምድር ውሃ አዘል አካላት እንደሚከተለው ቀርቦዋል።

(1ኛ) ባልተጠቀጠቀ አፈር ውስጥ ባሉ ክፍተቶች ውስጥ በመካከለኛ የውሃ ይዘት ኖሮዋቸው በስፋት የሚገኙ ወይም ከፍተኛ የሆነ የውሃ ይዘት ኖሮዋቸው ውሱን (አነስተኛ) በሆነ ስፋት የሚገኙ የውሃ አዘል አካላት በካርታው ላይ 243 ስኩዌር ኪሎሜትር የክልሉን ስፍራ ሸፍነው የሚገኙ (Extensive and moderately productive or locally developed and highly productive porous aquifers) ሲሆን ከ0.5-5 ሊትር በስኮንድ በሆነ መጠን ውሃ ሊሰጡ የሚችሉ

(2ኛ) በጠጣር የእሳተ-ጎሞራ ቅልጤ አለቶች ስንጥቅ ውስጥ በመካከለኛ የውሃ ይዘት መጠን በስፋት 1395 ስኩዌር ኪሎሜትር የሚሆነውን የክልሉን ስፍራ ሸፍነው የሚገኙ (Extensive and moderately productive fissured aquifer) በተመሳሳይ ከ0.5-5 ሊትር በስኮንድ በሆነ ምጣኔ የከርሰ-ምድር ውሃ ሊያመነጩ የሚችሉ ነገር ግን በጠንካራ አለቶች ውስጥ እንደመገኘታቸው ለማልማት ከፍተኛ መዋእለ ንዋይ የሚፈልጉ ፤

(3ኛ) ባልተጠቀጠቀ አፈር ውስጥ ባሉ ክፍተቶች ወይም በጠጣር እና ልል ከእሳተ-ጎሞራ ቅልጤ የተፈጠሩ ጠጣር አለቶች ስንጥቅና በልል ፍንጥቅጣቂ ክምችት ውስጣዊ ክፍተቶች ውስጥ መካከለኛ የውሃ ይዘት ኖሮዋቸው በስፋት የሚገኙ ወይም ከፍተኛ የሆነ የውሃ ይዘት ኖሮዋቸው ውሱን (አነስተኛ) በሆነ ስፋት የሚገኙ ቅልቅል የውሃ አዘል አካላት በካርታው ላይ 3 ስኩዌር ኪሎሜትር የክልሉን ስፍራ ሸፍነው የሚገኙ (Extensive and moderately or locally developed and highly productive mixed porous and fissured aquifers) ሲሆን ፤ ከ0.5-5 ሊትር በስኮንድ በሆነ መጠን ውሃ ሊሰጡ የሚችሉ

(4ኛ) ወደ በሃነት እና ብሎም ወደ ኮረታማ አፈር በተቀየሩ ጠጣር የእሳተ-ጎሞራ ቅልጤ አለቶች ውስጥ የሚገኙ ሰፊ ስፍራን የሚያካልሉ ነገር ግን አነስጠኛ የውሃ ይዘት በቅርብ ጥልቀት ያላቸው የውሃ አዘል አካላት በካርታው ላይ 104 ስኩዌር ኪሎሜትር የክልሉን ስፍራ ሸፍነው የሚገኙ (Extensive and low productive aquifers) ሲሆኑ ከ0.25-0.6 ሊትር በስኮንድ በሆነ መጠን ውሃ ሊሰጡ የሚችሉ ናቸው።

1) INTRODUCTION

The present work is a continuation of previously implemented development intervention through natural resources mapping and management studies in selected specific locations in the SNNP Region and the Sidama Region. The limitation of the maps in terms of areal coverage prompted a growing need to apply similar mapping schemes to the entire administrative area of the Gedeo Zone at a scale of 1:100,000. Hence, the maps pertaining to geological setting, soil variability, geohazard status, and groundwater conditions of the entire Gedeo Zone have been undertaken at a scale of 1:100,000. This mapping is further corroborated with additional detailed surveys in a few kebele administrative units to demonstrate the use of the prepared maps to develop Land Management Plans (LMP) along with appropriate maps at a scale of 1:10,000. It is envisaged that through the experience and technical skills transfered during this project, similar LMP studies could eventually be carried out by the regional and local administrations responsible for the utilization and preservation of natural resources.

The project was implemented within the framework of the Memorandum of Understanding signed between the Czech Development Agency (CZDA) and the Federal Democratic Republic of Ethiopia (FDRE) for cooperation on priority issues. It was financially supported by the CZDA through the partner organization of the Czech Geological Survey (CGS) in response to the request for technical assistance raised by the Geological Survey of Ethiopia (GSE) which also made an in-kind contribution to successfully carry out the project objectives. In addition to the project outputs related to the areas investigated, the skills and methodologies of the Geological Survey of Ethiopia professionals in the field of geosciences were significantly enhanced.

The major objective of the project was to characterize the natural environment with respect to the efficient and safe utilization of natural resources including soil, groundwater and mineral resources, and also interaction with the geohazards that arise in the region. This has been achieved through three sets of maps at a scale of 1:100,000; a geological map, a soil map and a hydrogeological map.

The current sharp increase in population and settlements and demands for farmland has merged with an adverse competition in the search for available natural resources such as land for farming, groundwater, pasture, settlement areas, and the like, resulting in increasing conflicts of interest. The extensive deforestation endangers the indigenous vegetation due to the expansion of settlements and farmland into marginal lands (e.g., Kibret et al., 2016; Debeko et al., 2018). Hence, the expansion of agricultural land to often hazard-prone areas due to lack of space is becoming a common practice and increases the risk of susceptibility to various forms of geohazards. Without reasonable land management, it is inevitable that soon the land expansion will result in accelerated erosion, formation of deep erosion furrows, and the overall degradation of farmland leading to falling long-term viability and productivity. These processes can lead to the formation of the so-called “badlands”, which are areas with no soil cover, without vegetation, and with a high density of erosion furrows, which subsequently become unsuitable to sustain the population in place if the area is not treated and managed appropriately.

The interplay of different geological environments of MER (Main Ethiopian Rift, part of the great East African Rift Valley) lends itself to investigation of the various impacts this has on the variability of the geomorphological and geo-hazard processes, groundwater dynamics, soil and land cover systems across the region. Comprehensive research and investigation of geology and lithology, including the analysis of possible geological hazards in both the tectonically active and older stable terrain of the region at a scale of 1:100,000, are hence crucial for effective management and planning of development activities for sustainable agro-practice, improved quality and long-term protection of agricultural lands. The study also helps direct and constrain the search for water resources, which can avoid considerable financial expenditures associated with having to remedy negative phenomena arising from adverse geological processes. The level of information compiled on the maps is envisaged to be practical enough to be implemented and therefore allow a sufficient assessment of natural resources with strategic importance (e.g., current agglomerations, areas with a rapidly growing population, areas susceptible to negative impacts of climate change, and areas with possible recent tectonic and seismic activity).

The objectives of the study are to produce a set of geological and thematic geoscientific maps with explanatory notes for the selected areas that are susceptible to various forms of geohazards. This includes large-scale geological mapping at a scale of 1:100,000 showing the lithological, geochemical, and structural characteristics of the area along with hydrogeological and soil maps supplemented by geohazard and land cover map schemes of the area. The maps and explanatory notes are intended to be easily understood and to be informative enough for the local authorities and development officers. It is anticipated that the maps will aid the effort for natural resources management and planning of land use practice and local development strategies.

The Gedeo Zone

The Gedeo Zone is located in the southern part of Ethiopia (Fig. 1-1). It occupies the eastern margin of the southern Main Ethiopian Rift between Lake Abaya (1,200 meters a.s.l.) in the west, and mountains that reach 3200 meters a.s.l. to the east. The terrain ascends to the east with slopes of between 30–40%. Gedeo as a whole extends over the distance of 150 km from north to south and 40 km from east to west. This hilly terrain with an area of 1,347 km² hosts over 1.5 million people. This makes it the most densely populated zone in the Southern Nations, Nationalities and Peoples' Region, Ethiopia. It is bordered by the Sidama Zone in the north, and by the Oromia Region in the south, east and west. The exact location of the Gedeo Zone lies between 5º50′26″ to 6º12′48″N latitude and 38º12′48″ to 38º13′02″E longitude. Gedeo is very well known for its indigenous knowledge-based self-sustaining land use system. The Gedeo cultural landscape has multiple facets.

The Agroforestry system developed and adopted locally to sustain livelihoods, and the megalithic monuments, Rock art sites and traditionally protected ritual forests which abound in the landscape are its main components (Gedeo Cultural Landscape, 2021). Woreda divisions of the Gedeo Zone are: Bule, Dila Town, Dila Zuria, Gedeb, Kochere, Wenago, and Yirga Chefe.

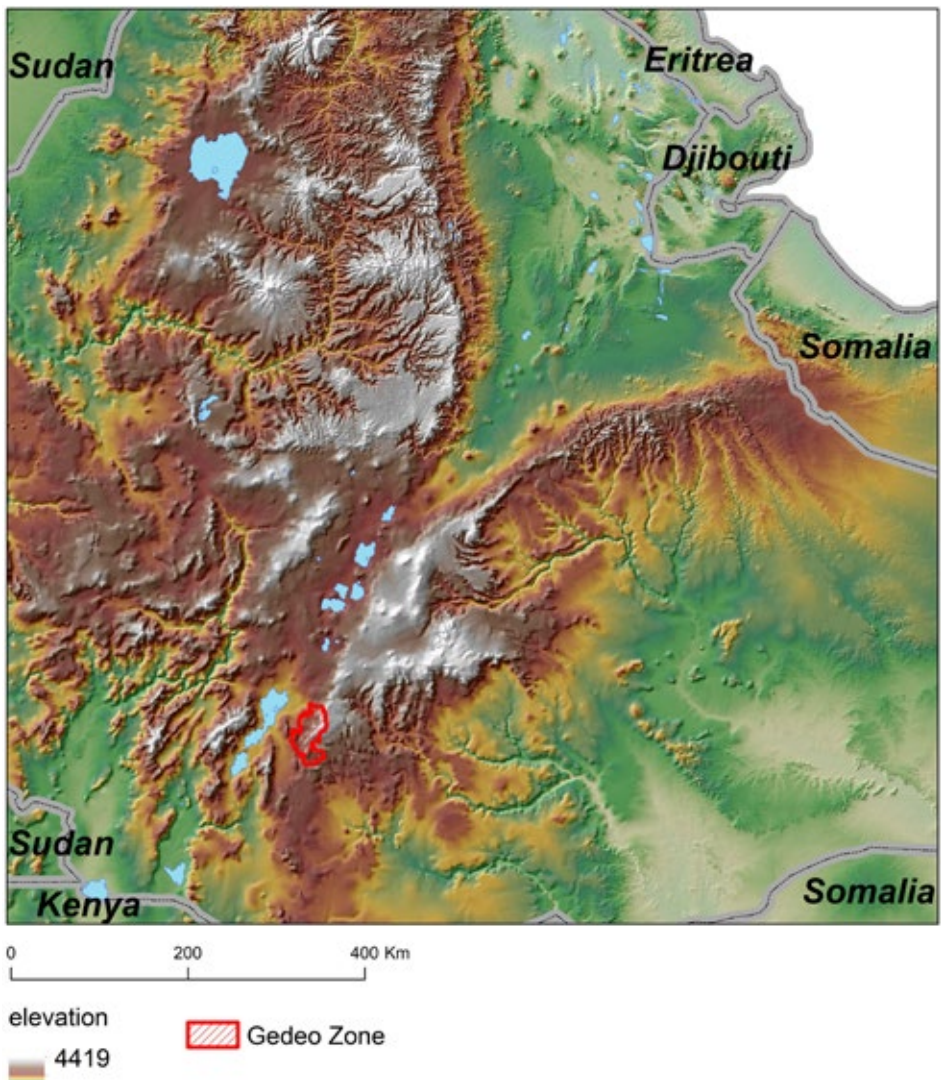

Figure 1-1. *Position of the Gedeo Zone in Ethiopia and the Main Ethiopian Rift.*

2) ENVIRONMENTAL SETTINGS

2.1 Topography and morphology

The Gedeo Zone is located in the eastern margin of the southern Main Ethiopian Rift. Most of the area is covered by the erosional landscape separating the lowland of the rift floor around Lake Abaya to the west from the plateau upland to the east (Fig. 2-1).

This *erosional landscape* is characterized by relatively steep slopes modified by water erosion, a dense drainage network with deep and narrow valleys. The slopes are often remodelled by slope processes. In the west, the erosional landscape is locally formed by badlands.

The *fault scarps* emerging in the erosion relief are linear steeply sloping surfaces which are straight or slightly curved. The majority of fault scarps in the area run N–S or NE–SW.

Planation surface is formed by the upland plateau in the east of the area. It is characterized by gently undulating to flat landforms as a result of long-term denudation and planation processes of low intensity of headward erosion impact.

The *volcanic plateau* extending marginally into the northern part of the region is a predominantly flat or gently sloping surface determined by the bedding of pyroclastic or lava flows.

The *tectonic depressions* are formed north of Yirga Alem and in the vicinity of Chelelektu and are characterised by distinct flat-bottomed, limited drainage depressions filled with Quaternary cover.

2.2 Climatic conditions

The climate of the study area is generally influenced by its topographic features. The main part of the area is located at the bottom of the Ethiopian Rift Valley with altitude ranging from 1,200 near Lake Abaya to 1,700 m a.s.l. at the foot of the eastern escarpment. The eastern part of the area consists of the eastern escarpment with altitude ranging from 1,700 to 2,600 m a.s.l. and a part of the eastern plateau with altitude ranging from 2,600 to more than 3,000 m a.s.l. with its highest peaks on the edge of the eastern plateau (Meraro Mt. 3,064 m a.s.l.) along the surface water divide between the Rift Valley Lake Basin and the Genale River Basin, between the villages of Repe and Kofele. Despite the fact that the study area is relatively small, it is climatically highly variable. The area is mainly characterized by the subtropical Weina Dega on the rift floor and the temperate to humid Dega climatic zones on the escarpment.

The mean monthly value of relative humidity shown for Dila is 70.5% and the average wind speed is 0.5 m/s. The total annual crop evapotranspiration of 1,272 mm (CropWat 4 Windows Version 4.3 software) is dependent on the total daily sunshine hours (6.1 hours).

The Ethiopian territory is divided into four zones, each of them with a different precipitation pattern. The study area is mainly located in a zone characterized by three

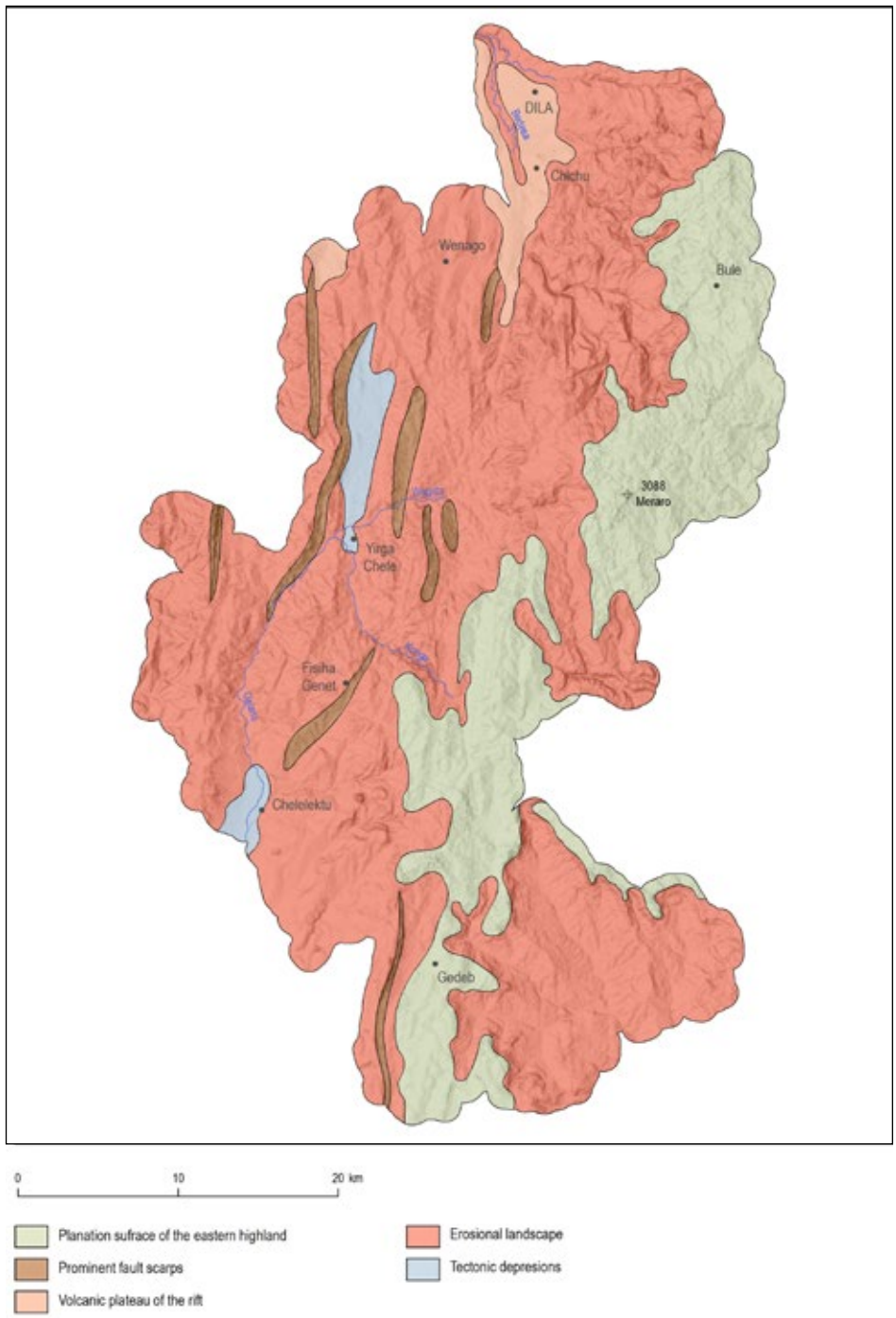

Figure 2-1.
Geomorphological map scheme of the Gedeo Zone.

distinct seasons and bimodal precipitation patterns with two peaks, the first occurring in April to May and the second from September to October (see Fig. 2-2).

The results of analyses by the Japan International Cooperation Agency (JICA, 2012) for the average annual rainfall show that the values range from 492 mm to 2,582 mm, which is a 5-fold difference. This is a relatively large difference but there is a relatively

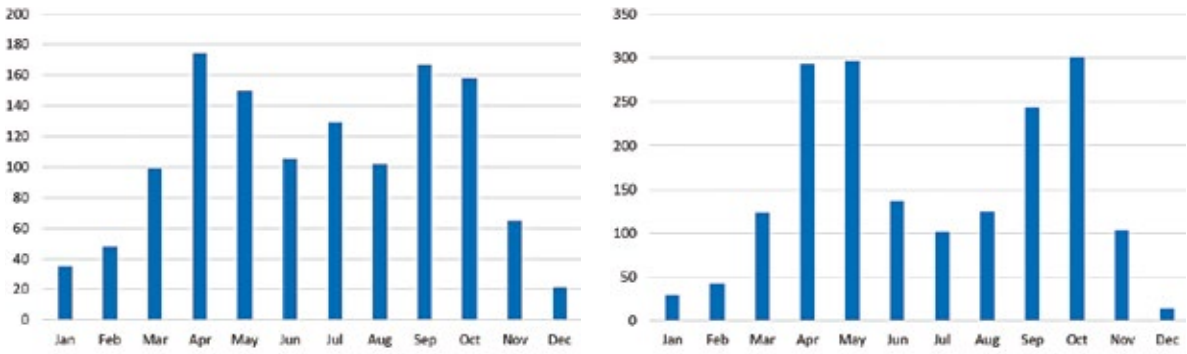

Figure 2-2. *Rainfall patterns at the Dila (left) and Yirga Chefe (right) meteostations (data in mm). Source of data: http://www.levoyageur.net/weather-city-YIRGA-CHEFE/DILLA.html.*

small difference in the values of minimum and maximum rainfall at the individual stations. The main Japan International Cooperation Agency report calculated a precipitation of 1,079 mm as the simple average from 72 stations located within the Rift Valley Lakes Basin (RVLB). The arithmetic value of annual average precipitation was assessed to be 1,012 mm for the Rift Valley Lakes Basin, and 1,000 mm for the Wabe Shebelle Basin in the study area.

The annual average precipitation observed in Dila in the period from 2009 to 2020 was 1,253 mm. It is necessary to point out that years 2019 and 2020 had an exceptionally high rainfall (2,484.7 and 3,053 mm) for southern Ethiopia. **The precipitation value adopted for further calculations was 1,200 mm for the study area.**

2.3 Land cover

Land cover refers to the surface cover on the ground, e.g., vegetation, water, bare soil or other. Identifying and mapping land cover is important for local or global monitoring studies, resource management, and planning activities. Identification of land cover establishes the baseline from which monitoring activities (change detection) can be performed and provides the ground cover information for thematic maps. Remote sensing and geospatial data provide crucial information and methods for land cover monitoring. Land cover studies are mostly multidisciplinary and thus the participants involved in such work are numerous and varied, ranging from international wildlife and conservation foundations to university and government researchers. In addition to facilitating sustainable management of the land, land cover information is often used for planning, monitoring, and evaluation of development, industrial activity, or reclamation. The spatial structure of land cover reflects both physical and socio-economic factors, e.g. climatic conditions, quality of soil, population density, agricultural and industry activities (Land Cover & Land Use, 2019).

The Global Land Cover Database from Copernicus data services was used for this purpose. For these global 100m resolution maps, the main inputs are PROBA-V satellite images, organized into Sentinel-2 tiles. The processing in this tiling grid ensures high quality data and facilitates the continuity with Sentinel-2 from the Copernicus programme. The available global annual maps include a discrete classification with 23 classes observed

Figure 2-3. *A typical landscape of the rift floor near the Abaya Lake.*

with a minimal mapping unit of 100 × 100 m (Land Cover & Land Use, 2019). Images from 2019 were used for this analysis. Nine classes were determined: cropland, grassland, closed forest, open forest, shrubs, built up, bareland, water bodies and wetland.

Gedeo landscape comprises natural land cover classes, e.g., forest, water bodies, and a locally adopted agroforestry system (Fig. 2-3). The components of the agroforestry are mainly coffee, enset, indigenous trees, root crops, shrubs, etc. in which every plant occupies distinct layers of the vertical space of the plant community (Tefera et al., 2007). The landscape – at between 1,000 m and 3,200 m a.s.l. – has rich volcanic soil. This hilly terrain with an area of 1,347 km² hosts over 1.5 million people. Owing to the topographic characteristics, the area is not suitable for monocrop agriculture. The Gedeo Cultural Landscape is part of the tentative list of Ethiopia in order to qualify for inclusion in the UNESCO World Heritage List (Gedeo Cultural Landscape, 2021).

The mountains and the less inhibited area of Gedeo are dominated by a forestry landscape pattern. Closed and open forests cover more than two thirds of the total area in Gedeo. Mountainous areas in the west, central and south-eastern parts are mostly covered by forests. From an environmental point of view, a high share of closed forest (more than 35%) is valuable, having a canopy density of > 70%. Croplands with grasslands provide the most favourable conditions for agriculture in an area located in the east and south of the Gedeo Zone. These agricultural classes occupy ca 30% of the total area. The built up areas include the biggest towns: Dila and Abel. Wetlands and shrubs cover less than 1% of the total area (Tab. 2-1 and Figs 2-3 to 2-5).

The agroforestry system implemented in Gedeo has not radically impacted the original features of landscape and the proportion of forest has been preserved without marked degradation and loss of biodiversity because it is based on the indigenous knowledge of environmental management (Kifle et al., 2016). A continued dependence on subsistence agriculture, which relies on archaic technology and limited nature resources coupled with a massive growth in rural population, and limited rural development, could be a risk both for the local population and landscape diversity together with protection against land degradation.

Table 2-1. Gedeo – land cover in 2019. Source: Copernicus programme, the Global Land Cover Database

Land cover class	Ha	%
Cropland	28,914	25.57
Grassland	5,428	4.80
Closed forest	40,196	35.54
Open forest	36,392	32.18
Shrubs	453,000	0.40
Built up	1,674	1.48
Wetland	38,000	0.03
Total	**113,095**	**100.00**

Figure 2-5. *A typical rural area of the rift slopes (left) and diverse vegetation cover on the highland plateau (right).*

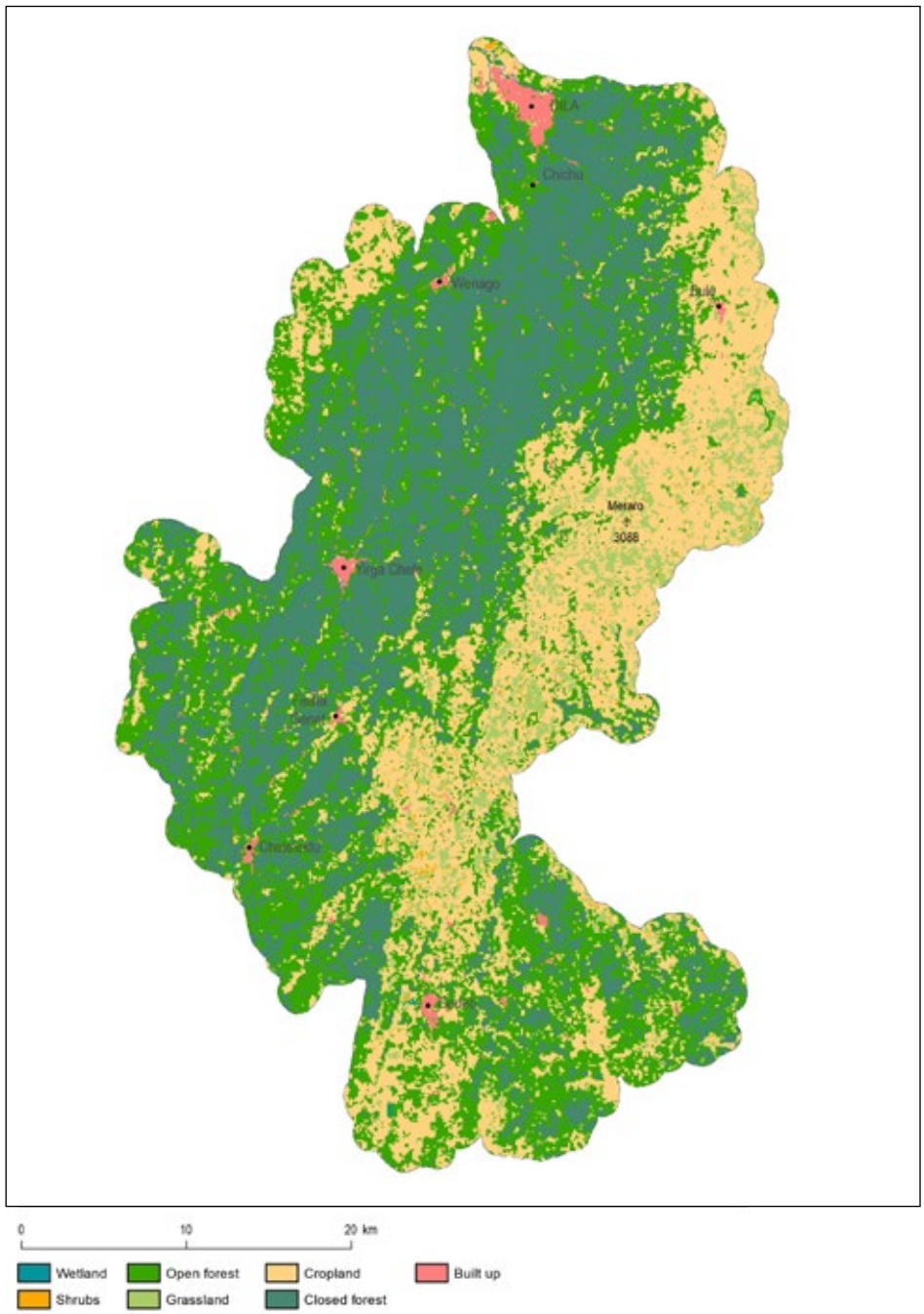

Figure 2-4. *Land cover map scheme in 2019. Source: Copernicus programme, the Global Land Cover Database.*

3) REMOTE SENSING ANALYSIS

3.1 Optical imagery

Nowadays, vast repositories of optical images of various spatial, spectral and temporal resolution are available for free. These include the Sentinel-2 data (exceptional spatial resolution of 10 meters for VIS-NIR bands), Landsat 8 (the longest continuous satellite remote sensing mission) and ASTER (best spectral resolution of all the free satellite data). These data were used and analyzed in order to improve in-situ knowledge of the mapped area of Gedeo. Due to the size of the area, which is covered by different orbital tracks, it was not possible to create one merged satellite product with unified reflectance features. Therefore, the area was divided into several parts according to specific geometries of each satellite imagery. All data were projected in UTM Zone 37N, WGS 1984. This projection was selected as being the best for data exchange with the field experts and office analysts and is best for use by Global Positioning System (GPS) gadgets as well. All satellite data were selected from the dry season period (January to April), which minimized cloud cover. Since vegetation covers more than 80% of the Gedeo area, it was necessary to mask vegetated pixels. Usually by omitting vegetation, it is possible to observe much higher variability in the rest of the pixels which further helps distinguish different lithologies and types of surfaces. In case of the Gedeo area, there are very few pixels not covered by vegetation which makes it hard to utilize optical imagery.

The **Sentinel-2** imagery has a unique spatial resolution of 10 meters for four of its bands (visible and near-infrared) and also a very good resolution of its SWIR bands (20 meters) which are suitable for geological studies. For the Gedeo area, two images of Sentinel-2 were used. Both were acquired on 10th March 2019 with minimum clouds present in the scenes. Due to difficulties in mosaicking these scenes, each was processed separately – the south scene covering most of the area, except for the northern tip of the area. The northern part was thus covered by the other scene used for the Sidama area.

Sentinel-2 data were preprocessedand atmospherically corrected using professional remote sensing and GIS software. All spectral bands were included in the final stacked product. These data were further masked for vegetation and Principal Component Analysis (PCA) was performed on the resulting data. The PCA result features a new set of bands in which the first three bands contain the largest variability of original information. As a result, this representation offers another view of the surface variability and uncovers possibly hidden information (Fig. 3-1). Experimentally, the transformed PCA image has been further interpolated to test if it would be possible to fill vegetation pixels which were previously masked out and which form substantial portion of the surveyed area and to obtain missing information beneath the vegetation cover (Fig. 3-1). The vegetation cover is dense and covers the majority of pixels and thus the remaining pixels in between are biased. Therefore, the interpolation provides useful information only in the less vegetated areas in the west and east of the Gedeo Zone.

Landsat 8 imagery has a standard spatial resolution of 30 meters for all its bands. Landsat 8 is the latest satellite from the Landsat family which forms the longest time

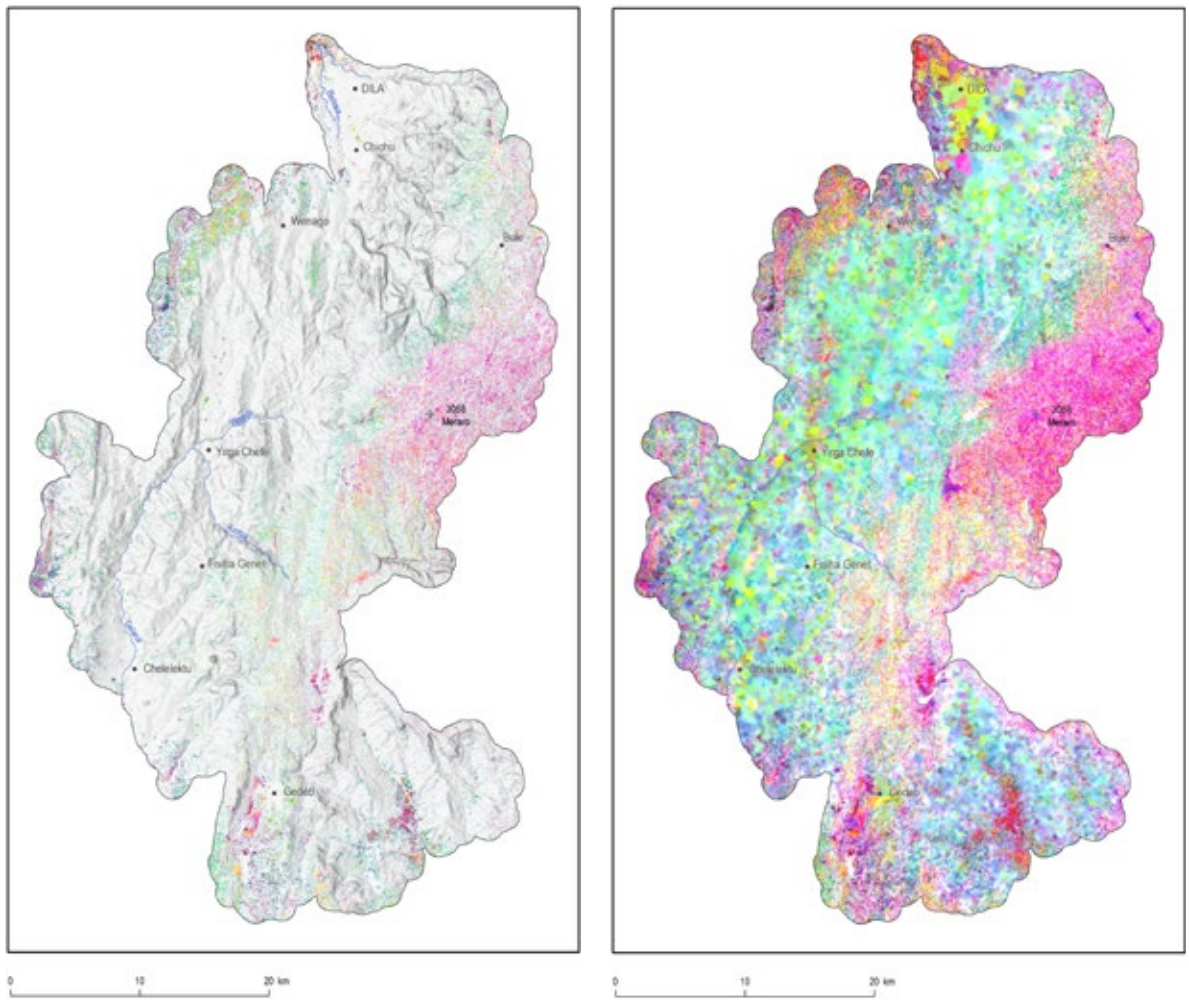

Figure 3-1. *PCA transformation of the Sentinel-2 imagery over Gedeo area (left) and interpolation of missing pixels of PCA transformation (right).*

series of continuous Earth remote sensing. Landsat also contains two SWIR bands and two thermal bands which are useful for field geological mapping. Both Landsat 8 images were acquired on 1st February 2019. Landsat 8 data were professionally preprocessed using an atmospheric correction. Also, Landsat 8 data were used for band combination products which enhance lithological/pedological information. Thermal bands were also used in order to distinguish different surface classes, although the spatial resolution of these bands is 100 m per pixel, thus reducing the detail.

ASTER imagery has three groups of bands: Visible-NIR with a spatial resolution of 15 meters, SWIR bands with a resolution of 30 meters and Thermal bands with a resolution of 90 meters. ASTER imagery was created especially for geological studies, and its high number of bands in the SWIR and TIR parts of the spectrum corresponds to this objective. ASTER data comes in tiles with much smaller spatial coverage.

Therefore, it was necessary to process three distinct tiles (west, middle and east) which were acquired on 12th May 2015, 22nd May 2015 and 8th June 2015. ASTER data were preprocessed using atmospheric and radiometric calibration. Due to the very high vegetation cover, the ASTER products for the Gedeo area were not usable for geological interpretations.

3.2 Morpho-tectonic analysis

Aster DEM, SRTM3 and Landsat 7 ETM+ imagery were used for morphotectonic analysis. The main approach for the morphotectonic analysis followed that used by Dhont and Chorowicz (2006) and Le Turdu et al. (1999) for Ziway and Shala lakes. The main aim was to use Digital Elevation Model (DEM) images to interpret the largest neotectonic structures in the Sidama Region. Single-directional and multi-directional shaded reliefs and an elevation-coloured ASTER DEM image (Fig. 3-2) were generated using ArcMap 10.6 (www.esri.com). The faults mapped can be considered as the main neotectonic faults because they have a prominent expression in the morphology. In some cases, they form asymmetric ranges with one side corresponding to breaks in slope or scarps; by the displacement of Pleistocene and Neogene lithological boundaries; by the occurrence of straight lines of kilometres to several tens of kilometres in length. The images were compared with field geological mapping data to distinguish the scarps formed by active faults from those formed by differential erosion of contrasted lithologies.

The result of the interpretation is called "linear indices", which mostly represent active faults (normal and normal-oblique slip, in a few cases probably strike-slip faults). However, because of uncertainties as to the detailed lithology in some areas and a lack of field verification in some cases, the "linear indices" may also represent prominent fracture zones in exceptional cases as well as lithological boundaries.

Shaded relief maps, derived from the maps of the Czech Development Agency with NW, N and NE illumination, and multidirectional shaded relief maps were used as a base map for morphotectonic interpretation. Based on a comparison with geological maps, lineaments representing lithological boundaries, without evidence of faults, were removed during the next stage. Thus, the interpreted lineaments mostly represent present-day active faults, fault zones, important fracture zones which are exhibited in morphology. Moreover, older faults with a prominent lithological contrast can also be reflected in morphology. The interpretation was made at a scale of 1:250,000, so only the lineaments considered to represent a main fault or other tectonic zones have been mapped.

The study area is characterised by a predominance of NNE–SSW and N–S to NNW–SSE oriented lineaments mostly representing the major normal faults of the rift valley. The westernmost part of the Gedeo Zone represents the rift floor with local horsts and grabens. The subordinate populations of lineaments, mostly perpendicular to the strike of the rift, have an E–W to WNW trend, also showing vertical displacement. SW and NW striking lineaments occur locally. The eastern part of the Gedeo Zone represents a highland plateau on the rift flank that is formed by rigid volcanic rocks. NE–SW lineaments play an important role there.

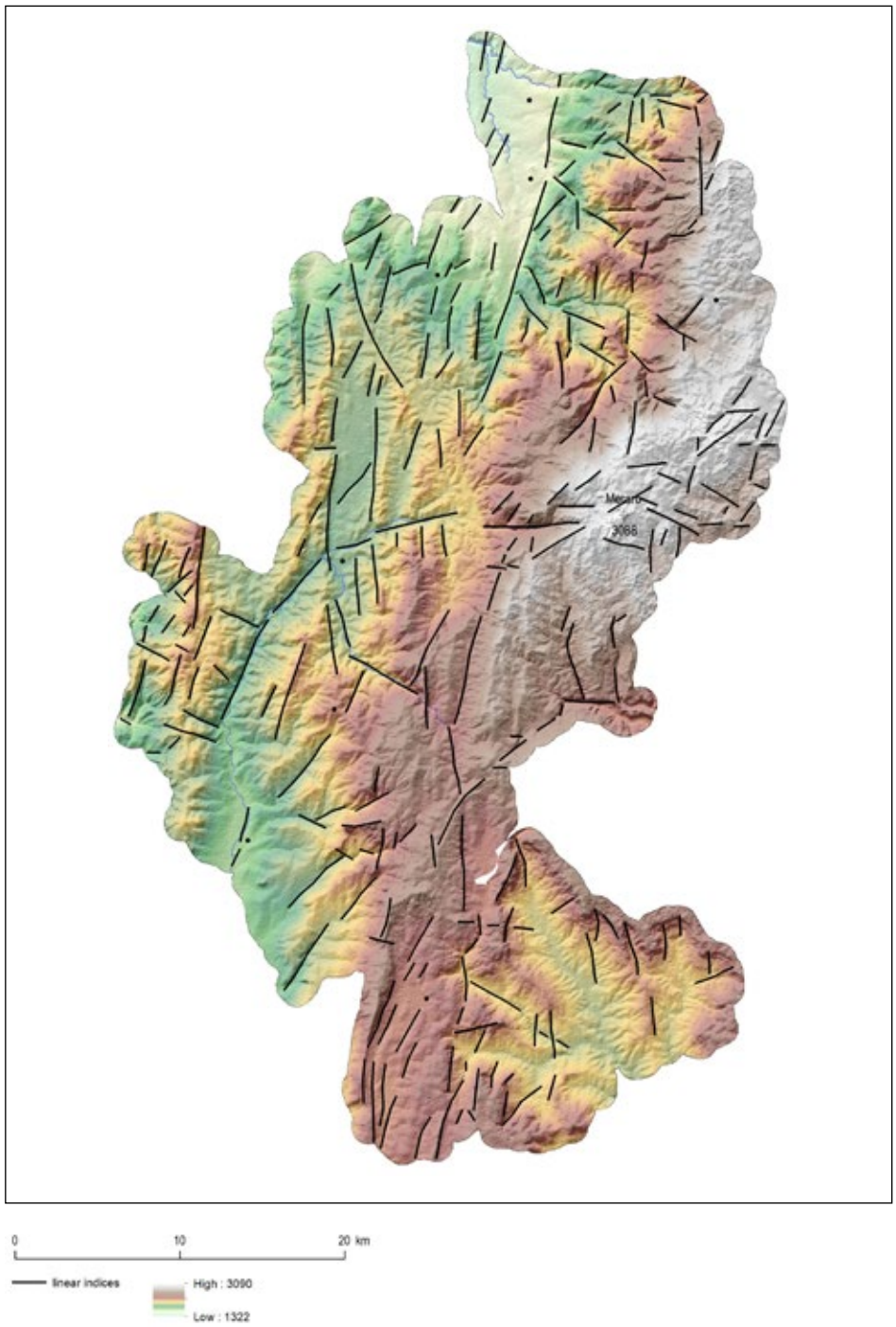

Figure 3-2.
Morphotectonic linear indices map scheme.

4) GEOLOGY

4.1 Previous studies

The Gedeo Zone is partly covered by regional geological, hydrogeological and geohazard maps at the scale of 1:250,000 (Agezew et al., 2014; Rapprich et al., 2014). The geohazard map identified the pertinent exogenous and endogenous hazards in the mapped area (Rapprich et al., 2014). The hydrogeological maps delineated the extents of variably productive aquifers along with zoning of hydrochemical affinity (Agezew et al., 2014). The study by the Japan International Cooperation Agency (JICA) also carried out an assessment of the entire Main Ethiopian Rift valley groundwater resources which generated vast baseline data for subsequent works (JICA, 2012). Regional groundwater and surface water resources have been widely studied (Halcrow, 2008; JICA, 2012). An earlier integrated master plan study for the Rift Valley Lakes Basin was carried out by Halcrow (2018) with a broad-spectrum and long-term forecast on the perspectives for water resources utilization.

The regional geological map of the Dila map sheet, which covers most of the Gedeo Zone, was compiled recently at a scale of 1:250,000 by the Geological Survey of Ethiopia (Yismaw et al., 2015). Also, it has been extended to be used as the base map for producing an integrated geohazards map of the same map sheet (Rapprich et al., 2014) and a hydrogeological map (Agezew et al., 2014). The hydrogeological map identifies the regional aquifer systems along with the regional hydrochemical affinity, giving an extensive inventory of water points in the region (Agezew et al., 2014).

Also the set of geoscience maps at a scale of 1:50,000 of the Dila map sheet was created in the framework of a development project financed by the Czech Development Agency from 2015 to 2018 (Buriánek ed., 2018). It provides detailed information on the northern part of the study area.

4.2 Regional geological setting

The Gedeo Zone (Fig. 4-1) is made up of rift-related volcanic and volcaniclastic deposits belonging to the Southern Main Ethiopian Rift of Eocene to recent ages (e.g. Hayward and Ebinger, 1996; Bonini et al., 2005; Corti, 2009). The Main Ethiopian Rift, as a northern part of the East African Rift System (EARS), is an active intra-continental rift involving magma-dominated extension of the African (Nubian), Somalian, and Arabian lithospheric plates (e.g. Acocella, 2010; Agostini et al., 2011). Three segments of the Main Ethiopian Rift reflecting temporally and spatially different stages of regional extension (transtension) and related volcanic activity have been defined (e.g. Hayward and Ebinger, 1996; Muluneh et al., 2014): (a) the Northern Main Ethiopian Rift, (b) the Central Main Ethiopian Rift and (c) the Southern Main Ethiopian Rift where the studied area belongs. In the Southern Main Ethiopian Rift, the current rate of ~E–W oriented extension between the African and Somalian plates amounts to 5.2 ± 0.9 mm/yr (Saria et al., 2014). The

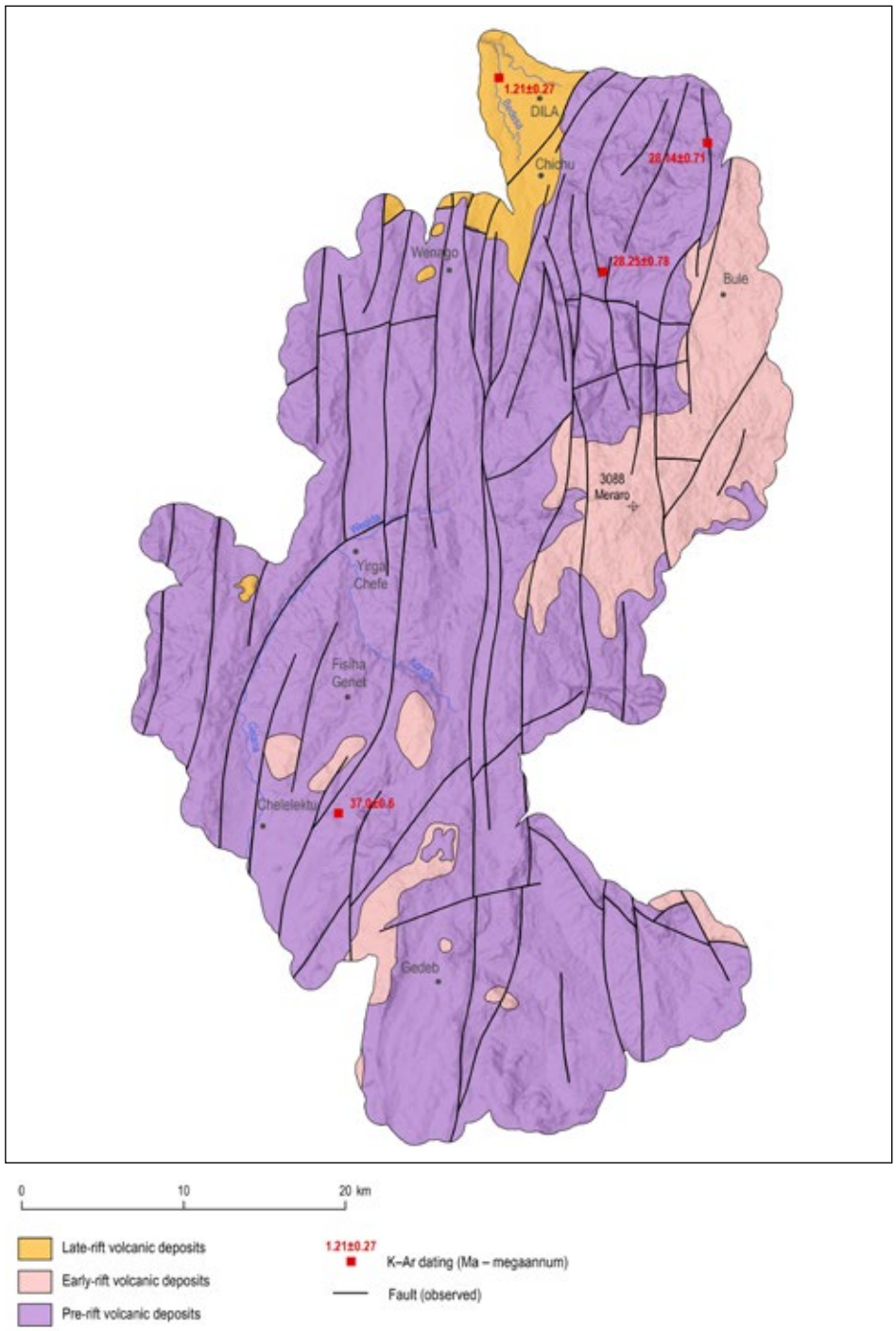

Figure 4-1.
Map scheme of the main geological units.

eastern volcanic highland forming the Sidama Region belongs to the Trap Series of the Somali Plateau (Abbate et al., 2015).

The volcanic activity in the mapped segment of the Southern Main Ethiopian Rift (Fig. 4-1) can be divided into three major episodes (e.g. Hayward and Ebinger, 1996; Bonini et al., 2005; Corti, 2009). The Eocene to Oligocene **pre-rift volcanic deposits**

(Eocene to Oligocene; ~45 to 27 million years – Ma) ago comprise mainly tholeiite to alkaline basalt lava flows and the associated volcaniclastic deposits (Amaro–Gamo basalts) with the presence of rhyolite ignimbrites (Shole ignimbrites) and minor trachytes (Buriánek ed., 2018, Verner and Megerssa eds, 2018). The Miocene **syn-rift volcanic deposits** (Miocene; ~22 to 7 Ma) are represented mainly by basalts, felsic volcanic and volcaniclastic rocks (e.g. rhyolite lava, minor ignimbrites, trachyte lava flows and related pyroclastic deposits) belonging mainly to the Getra-Kele sequences (Ebinger et al., 1993, 2000; Bonini et al., 2005) or to the Arussi and Bale basalts of Miocene age (23 to 9 Ma) with compositions ranging from transitional to alkaline with intercalations of rhyolite lava flows (Juch, 1975; Kunz et al., 1975; Morbidelli et al., 1975; Merla et al., 1979; Zanettin et al., 1980). These volcanic events were followed by a period of volcanic quiescence except for a small eruption of peralkaline pantelleritic ignimbrites intercalated with minor basaltic lava flows in the areas beyond the rift escarpments (Bonini et al., 2005). The subsequent products of Pleistocene to Holocene **post-rift volcanic deposits** (Pliocene–Pleistocene; ~7 Ma to recent) are mainly bimodal volcanic and volcaniclastic rocks such as, for example, the massive Nech-Sar basalts, rhyolites, strongly welded rhyolitic ignimbrites and other pyroclastic deposits (Ebinger et al., 1993). A typical example of post-rift volcanic activity in the northern flank of the Southern Main Ethiopian Rift is the lower Pleistocene formation of unconsolidated pyroclastic deposits on the rift floor (e.g. the Corbetti volcanic system, Rapprich et al., 2014), which were consequently disturbed by tectonic movements and erosion.

The Gedeo Zone is located near the southern termination of the Main Ethiopian Rift and is characterized by predominantly Paleogene–Neogene volcanic rocks split into numerous horsts and grabens by Miocene to Recent faults (Davidson, 1983; Woldegabriel and Aronson, 1987; Ebinger et al., 2000). Also, modern tectonic activity related to the southwestward migration of the Main Ethiopian Rift is common, with the main deformation affecting the southern Main Ethiopian Rift in Pliocene–Pleistocene (Bonini et al., 2005).

4.3 Methods

In addition to standard field hand specimen rock descriptions, laboratory analyses of rocks and minerals were carried out. Laboratory investigations and analyses of collected samples aimed at classifying the local lithologies and describing and establishing geochemical and hydrochemical characteristics of the surveyed areas. These were used as a basis for the geological interpretation of potential geohazard risks. Laboratory studies and analyses of the collected samples were carried out by various organizations and institutes. Physical properties of rocks were analysed in Ethiopia at the Geological Survey of Ethiopia Central Laboratory. Geochemical analyses were made at the ACME Labs in Canada, soil chemistry and microanalysis of polished sections were carried out at the Czech Geological Survey Laboratories in Prague.

Mineral chemistry

Chemical analyses of minerals were obtained using a Cameca SX-100 electron microprobe at the Joint Laboratory of the Department of Geological Sciences, Faculty of Science, Masaryk University in Brno and the Czech Geological Survey, Brno. The measurements

were carried out in a wave-dispersion mode under the following conditions: acceleration voltage of 15 kV, beam diameter of 5 μm and probe current of 30 nA. The integration time was 20 seconds and the standards employed (Kα lines) were: augite (Si, Mg), orthoclase (K), jadeite (Na), chromite (Cr), almandine (Al), andradite (Fe, Ca), rhodonite (Mn) and TiO_2 (Ti). Data were reduced on-line using the PAP routine procedure (Pouchou and Pichoir, 1985). The empirical formulae of feldspars were recalculated to 8 oxygen atoms. The amphibole formulae were obtained on the basis of 23 oxygen atoms (Leake et al., 1997). The Fe^{2+}/Fe^{3+} ratios in amphiboles were estimated assuming the cation sum of 13 without Ca, Na and K (13 eCNK). Pyroxenes are classified according to Morimoto et al. (1988). The formulae were obtained on the basis of 4 cations and the ferric iron estimated after Droop (1987).

Whole-rock geochemistry

About 4 kg samples were crushed (jaw crusher) and homogenized in an agate planetary ball mill for the whole-rock chemical analyses (Annex 1). Major and trace elements were determined at the Acme Analytical Laboratories, Ltd., Vancouver, Canada. Major oxides were analyzed by the ICP-OES method. Loss on ignition (LOI) was calculated from the weight difference after ignition at 1,000 ºC. The rare earth and other trace elements were analysed by ICP-MS following $LiBO_2$ fusion (analytic code: A4B4 – major oxides, Ba, Be, Co, Cr, Cs, Ga, Hf, Nb, Ni, Rb, Sc, Sr, Ta, Th, U, V, W, Y, Zr, REE; 1DX – Ag, As, Au, Bi, Cd, Cu, Hg, Mo, Ni, Pb, Sb, Se, Tl, Zn; 2ALeco – C_{tot}, S_{tot}; for analytical details, reproducibility, and detection limits see http://acmelab.com). Geochemical data were handled and plotted using the GCDkit software package (Janoušek et al., 2006).

4.4 Lithology and petrology

Pre-rift stage

Eocene–Oligocene

13. Basalts to trachybasalts with subordinate basaltic pyroclastic deposits are the oldest rocks exposed in the Gedeo Zone. This unit crops out in the southeast quadrant of the Gedeo area between Dugda YA-A and Gedeb. Numerous outcrops are situated to the south of Dila, and around Yirga Chefe. The Amaro–Gamo basalt sequence mainly consists of alternations of thick massive lava flows, up to 3 m thick, with slightly to strongly weathered surfaces. Often a layer of reddish buried soil up to 0.5 m thick is present at the contact with overlying rocks. Lenticular or tabular bodies of pyroclastic deposits are scarce. Dark-grey basalts to trachybasalts are characterized by a hyaloophitic to ophitic texture in their groundmass with a flow structure shown by the plagioclase (Fig. 4-2) and/or clinopyroxene phenocrysts (Fig. 4-3). Rare alkali feldspars ($An_{9–12}$ $Ab_{70–71}$ $Or_{18–20}$) are present. Clinopyroxene (diopside and augite, Fig. 4-4a) shows X_{Mg} values from 0.64 to 0.69 and Ca from 0.76 to 0.89 atoms per formula units (apfu, see Annex 2). The plagioclase forms elongated laths with a weak oscillatory zoning (Fig. 4-4b; $An_{43–61}$ $Ab_{37–56}$ $Or_{0–2}$; Annex 2). Subhedral olivine ($Fo_{53–54}$; Annex 2) is largely replaced by iddingsite and minerals from the serpentine group. The volcanic glass is affected by alteration and replaced by clay minerals and chlorite. Accessory minerals include ilmenite and magnetite.

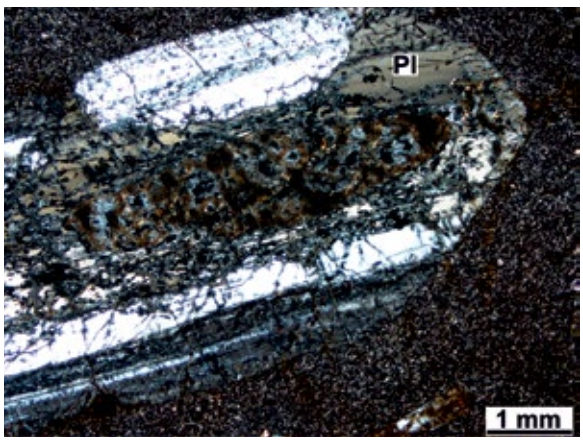

Figure 4-2. *Photomicrograph of plagioclase phenocryst (Pl) from the Amaro–Gamo basalt, from an outcrop in Kara Soditi (TD029), SW of Dila; XPL image*

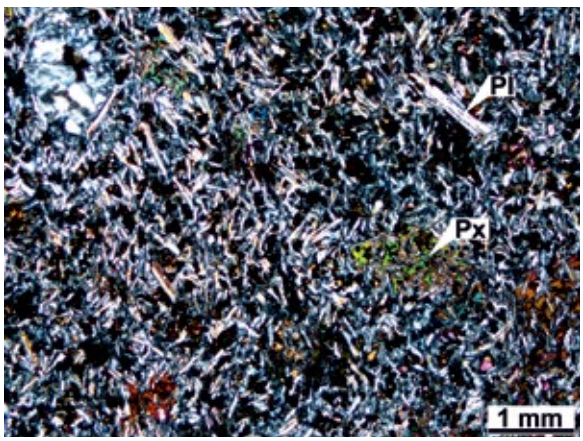

Figure 4-3. *Photomicrograph of pyroxene basalt Aricha (TD032), NE of Yirga Chefe (Pl = plagioclase, Px = pyroxene); XPL image.*

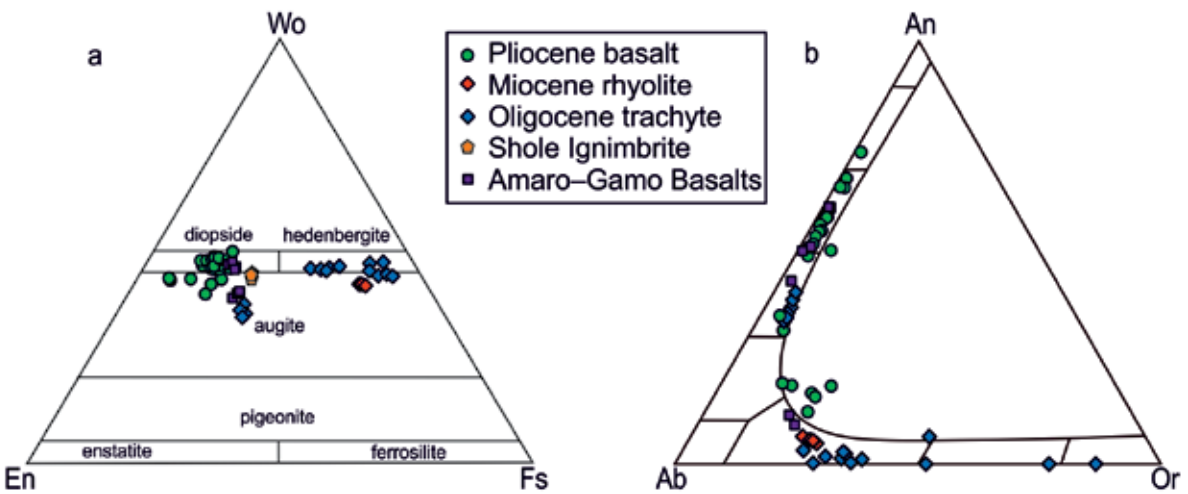

Figure 4-4. *Classification diagrams for Ca-Fe-Mg pyroxenes (a) and feldspars (b) from volcanic rocks.*

12. Rhyolitic ignimbrite and minor rhyolites are exposed in a wide area between Bedesa and Yirga Chefe. These rocks often cap the top of hills or form steep valley walls. Exposures also occur in numerous valleys between Yirga Chefe and Dila. A sequence of densely to moderately welded ignimbrites (Fig. 4-5) has a total thickness of 150–300 m and consists of a package of 3–20 m thick layers of ignimbrites with minor rhyolitic lava, ash fall deposits and buried soil horizons. The ignimbrite deposits show vertical and lateral variations in welding intensity. The proximal parts of ignimbrite flows are generally welded and characterized by the presence of glassy fiamme, while rarely occurring distal facies contain pumices up to 3 cm in diameter. Columnar jointing commonly occurs in densely welded facies of ignimbrites. Fine-grained, densely welded, yellowish to reddish, rhyolitic ignimbrites are predominant. The groundmass is fine-grained and contains flattened glass shards up to 1 mm in length. Crystal fragments comprise 5–35 vol. % and are dominated by subhedral to euhedral quartz as well as sanidine and plagioclase crystals (Fig. 4-6). Clinopyroxene (Fig. 5-3a; X_{Mg} 0.60 to 0.61 and Ca 0.86 to 0.88 atoms

Figure 4-5. *Densely welded ignimbrite deposits exposed near Boytu (TD122), NNE of Yirga Chefe.*

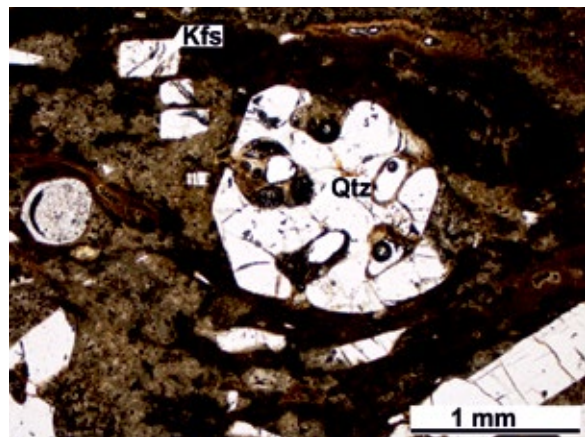

Figure 4-6. *Densely welded ignimbrite with sanidine (Kfs) and corroded quartz (Qtz) phenocrysts (TD103) from Cimeti, SW of Abel; PPL image.*

per formula units; Annex 2) and magnetite are also present. Flattened fiamme are usually eutaxitic and reach a maximum length of 4 cm. Massive, dark grey glassy ignimbrites, sometimes with relicts of petrified wood (Buriánek ed., 2018), are locally present.

11. Trachytes to trachybasalts are exposed on small ridges, small mesas and volcanic necks east of Dila, and between Guanguwa and Gedeb. Light grey to grey trachytes and dark grey trachybasalts (Fig. 4-7) are fine-grained, porphyritic rocks with a trachytic texture. Trachyte and trachyandesite consist of subhedral to euhedral plagioclase ($An_{34–41}$ $Ab_{55–61}$ $Or_{5–6}$; Annex 3, sanidine ($Ab_{14–48}$ $Or_{52–86}$) and/or anorthoclase (Fig. 4-4b; $An_{0–3}$ $Ab_{61–72}$ $Or_{25–38}$). Feldspar laths (57–72 vol. %) have a preferred orientation and the interstices in feldspar crystals are occupied by clinopyroxene (hedenbergite to augite; X_{Mg} 0.11 to 0.64 and Ca 0.67 to 0.94 atoms per formula units) or alterated glass (Fig. 4-8). Weathering, which transforms the dark trachyte into white, clay-rich rocks, is common.

Figure 4-7. *Trachybasalt on an outcrop WSW of Gedeb (TD127).*

Figure 4-8. *Photomicrograph of trachybasalt with trachytic texture (BM034), NW of Abel, XPL image.*

Early-rift stage

Miocene

10. Rhyolites, volcanic breccias, and minor ignimbrites form small lava flows (west of Bule), lava domes, volcanic necks, and up to 2 m thick glassy ignimbrite layers (Buriánek ed., 2018). Rhyolites can be subdivided into three main lithofacies: porphyritic rhyolite, flow-banded rhyolite, carapace breccia and ignimbrites (Fig. 4-9). Porphyritic rhyolites are light grey to red fine-grained rocks with phenocrysts of quartz (45–60 vol. %), anorthoclase ($An_{5–7}$ $Ab_{68–70}$ $Or_{23–27}$), with rare clinopyroxene (hedenbergite to augite; X_{Mg} 0.22 to 0.24 and Ca 0.84 to 0.82 atoms per formula units; Annex 2). The groundmass is fairly equigranular, sometimes trachytic and consists of quartz, anorthoclase, rare albite and volcanic glass in all stages of alteration. Pink or red flow banded rhyolites are aphanitic rocks with fluidal textures. The groundmass is glassy (Fig. 4-10) and usually strongly devitrified (spherulite). Carapace breccia is matrix or clast-supported breccia with mainly angular to subangular rhyolite clasts up to 70 cm in diameter. Ignimbrites are dark-

Figure 4-9. *Rhyolite lava and ignimbrite from an outcrop near Wenago (TD028).*

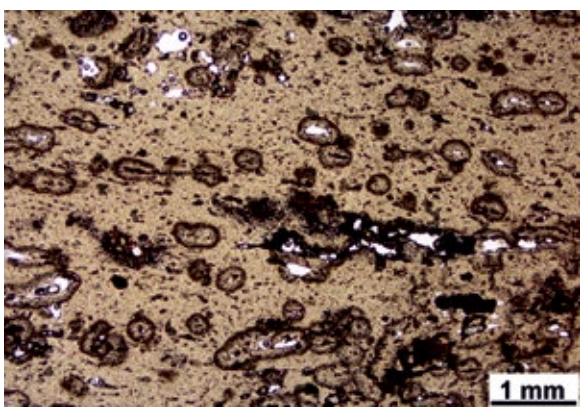

Figure 4-10. *Photomicrograph of glassy rhyolite (TD028), PPL image.*

grey with a glassy, vitroporphyric texture. The groundmass is usually dominated by fresh volcanic glass, feldspar phenocrysts, small rhyolite lithoclasts, with vesicles commonly occurring. Locally a rheomorphic texture is visible as a result of the deformation of layering during emplacement. In thick ignimbrites, columnar jointing occurs due to the contraction during cooling.

Pliocene

9. Welded rhyolitic ignimbrite. Individual bluish-grey to white ignimbrite layers, locally with columnar jointing, vary from less than 1 to 8 m in thickness. Exposures occur in the eastern part of the Gedeo Zone and are best seen on the slopes of the platform around Bule. The most common volcanic lithofacies contain welded ignimbrite (Fig. 4-11) with varying amounts of fiamme and feldspar crystals (Fig. 4-12). The fiamme (few mm to 3 cm in length) consist of glassy groundmass (partially recrystallised), occasionally with visible structural remnants of the original pumices. Euhedral anorthoclase phenocrysts

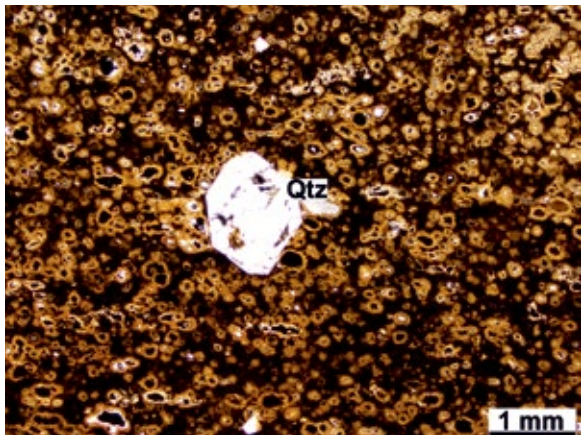

Figure 4-11. *Welded Pliocene rhyolitic ignimbrite with quartz phenocrysts (TD041B), Kurumi, E of Abel, PPL image.*

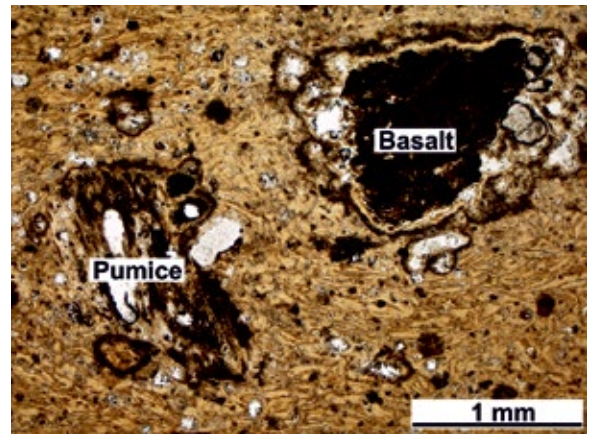

Figure 4-12. *Welded Pliocene rhyolitic ignimbrite with pumice and lithic clasts (TD81B), Hama, SW of Abel, PPL image.*

are up to 0.2–0.6 mm in length. The matrix contains feldspar phenocrysts, lithic fragments and flattened glass shards displaying a well-developed parallel alignment.

8. Basalts with minor volcaniclastic deposits are exposed mainly in the eastern part of the Gedeo Zone sheet between Bule and Wachile. Dominant basalts are massive, dark-coloured rocks (Fig. 4-13) with columnar jointing, which exhibit brown to reddish crusts when weathered. Lava flows are locally intercalated with palaeosoils and fine basaltic scoria layers several m thick, or epiclastic deposits up to 1 m thick. The basalts show an aphanitic or porphyric structure, while consisting of plagioclase (41–59 vol. %), clinopyroxene (25–42 vol. %), interstitial glass (5–22 vol. %) and often subordinate amounts of olivine. Fine-grained ophitic or sub-ophitic groundmass is dominated by plagioclase laths, interstitial clinopyroxene and volcanic glass (Fig. 4-14). Plagioclase ($An_{32–74}$ $Ab_{25–62}$ $Or_{1–7}$) phenocrysts occur as subhedral laths up to 2 mm in size. Rare

Figure 4-13. *Hand specimen of Pliocene olivine alkali basalt (TD126), Gerse, E of Yirga Chefe.*

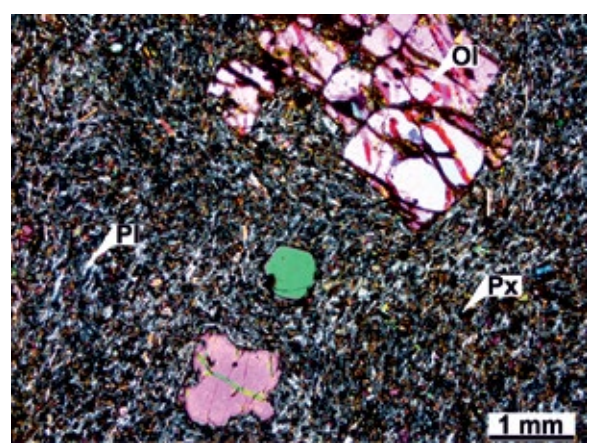

Figure 4-14. *Photomicrograph of Pliocene olivine alkali basalt (BM061), NE of Yirga Chefe (Ol = olivine, Pl = plagioclase, Px = pyroxene), XPL image.*

alkali feldspars ($An_{12–19}$ $Ab_{59–68}$ $Or_{13–23}$) are present. Subhedral to anhedral clinopyroxene phenocrysts are up to 0.4 mm in size (diopside to augite, X_{Mg} = 0.68 to 0.89 and Ca = 0.70 to 0.93 atoms per formula units). Olivine ($Fo_{56–89}$) forms subhedral crystals up to 0.8 mm in size and is largely replaced by red-brown iddingsite. Magnetite and spinel (often associated with olivine) occur as abundant accessory minerals. Volcanic glass or clinopyroxene is partially replaced by chlorite.

Basaltic agglomerate, tuff breccia and minor lapilli tuff consist of several m thick beds of reddish, dark-brown to grey pyroclastic rocks alternating with basaltic lava flow. Ash-supported or clast-supported bed agglomerates and tuff breccias are usually strongly weathered. Volcanic bombs are relatively abundant; however, angular to sub-angular lava blocks are locally present as well. The clasts, cm to dm in size, often display porphyritic texture (plagioclase phenocrysts).

Late-rift stage

Middle Pleistocene – Upper Pleistocene

7. Welded to unwelded rhyolitic and trachytic ignimbrite is exposed mainly in the north-western edge of the Gedeo Zone in the vicinity of the town of Dila. Grey to yellowish ignimbrite (Fig. 4-15) displays distinct lateral and vertical variation in terms of degree of welding, feldspar phenocrysts and clast abundances. Up to 5 m thick layers of welded to unwelded ignimbrites also alternate with ash fall deposits. Rhyolitic ignimbrite often contains feldspar phenocrysts (15–50 vol. %), dark grey glassy fiamme of 3 mm to 2 cm in length (5–10 vol. %), basaltic and rhyolitic subangular to rounded fragments (0–15 vol. %). The fine-grained groundmass has a well-developed parallel alignment of glass shards (Fig. 4-16) caused by compaction.

6. Pyroclastic deposits with subordinated ignimbrite are exposed in the northwestern part of the Gedeo Zone (e.g. roadcuts in the western part of Dila). Pyroclastic deposits are composed of several cm to dm thick layers of well-sorted acid volcanic ash and/or

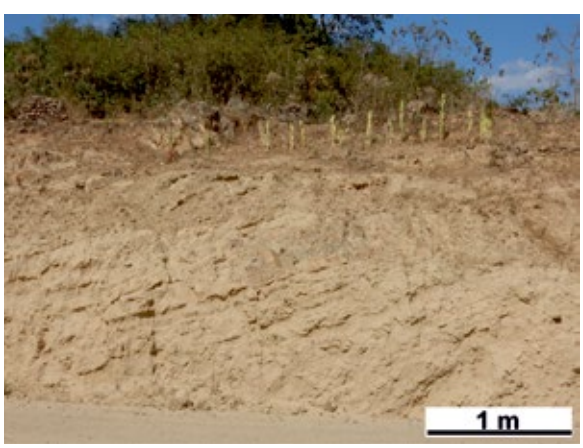

Figure 4-15. *Outcrop of unwelded Pleistocene ignimbrite (DE340), W of Kebado.*

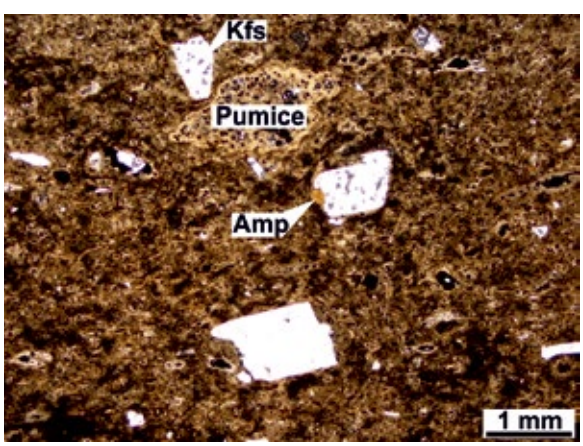

Figure 4-16. *Welded Pleistocene rhyolitic ignimbrite with pumice and lithic clasts (TD050), Yirga Chefe (Kfs = sanidine, Amp = amphibole), PPL image.*

fine to medium-grained lapilli (2–25 mm). At the outcrops, these reach 5 m in thickness; however, the original thickness is unknown. In the ash layers, accretionary lapilli of 0.1 to 0.5 cm in size are locally present.

Quaternary sediments

Pleistocene–Holocene

5. Colluvial sediments are associated with different types of gravity processes, which are very common in tectonically dynamic relief. They are represented by accumulations of rock-falls, landslides, earth flows and creep preserved mainly in the foot of the scarps. It forms heterogeneous admixtures of sediments with different granular size. Most voluminous deposits represent the accumulation zones of deep-seated fossil rockslides and landslides. The lithology of these deposits is characterized by unsorted sediments with boulders up to several meters in diameter composed of competent volcanic rocks such as welded ignimbrites, trachyte and basalt (Fig. 4-17). In the areas with a thicker layer of weathering, the colluvial sediments are represented by finer-grained re-sedimented sandy to clayey soils with a low content of small rock fragments.

4. Polygenetic sediments consist of a mixture of colluvial, alluvial and lacustrine sediments filling the tectonic depression between Yirga Chefe and Wenago. They are characterized by a heterogeneous sequence of reddish or brownish loamy sands and silt representing reworked residual soils. In the northern margin of Yirga Chefe, intercalations of grain-supported gravels with subrounded to rounded clasts of basalts were investigated. The thickness of the sequence is estimated at several meters to a few tens of meters.

Holocene

3. Lacustrine sediments are preserved in two partially undrained depressions south of the town of Gedeb. The lithology of the lacustrine deposits is generally controlled by the

Figure 4-17. *Outcrop of sandy colluvial soils with an angular clast of basalts.*

Figure 4-18. *Undrained depression with wetland infilled by lacustrine sediments, S of Gedeb.*

Figure 4-19. *Floodplain with a small meandering channel in the upper highland, S of Mora.*

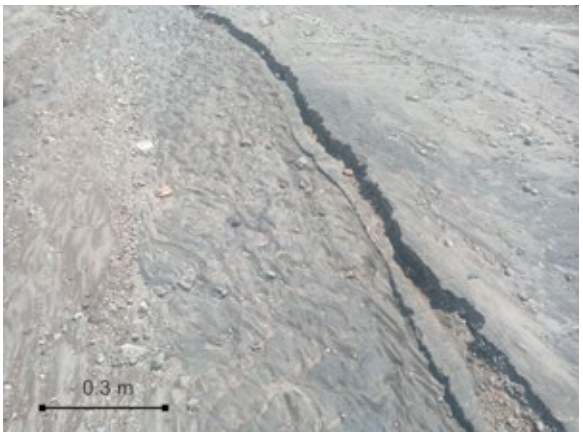

Figure 4-20. *Fine-grained sands with ripplemarks infilling a temporal fluvial channel, E of Wenago.*

transport and supply of clastic material from fluvial channels flowing into the depression (Fig. 4-18). The lacustrine deposits are mainly formed of fine-grained accumulations of clays and silts with a high portion of organic matter; however, the coarser sandy deposits could have accumulated at the mouths of fluvial channels and streams.

2. Alluvial fan deposits generally form at the mouths of narrow erosional valleys and canyons where they spread onto flatter relief. Deposits of alluvial fans are made up of a range of sediments with varying grain sizes. Most of the alluvial fans are formed by debris-flow deposits characterized by coarse-grained matrix-supported massive gravels with angular to subrounded clasts of basalts, trachyte and welded ignimbrites, locally with boulders up to 1 m in size. The matrix is usually formed of reddish to brownish sandy to silty clays. The alluvial fans with sheet-flood deposits have been documented around the town of Dila. Compared to the previous type, the bodies of these alluvial fans are flatter and wider. The accumulations of sheet floods are clearly stratified with an alternation of layers centimeters to a few decimeters thick of grain-supported gravel and sands with subordinate intercalation of sandy and silty clay loams. The thickness of deposits is usually several meters, the greatest thicknesses being preserved in the upper part of the alluvial fan and decreasing towards the distal parts.

1. Fluvial sediments are associated with the occurrence of fluvial channels and adjacent floodplains. The nature of the sediments depends on the type of fluvial system, topographic gradient and sinuosity of the river channel. Most of the rivers have small temporal streams with straight and braided channels. The accumulations are reduced to a narrow infill of the channel and lateral or in-channel bars formed by clast-supported gravels. In the highland plateau, small meandering streams develop on floodplains, being several tens of meters wide (Fig. 4-19). The fluvial sediments of this area are characterized by unconsolidated silty to sandy accumulations (Fig. 4-20), while silts and clays with a high content of organic matter are associated with sparse wetlands located in the floodplains. The thickness of fluvial sediments is estimated at several meters.

4.5 Geochemistry

The variation in chemical composition of the studied volcanic rocks is similar to those of previous works. Location of the sampling points is shown in Fig. 4-21. According

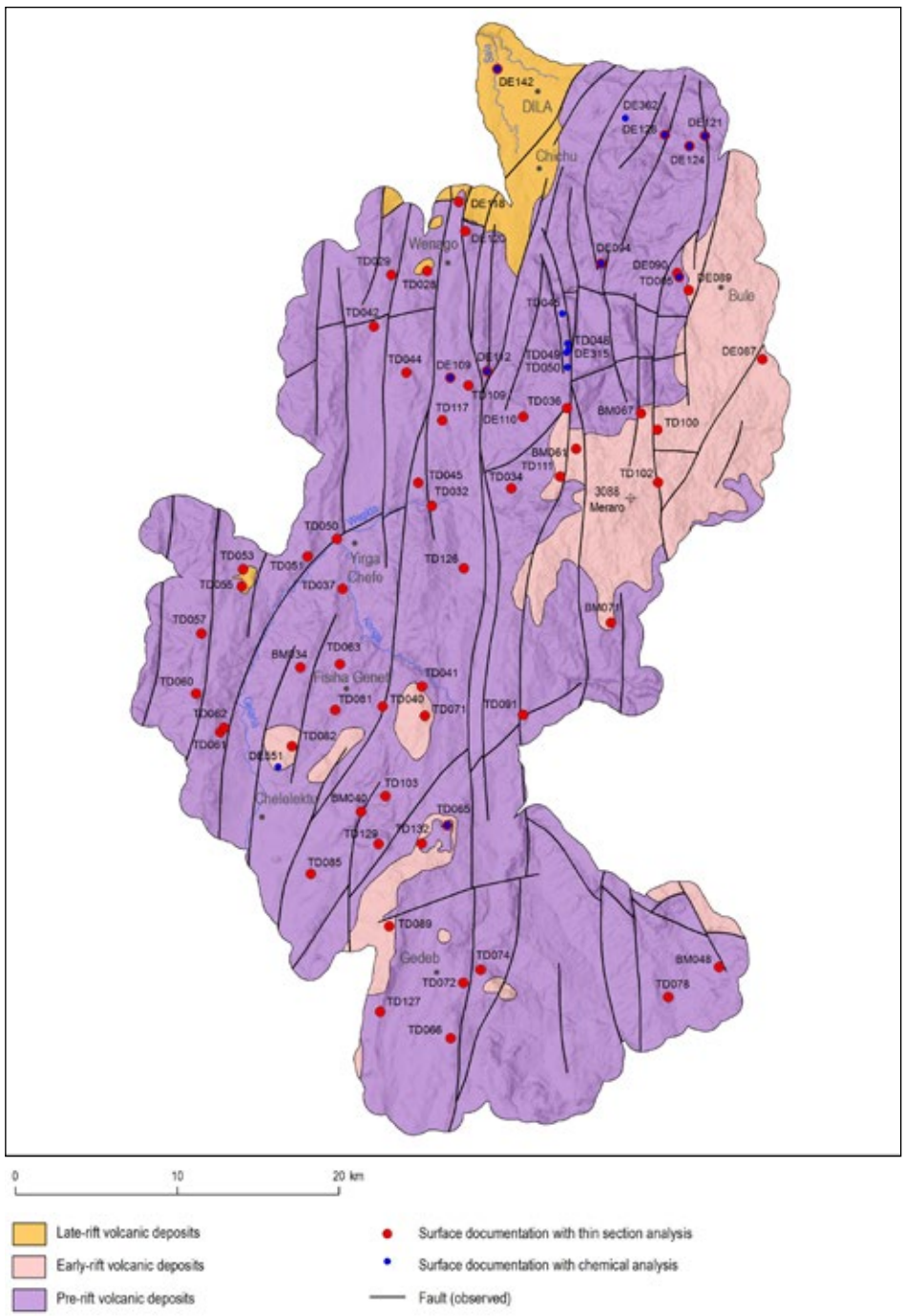

Figure 4-21. *Location of thin section and geochemical analyses samples.*

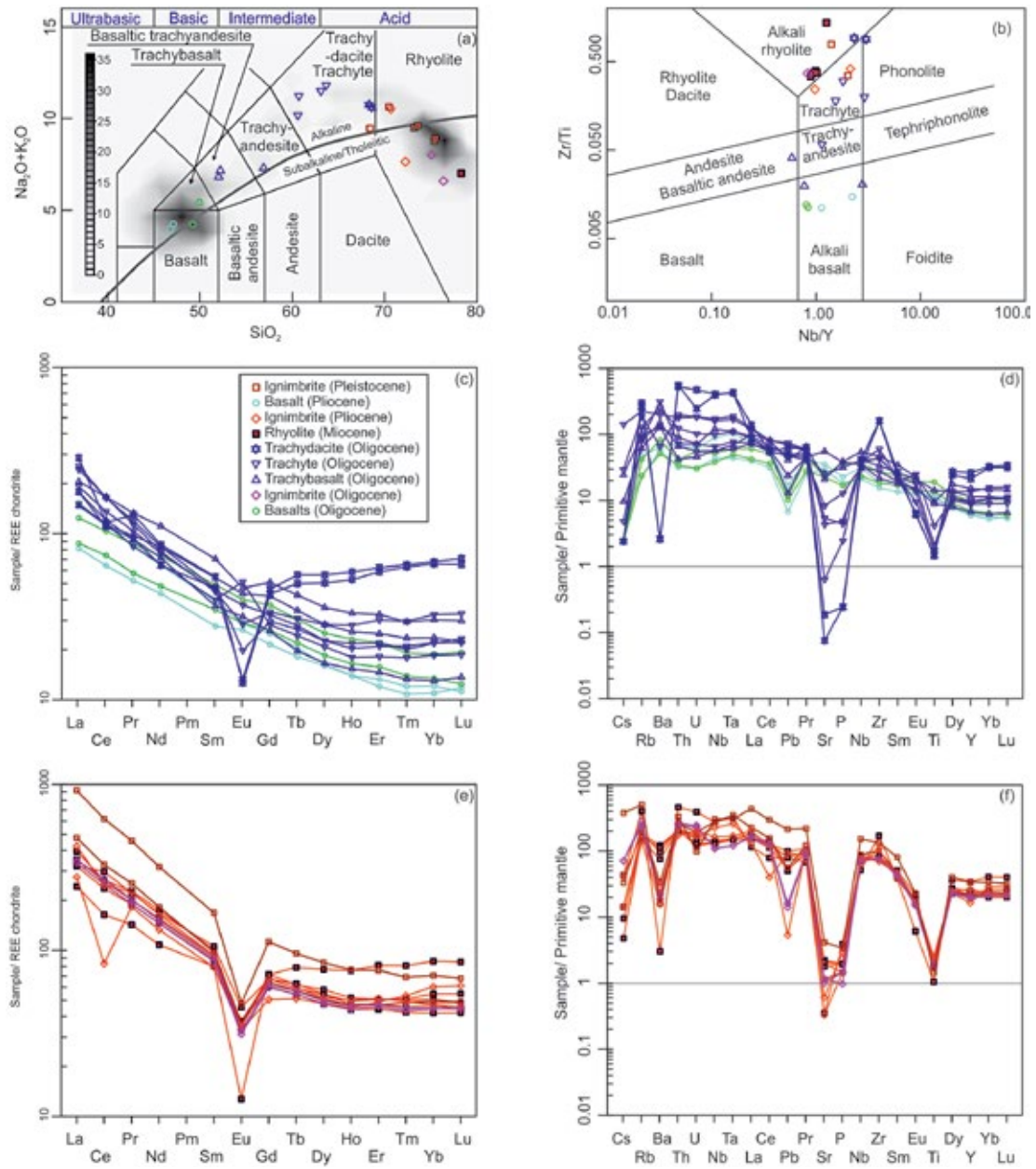

Figure 4-22. *Chemical composition of volcanic rocks: (a) $Na_2O + K_2O$ versus SiO_2 (TAS; Le Bas et al., 1986), shaded areas portray the frequency of other volcanic rocks in the Southern Main Ethiopian Rift (MacDonald and Gibson, 1969; Brown and Carmichael, 1969, 1971; Di Paola, 1971, 1972; Zanettin et al., 1978a, b; Bloomer et al., 1989; Hart et al., 1989; Asfaw et al., 1991; Woldegabriel et al., 1991, 2005; Wolde and Widenfalk, 1994; Stewart and Rogers, 1996; Ayalew et al., 1999, 2002, 2006; George and Rogers, 1999; Trua et al., 1999; Yemane et al., 1999; Katoh et al., 2000; Rogers et al., 2000; Furman et al., 2004; Haileab et al., 2004; Rooney, 2010; Shinjo et al., 2011; Rooney et al., 2012; Wolela, 2014; Rapprich et al., 2016); (b) Zr/Ti vs. Nb/Y discrimination diagram (Pearce, 1996); (c) chondrite-normalised rare earth element (REE) patterns (values for normalization are based on Boynton, 1984) for mafic rocks trachyte and trachydacite; (d) primitive mantle-normalized multi-element spider diagram (values for normalization are based on McDonough and Sun, 1995) for mafic rocks trachyte and trachydacite; (e) chondrite-normalised rare earth element (REE) patterns (values for normalization are based on Boynton, 1984) for rhyolite and ignimbrite; (f) primitive mantle-normalized multi-element spider diagram (values for normalization are based on McDonough and Sun, 1995) for rhyolite and ignimbrite.*

to Shinjo et al. (2011), the Miocene basic volcanic activity in this area is characterized by typical alkali basalts and hawaiites, whereas Pliocene basalts show tholeiitic affinity.

According to the total alkalis vs. SiO_2 (TAS) classification diagram (Le Bas et al., 1986; Fig. 4-22a), the volcanic rocks of the Gedeo Zone belong to basalts, trachybasalts, basaltic-trachyandesites, trachytes, and rhyolites. The mafic rocks (basalts, trachybasalts, basaltic-trachyandesites) have relatively low SiO_2 contents (45.8–55.2 wt. %) and high Al_2O_3 (14.2–17.1 wt. %). They are characterized by higher contents of Na_2O (2.7–4.7 wt. %; K_2O/Na_2O = 0.3–0.9), CaO (5.3–10.3 wt. %), and Fe_2O_3t (9.5–14.1 wt. %). The Pliocene as well as the Eocene to Oligocene basalts are spread along the subalkaline (tholeiitic) / alkaline boundary (K_2O contents ranging from 1.0 to 1.6 wt. %) in the TAS diagram (Fig. 4-22a). The CIPW normative compositions of the mafic rocks show distinct variations. The Amaro–Gamo basalts and Oligocene trachybasalts are silica-oversaturated and contain 1.4–8.9 wt. % of normative quartz calculated by the CIPW norm, whereas Pliocene basalts are normative quartz-free. The Oligocene trachytes and trachydacites (SiO_2 58.8–67.2 wt. %) have high Na_2O (5.5–6.6 wt. %; K_2O/Na_2O = 0.7–0.9), Fe_2O_3t (5.2–7.2 wt. %) and low MgO (0.0–0.6 wt. %). The trachytes are characterized by a low content of normative quartz (Q 0.1–4.8 wt. %), whereas the trachydacites are enriched in normative quartz (Q 15.3–16.1 wt. %).

According to the $Na_2O + K_2O$ content, the rhyolite and ignimbrite samples are classified as alkaline to subalkaline (tholeiitic) rhyolites and trachydacite (one Pleistocene ignimbrite; Fig. 4-22a). The SiO_2 (64.0–76.6 wt. %), Al_2O_3 (10.6–14.1 wt. %) and K_2O (3.8–5.5 wt. %; K_2O/Na_2O = 1.0–2.0) contents are high. Almost all studied samples exhibit a high Nb/Y ratio (Fig. 4-22b) typical for alkaline rocks (Pearce, 1996).

Basalt and trachybasalt show similar REE patterns (Fig. 4-22c) with a gently decreasing trend from LREE to HREE (La_N/Yb_N = 6.2–13.7) and have either no Eu anomaly or a slightly negative or positive one (Eu/Eu*= 0.8–1.1). The REE contents in basalts (153–219 ppm) are lower than those in trachybasalts (236–342 ppm). The trachytes show similar REE contents (225–316 ppm) to the trachybasalts; however, LREE patterns are slightly fractionated (La_N/Sm_N = 4–5; Fig. 4-22c) and the Eu anomaly is positive or negative (Eu/Eu* = 0.5–1.5). Primitive mantle-normalised multi-element variation diagrams (Fig. 4-22d) for basalts and trachyte show intraplate volcanic patterns with enrichment mainly in Rb, Ba, Th, U, Nb and Ta accompanied by low values of Cs and Pb. Trachydacites show remarkable depletion in Ba, Sr, P and Ti.

Trachydacites (Fig. 4-22c) show similar REE patterns to alkaline rhyolites (Fig. 4-22e). Individual REE patterns for the rhyolites are subparallel, with differences in total REE contents (400–560 ppm). They are characterized by fractionation of LREE (La_N/Sm_N = 2.8–7.7), flat to slightly increasing HREE and a negative Eu anomaly (Eu/Eu*= 0.2–0.5). The chondrite-normalized REE patterns for ignimbrites are highly fractionated in LREE and relatively flat in HREE (La_N/Yb_N = 4.6–13.0), except for the Pleistocene ignimbrite. A negative Eu anomaly (Eu/Eu* = 0.5–1.5) is common. One ignimbrite sample (DE159) exhibits a pattern with a significantly negative Ce anomaly (Fig. 4-22e). Primitive mantle-normalised multi-element variation diagrams (Fig. 4-22f) for ignimbrites and rhyolites display marked negative peaks of Cs, Ba, Sr, P and Ti, which are possibly the consequence of fractionation of feldspars, apatite and Fe-Ti oxide, respectively.

4.6 Tectonics

The Gedeo Zone (SNNPR) is located along the eastern edge of the NNE–SSW trending Southern Main Ethiopian Rift, which is part of the East African Rift System (e.g. Ebinger, 2000; Bonini et al., 2005; Corti et al., 2018). Individual segments of the Main Ethiopian

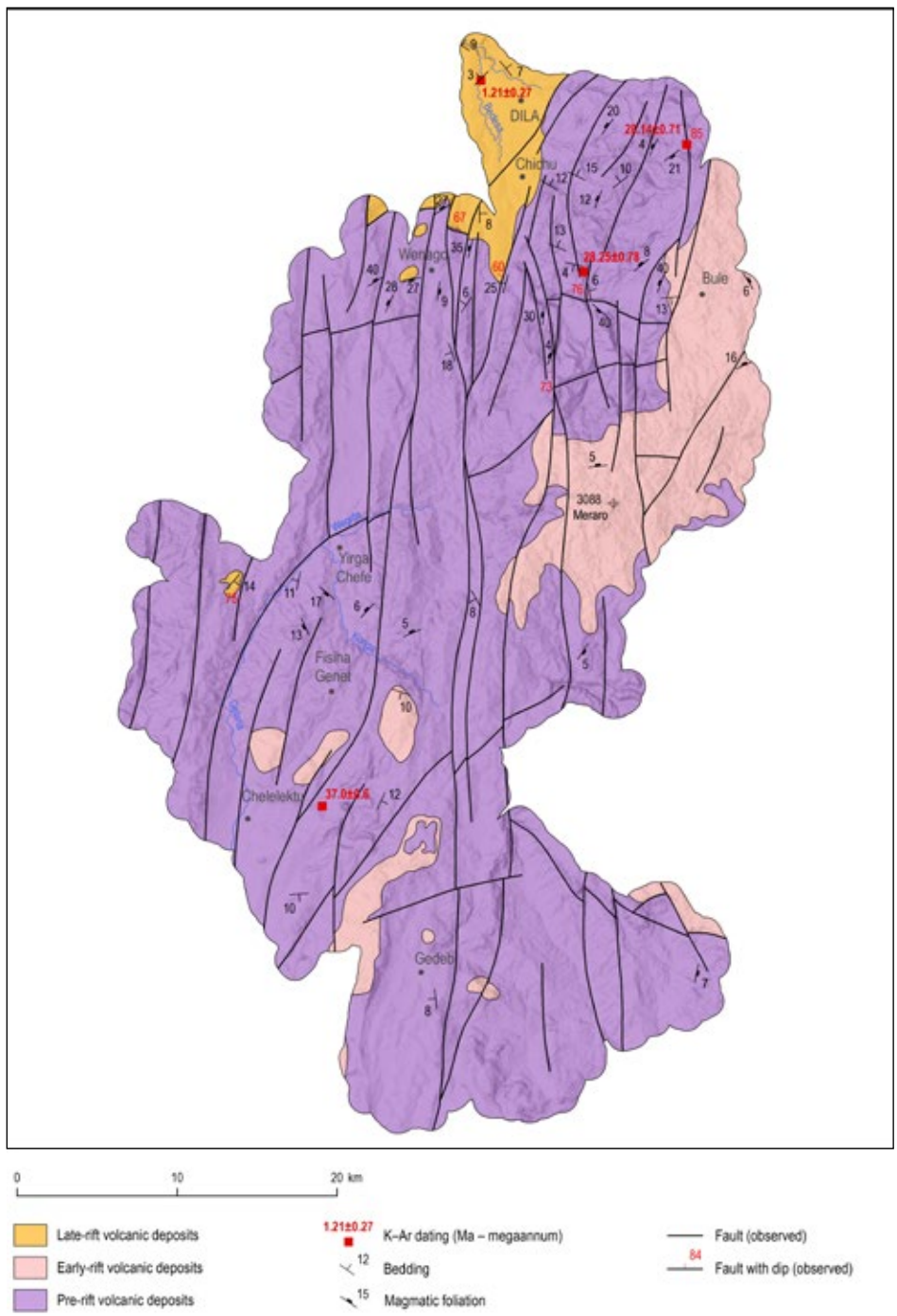

Figure 4-23. *Tectonic map scheme with location of dated rock samples.*

Rift reflect different stages of a regional ~E–W continental extension between the Nubian and Somalian plates. The continental extension started with early rifting in the Southern Main Ethiopian Rift in Lower Miocene and moved to a more prominent extension in the central and northern parts at present (e.g. Corti, 2009). On a regional scale, the initial ~WNW–ESE trending extension has changed to the recent ~W(WSW)–E(ENE) direction. Apparent reactivation of earlier normal faults resulting in those changes in orientation of regional stress field from rift-perpendicular extension to ~WSW–ESE transtension are observed at several domains across the Main Ethiopian Rift (Agostini et al., 2011).

The mapped area is composed of several lithotectonic units in terms of geodynamic and volcanic evolution of the Southern Main Ethiopian Rift (Fig. 4-23), described from the bottom: (a) **Pre-rift effusive rocks and volcanoclastic deposits** of Eocene to Oligocene ages. This sequence consists of several compositionally different rocks such as the Amaro–Gamo basalts, interleaved with ignimbrites and related acid pyroclastic deposits. (b) **The syn-rift volcanic deposits** which are mainly basalt lava flows with subordinate welded rhyolitic ignimbrites, and rhyolite lava domes with subordinate volcanic breccias of Miocene to Pliocene ages. The pre- and syn-rift volcanic deposits are followed by (c) **post-rift rift-floor volcanic deposits** of Pleistocene age, including mainly sequences of rhyolitic to trachytic ignimbrites associated with pyroclastic fall deposits, all commonly known as the Dino Formation.

The set of primary volcanic and volcano-sedimentary fabrics were locally modified by brittle rift-related structures (normal faults and extensional joints).

Primary structures

The primary volcanic and volcano-sedimentary fabrics are represented mainly by planar preferred orientation of rock-forming minerals, micro-vesicles or micro-crystals and elongated mineral grains, lithic fragments or stretched and welded pumice fragments in ignimbrites. The pre-rift volcanic sequence reveals a mainly subhorizontal or ~NW to WSW gently dipping flow foliation defined by planar (or linear-planar) preferred orientation of vesicles and crystals in basalt lava flows (Figs 4-24, 4-26a). Commonly,

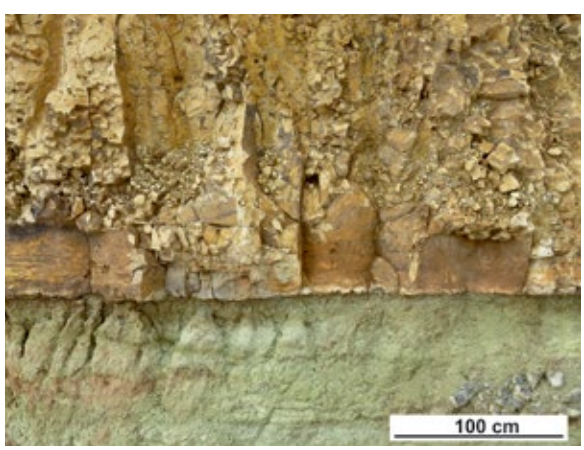

Figure 4-24. *Gently dipping bedding plane in pyroclastic fall deposits overlayed by a basalt lava flow (the crossroad 1.5 km NNE of Wenago village).*

Figure 4-25. *Rheomorphic folding of flow-foliation in rhyolites (the quarry 2 km W of Bule village).*

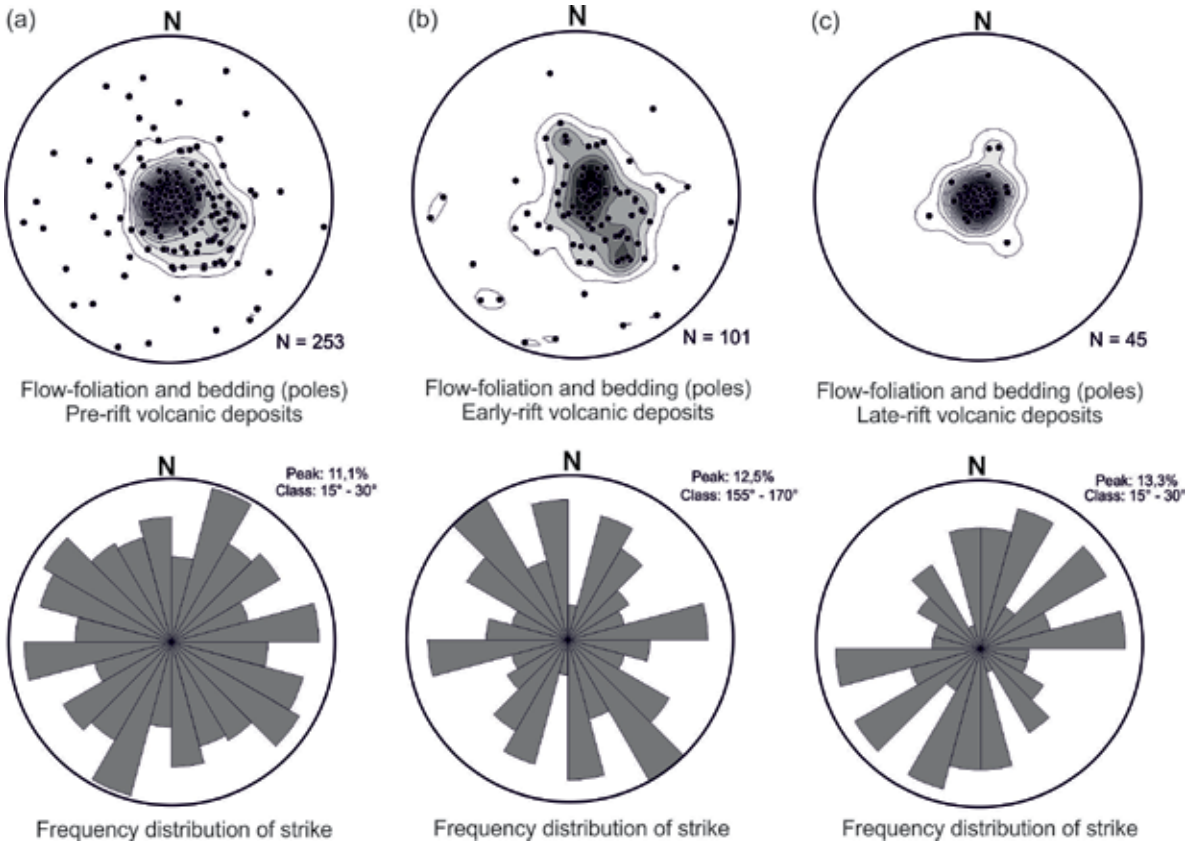

Figure 4-26. *Orientation diagrams of the primary structures in pre- to post-rift volcanic and volcano-sedimentary sequences: (a) flow foliation and bedding planes (poles) in ignimbrites and volcaniclastic rocks of the pre-rift deposits and frequency distribution of strike; (b) flow foliation and bedding planes in syn-rift deposits and (c) bedding planes (poles) in ignimbrites and pyroclastic deposits of the post-rift deposits. Equal projection to the lower hemisphere.*

welded ignimbrites reveal a flow-stretching of viscous silicic lava or hot glass fragments during the flow with a similar subhorizontal to WNW gently plunging dip. No linear alignment of the fragments or minerals is apparent. The syn-rift volcanic deposits, mainly basalt lava flows and associated pyroclastic deposits, show prevailing gently to moderately dipping flow foliation defined by the planar preferred distribution of rock-forming minerals and vesicles. The orientation of these flow-foliations exhibits relatively higher variability in orientation showing a weaker maximum reflecting ~NNW(NW) or SSE(SE) gently to moderately dipping planes (Fig. 4-26b) and associated weak stretching lineation gently plunging to E or W. In isolated rhyolitic lava flows, a variable dip of the planar preferred orientation of crystals was found, forming mostly the structure of asymmetric domes. These planar fabrics in rhyolites were locally folded into asymmetric open folds (Fig. 4-25) due to a highly viscous lava flow. In the post-rift deposits (with thickness up to ca. 70 meters), the prevailing rhyolitic to trachytic ignimbrites and pyroclastic fall deposits had mainly subhorizontal bedding planes (Fig. 4-26c). Contacts of individual volcanic flows and other lithological boundaries are mostly parallel to the gently-dipping to flat-lying planar fabrics. In some places, the contacts were also modified by normal faulting or locally by exodynamic processes such as rockfalls or landslides.

Figure 4-27. *Steeply W dipping, N–S trending fault plane with steeply plunging slickensides and normal kinematic indicators (a quarry east of Haru town).*

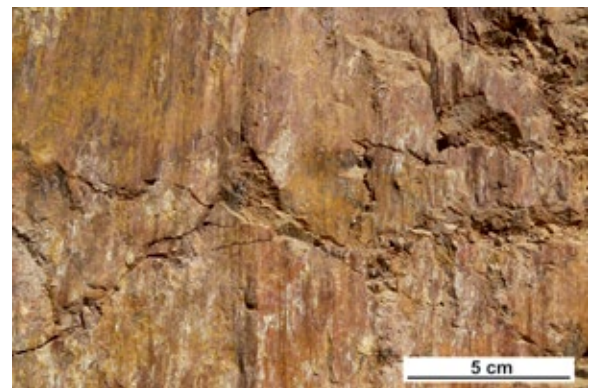

Figure 4-28. *Steeply dipping, N–S oriented fault plane with steeply plunging slickensides and normal kinematic indicators (a quarry west of Dila town).*

Brittle structures

Sets of brittle structures such as extensional joints, faults and fault zones bearing normal or oblique-slip kinematics were observed across the mapped area. The faults modified the entire geological pattern forming typical fault-dominated rift morphology. Prevailing rift-

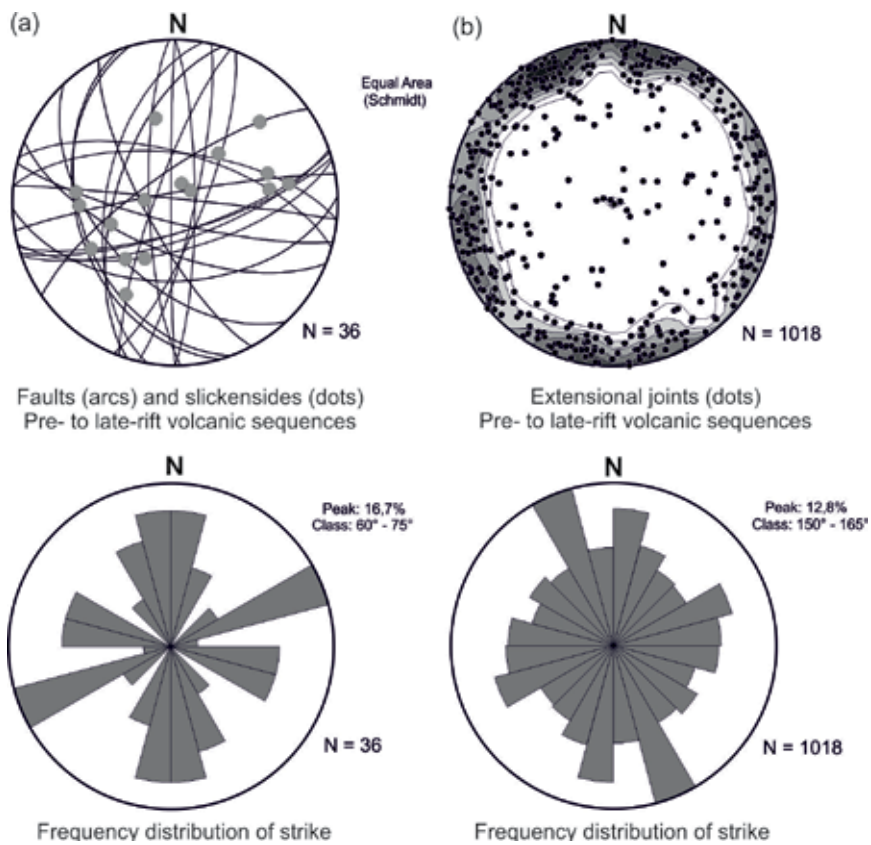

Figure 4-29. *Orientation diagrams of brittle structures: (a) normal faults / fault zones (arcs) in all lithologies with steeply plunging slickensides (dots) and frequency diagram showing the dip direction of faults and fault zones; (b) extensional joints in all lithologies (poles) and frequency diagram showing the dip direction of extensional joints in all units. Equal projection to the lower hemisphere.*

related faults dip steeply to ~W, or less commonly to ~E, with a prominent ~N–S strike (Fig. 4-27, Fig. 4-29a). These faults are often associated with fault lineation (slickensides) plunging steeply to W(SW) bearing evidence of normal kinematics (Figs 4-28, 4-29a). A continuous change in the orientation of the faults from the N–S to the NNE–SSW direction is apparent in the northern part of the Gedeo Zone, mainly NE of Gurguwa town (Fig. 4-23). The most prominent fault zone trends N–S with the approximate location between the towns of Chichu and Edera (Fig. 4-23). Moreover, main subordinate normal faults with subvertical ~W(SW)–E(NE) trending have been identified between the towns of Bule and Wenago or south of Yirga Chefe (Fig. 4-23). These faults are perpendicular to the prevailing series of normal faults parallel to the Southern Main Ethiopian Rift.

Two sets of mostly subvertical extensional joints with no evidence of movement were identified in all pre-, syn- and post-rift formations (Fig. 4-29b). The first distinct orientational maxima form the joints trending from ~N(NNW)–S(SSE). The second set consists of joints trending from ~E(ENE)–W(WSW). Their orientation is largely consistent with the regional fault pattern.

4.7 Gravimetry

Gravity data collected in archives of the Geological Survey of Ethiopia were used to create the complete Bouguer anomaly map of the Sidama and Gedeo zones. Although the data density is relatively low (Fig. 4-30), the resulting map (Fig. 4-31) still enables general large-scale features to be identified.

The whole area is characterised by a transition between the deep gravity low (even below –250 mGal) NE of the Sidama boundary and the gravity high (above –140 mGal) on the west and south sides of both zones. The gravity high is related to the rifting processes within the Main Ethiopian Rift – asthenospheric upwelling and mantle intrusion (e.g. Mahatsente et al., 1999, 2000). These long wave gravity anomalies largely reflect the depth of the Moho, which varies between 42 km on the N and NE and 36 km on the S and SE (Kassa et al., 2021).

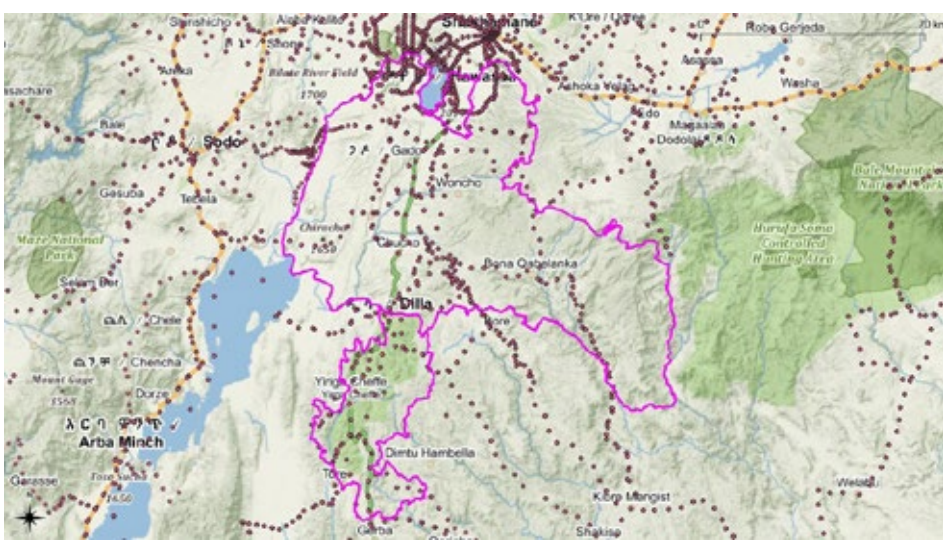

Figure 4-30.
A topographic map showing density of the gravity data points.

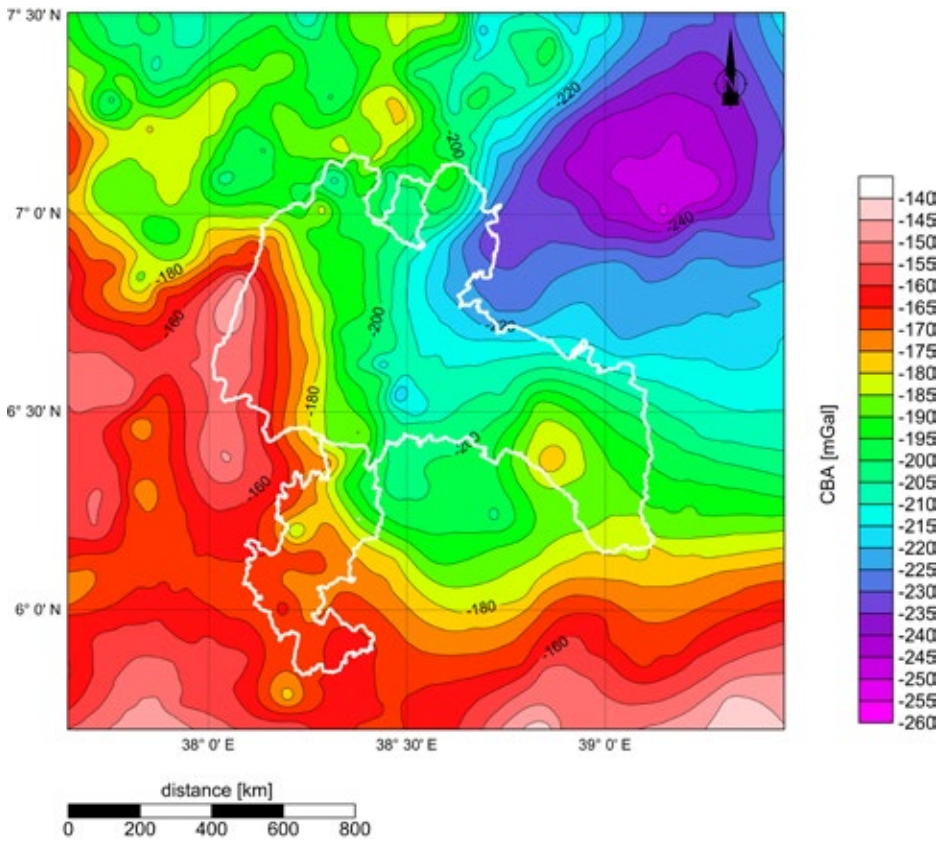

Figure 4-31. *Gravity map (complete Bouguer anomalies – CBA) of the Sidama and Gedeo zones.*

The gravity lows are related to the higher thickness of (relatively) low density upper crustal rocks. In the current map, these rock types are generally denoted as MG (igneous and metamorphic rock assemblage) and are mapped in the Sidama profile below the depths of 1500 m a.s.l. The densities of individual rocks in this assemblage obviously vary, but Mahatsente et al. (1999) uses an average density of 2700 kg/m^3 for the whole group of upper crystalline basement rocks (the Magdala Group in his work). The gravity data suggests that this group continues southwards to the Gideo map sheet mapped. There, it can be expected in the NE part of the area at an approximate depth of 0 m a.s.l. (east of the Bochesa River at the Gedeo profile).

The zone of high gravity values (up to –150 mGal) in the SE part of the Sidama Zone is probably connected with thick layers (even 1000 m) of Paleogene pre-rift basalt and trachybasalt lavas (βP2-3). Accumulations of these rock types generally correlate with local gravity highs, in contrast to the syn-rift Neogene basaltic lavas and pyroclastics (βN2), where the gravity highs are lower. The reason for this might be a lesser thickness of Neogene basalts and/or a higher content of pyroclastic deposits.

The young, post-rift, low density trachyte and rhyolite lavas forming a more than 1 km thick sheet in the west part of the Sidama Zone decrease the measured values of gravity acceleration and are most likely (together with the rift sediments) the reason for the slightly negative residual anomaly of the rift centre mapped by Mahatsente et al. (1999).

4.8 Geological evolution

Three distinct Cenozoic volcanic events took place within the Gedeo Zone (Southern Main Ethiopian Rift): pre-rift (Eocene to Oligocene), early-rift (Miocene), and late-rift stage (Pliocene–Pleistocene).

The volcanic activity started with the pre-rift volcanic sequences of the Amaro–Gamo basalts and Shole ignimbrites which reach a minimum thickness of ~1700 m. They were previously described as "Lower Basalts" (Hassen et al., 1997). The Eocene to Oligocene Amaro–Gamo basalts (45–28 Ma; Zanettin et al., 1978a; Ebinger et al., 1993, 2000; Buriánek ed., 2018; Steiner et al., 2021) form a dominant lithological unit in the Gedeo Zone and consist mainly of tholeiitic basalt to trachybasalt with minor basaltic pyroclastic deposits. The Amaro and Gamo basalts were originally attributed to an early phase of Afar-related volcanism (Stewart and Rogers, 1996). The Amaro basalts (45.2–39.58 Ma) represent geochemically primitive mantle melt, whereas the Gamo basalts (38–28 Ma) represent the mature main phase of flood basalt volcanism that has undergone significant processing within the lithosphere resulting in relatively homogeneous compositions (Steiner et al., 2021). Mainly in the upper part of the sequence, the Amaro–Gamo basalts are interbedded with strongly welded to welded Shole ignimbrites (38–17 Ma; Ebinger et al., 2000; Bonini et al., 2005; JICA, 2012; Buriánek ed., 2018). The Shole ignimbrites are also known as the Amaro tuffs (Ebinger et al., 1993; George et al., 1998; JICA, 2012) and have a rhyolitic composition. A subsequent eruptive event consisted of trachydacite to trachybasalt lavas which outcrop mainly to the east of the town of Dila. The K-Ar dates support this stratigraphic subdivision: Amaro basalts southeast of Sisota were dated at 37.0 ± 0.6 Ma (Ebinger et al., 1993) and the age of a Shole ignimbrite sample to the east of Wenago confirm an ignimbrite eruption at 28.25 ± 0.78 Ma (Buriánek ed., 2018). The K-Ar date for a trachyte sample situated close to the boundary with the Sidama Zone, east of Adida, provides a result of 28.14 ± 0.71 Ma (Buriánek ed., 2018).

The early-rift Miocene rhyolite volcanic sequence comprises rhyolite lava to volcanic breccia and minor glassy-rich ignimbrite.

The late-rift volcanic sequence consists of Pliocene ignimbrites (also described as the Bule Ignimbrite; Buriánek ed., 2018), partially covered by massive basalt lava flows and basaltic pyroclastic deposits. The Pliocene ignimbrite has been dated using the K-Ar method at 3.45 ± 0.36 (Buriánek ed., 2018). The Pleistocene volcaniclastic sequence includes ignimbrites (K-Ar 1.21 ± 0.27; Buriánek ed., 2018) and erosive relicts of acid volcaniclastic deposits crop out at the northwestern edge of the study area.

5) SOIL ENVIRONMENT

The soil represents an entire web of geological, hydrological, atmospheric and biological interactions. There are five major factors, which in various combinations create the large array of soils: time, climate, parent material, topography and organisms. The combination of all five factors determines the kind of soil development and distribution of soils in the area.

The relative influence of each factor varies from place to place, particularly in areas with a great diversity of the soil-forming factors. A detailed description of the soil-forming factors affecting the soil development in the area of the Gedeo Zone is given in the chapters.

Due to the very limited data available from the study area, a low intensity reconnaissance soil survey has been made to obtain representative profiles and characterization of the soil environment for the soil-environmental mapping at a scale of 1:100,000. Soil survey was conducted as a complement to the simultaneous geological mapping in cooperation with specialists of the Geological Survey of Ethiopia.

5.1 Genetic classification of soils – Reference Soil Groups

During the mapping campaign, 93 soil profiles (and/or soil landscapes) were georeferenced, documented and most of them sampled. Representative disturbed samples were taken for laboratory analyses using the boundaries of the horizon to define the vertical limits of sampling. The various road cuts and other soil disturbances, where a cross section of the soil is exposed, were used in the field work to provide the soil profile description, after a few centimeters of soil was scrapped off the profile to expose a fresh soil surface. In flat terrain a soil core sampler was used.

The major Reference Soil Groups were classified according to the latest update of World Reference Base for Soil Resources (WRB) classification system (International Union of Soil Sciences (IUSS) Working Group WRB, 2015). The morphological and other characteristics of the soil profiles and soil horizons were described according to Guidelines for Soil Description (Jahn et al., 2006).

The following major Reference Soil Groups (RSG) were mapped in the study area (Fig. 5-1).

Luvisols (LU) represent soils having an argic horizon (a subsurface horizon with a distinctly higher clay content than the overlying horizon, Fig. 5-2) with a cation exchange capacity equal to or more than 24 $cmol_c$ per kg clay throughout. They are moderately weathered, and, in the tropics, they occur on relatively young surfaces. Pedogenetic differentiation of clay content, with a lower content in the topsoil and a higher content in the subsoil without marked leaching of base cations or advanced weathering of high-activity clays results in the profile development of A – Bt – C. The Bt horizon often has a prismatic or sub-angular blocky structure. The illuvial nature of the argic horizon may be established using hand lens.

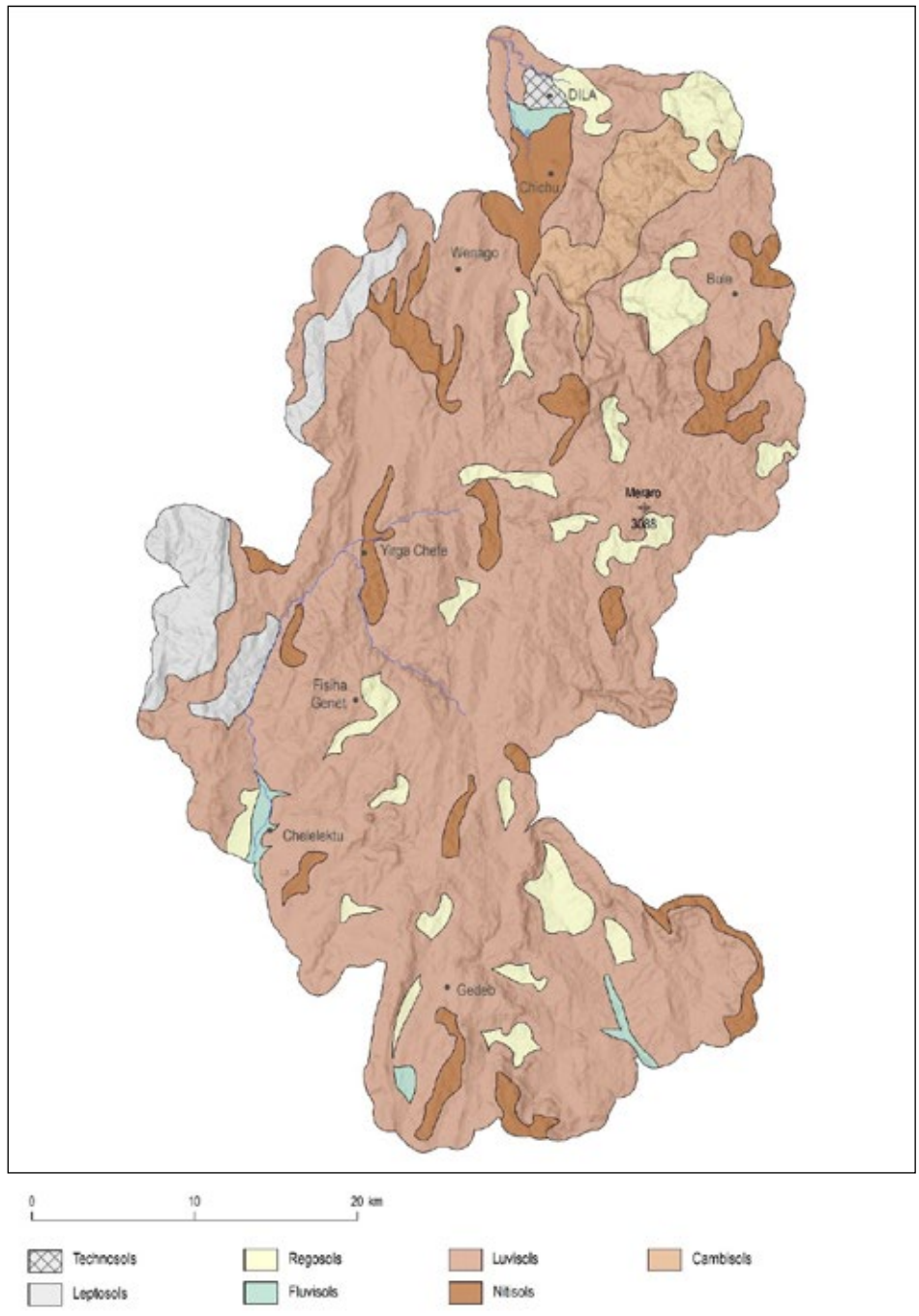

Figure 5-1. *Major Reference Soil Groups (RSG) in the Gedeo Zone.*

The clay coatings occur on soil aggregate surfaces, in fissures, pores and channels. The wide range of parent materials and environmental conditions led to a great diversity of soils in this Reference Soil Group.

Luvisols are fertile soils and suitable for a wide range of agricultural uses because of their moderate degree of weathering and high base saturation. Luvisols with a high silt

content are susceptible to structural deterioration if inappropriate farming technology is applied. Luvisols on steep slopes require erosion control measures.

Alisols (AL) occur predominantly alongside Luvisols on hilly or undulating topography. Most occurrences of Alisols are on the weathering products of basic rocks. Alisols are strongly acidic soils with an accumulation of high activity clays in the subsoil (Fig. 5-3). Similarly to Luvisols, Alisols have an A – Bt – C profile and a higher clay content in the subsoil than in the topsoil, as a result of pedogenetic processes (especially clay migration), leading to an argic subsoil horizon.

Alisols have a cation exchange capacity (CEC) equal to or more than 24 cmolc per kg clay throughout the argic horizon but differ from Luvisols in terms of having a low base saturation. The textural differentiation between surface and subsurface horizons impacts different physical properties.

Generally, Alisols are unproductive soils. The generally unstable surface soil of cultivated Alisols makes them susceptible to erosion; truncated soils are quite common. The use of acid-tolerant crops or low-volume grazing is common. The productivity of Alisols in subsistence agriculture is generally low. Where fully limed and fertilized, crops on Alisols may benefit from the considerable CEC and good water-holding capacity, and Alisols may eventually grade into Luvisols. Alisols are often planted with Al-tolerant crops such as coffee and sugar cane.

Nitisols (NT) seem to be one of the most common tropical soils on basic parental bedrock material. They occur on the gentle slopes and the relatively flat areas in the rolling to hilly plateaus in the mapped area.

Nitisols are deep, well-drained, red tropical soils with an A – B(t) – C profile development and a clayey nitic horizon. The nitic horizon is a clay-rich subsurface horizon

*<< **Figure 5-2.** Rhodic Luvisol in Repe; profile PPS21_005.*

***Figure 5-3.** Chromic Vertic Alisol (Clayic) to the SE of Fisiha Genet (Era location); profile SG047.*

with at least 30 percent clay and a silt to clay ratio < 0.4. The difference in clay content with the overlying and underlying horizons is gradual or diffuse. Nitic horizons have a typically angular blocky structure breaking into polyhedral or flat-edged or nut-shaped elements with shiny aggregate faces when moist, which cannot or can only partially be attributed to clay illuviation. There is no abrupt colour difference with the horizons directly above and below in the soil profile. The colours are of low value with hues often 2.5YR, moist, but sometimes redder or yellower.

The rapid rate of weathering in the tropics is responsible for the leaching of basic cations and relative accumulation of Fe and Al oxides in soils. Iron oxides influence the physical and chemical properties of the highly weathered soils that contain kaolinite as the major clay mineral. Goethite and hematite are responsible for the yellow-brown and red pigment, respectively. Due to their smaller crystal size and reactive surface sites, iron oxides are involved in the retention of anions such as phosphate (Singh and Gilkes, 1992). In a sub-humid tropical climate, the alternating dry and wet seasons and the relatively drier environment may affect the Fe-oxide and silicate clay species composition and formation from various parent materials *(*Fig. 5-4).

The exact origin of the shiny faces of the polyhedral, flat sided or nutty elements typical of the nitic horizon is still under debate. The development of these typical nitic properties, or the nitidization process, is assumed to be related to alternating micro-swelling and shrinking (Driessen et al., 2001). The soil moisture regime plays an important role because it influences the degree of swell–shrink behaviour, which will be strongest in a climate with contrasting wet and dry seasons.

Contributing factors to Nitisol development are:

– the presence of open 2/1 clays, in addition to dominant kaolinite, resulting in relatively high water-dispersible clay content and high swell-shrink potential,
– seasonal cycles of wetting and drying, contributing to strong blocky soil structure development,
– recurrent conditions of weak temporary hydromorphism, resulting in the redistribution of Fe-Mn oxides,
– exceptional Fe oxide characteristics, particularly an extremely small particle size. Together with the presence of abundant clay coatings, these Fe oxide characteristics explain the shiny aspect of ped faces that is characteristic of nitic horizons (De Wispelaere et al., 2015).

Nitisols are among the most productive soils of the humid tropics. The deep and porous solum and the stable soil structure of Nitisols permit deep rooting and make these soils quite resistant to erosion. The good workability of Nitisols, their good internal drainage and fair water holding properties are complemented by chemical (fertility) properties that compare favourably to those of most other tropical soils. Nitisols are used for coffee plantations and are also widely used for food crop production on smallholdings.

Cambisols (CM) occur where conditions are not favourable for other soil forming processes than weathering to take place, and often occur on steep slopes. Large occurrence of Cambisols is concentrated on the metamorphic rocks in the SE part of the area.

Cambisols are soils with an A – Bw – C soil profile and at least, the initial development of a subsurface cambic horizon shows the evidence of pedogenetic alteration that ranges from weak to relatively strong. If the underlying layer has the same parent material, the cambic horizon usually shows higher oxide and/or clay contents than this underlying layer (Fig. 5-5). The pedogenetic alteration of the cambic horizon can also be established by contrast with one of the overlying mineral horizons that are generally richer in organic

<< ***Figure 5-4.*** *Eutric Nitisol near Werka Chelbesa; profile UCS21-01-24-14.*

Figure 5-5. *Chromic Cambisol to the north of Wenago.*

matter and therefore have a darker and/or less intense colour. In this case, some well-developed soil structure is needed to prove pedogenetic alteration. The cambic horizon can be considered the predecessor of many other diagnostic horizons, which have specific properties that are not recognized in the cambic horizon – such as illuvial or residual accumulations, or the development of specific soil structures.

The processes that lead to the formation of a cambic subsurface horizon are fundamentally the same in all climate zones, but the intensity of the chemical and biological transformations is considerably greater in the tropics than elsewhere. Cambisols in the humid tropics can be formed in a few years. Generally, cambisols are not common in sub-humid and humid tropics because of the faster rate of weathering and soil formation than in the temperate climate. However, in the areas with active erosion, they may occur in association with mature tropical soils and/or with very young and weakly developed soils.

Eutric and Chromic Cambisols in undulating or hilly (mainly colluvial) terrain are planted to a variety of annual and perennial crops or are used as a grazing land.

Fluvisols (FL) cover a large amount of the polygenetic sediments (alluvial and resedimented pyroclastics) in the lowest part of the mapped area along the shores of the Lake Hawassa (Hawassa Caldera) as well as the fluvial and lacustrine sediments in the endorheic depressions and rare flood plains. They also occur on the alluvial fans.

Fluvisols represent genetically young soils with fluvic material lacking distinct horizon differentiation, where only a distinct topsoil horizon resulting from cultivation is present (Fig. 5-6). The texture of the parent material differs between riverbanks or lagoons and basins. Fluvic material refers to fluviatile and lacustrine sediments that receive fresh material or have received it in the past and still show stratification. Stratification may be reflected in different ways: variation in texture and/or the content or nature of coarse fragments, different colours related to the source materials, or alternating lighter and darker coloured soil layers, indicating an irregular decrease in organic carbon content in

Figure 5-6. *Eutric Fluvisol; Birda Bochesa; profile DKS21-01-21-16.*

the soil with depth. The great variability of fluvisols does not permit a characterization of the nutrient status for the group as a whole. The fertility of fluvisols is directly related to the materials from which they are derived. Flood hazard is a common constraint on fluvisols, especially in areas with seasonal rainfall patterns.

Severe erosion and land degradation occur in the mapped area: the gullies are deeply incised into the soils and underlying layers, and the barren and degraded badlands have total soil loss (the soil is washed out). Highly eroded areas and slopes with thin and stony soils generally have **Leptosols and Regosols.**

Regosols (RG) cover heterogeneous formations of colluvial sediments at the foot of steep eroded slopes throughout the mapped area.

Regosols are weakly developed soils in an unconsolidated material without diagnostic horizons. They show only slight signs of soil development – some accumulation of organic matter producing a darker topsoil is often the only evidence of soil formation (Fig. 5-7). Soil horizon development is minimal as a consequence of the young age. Regosols are generally associated with degrading and eroding surfaces. Colluvial material is a heterogeneous mixture of material that, by gravitational action, has moved down the slope. It has been transported as a result of erosion, wash or soil creep, and the transport may have been accelerated by particular land use practices (deforestation). It has been formed in relatively recent times. Colluvial material is generally moderately sorted. It may show some gross stratification, but stratification is not a typical feature due to the diffusion or chaotic nature of the deposition process.

Regosols suffer severe erosion and are often covered with tree and shrub vegetation.

Leptosols (LP) occur throughout the whole area where slopes are too steep to make any significant degree of soil development possible (Fig. 5-8). An additional factor is severe recent erosion on cultivated slopes.

Leptosols are azonal soils with an incomplete solum and/or without clearly expressed morphological features. They can be found on rocks that are resistant to weathering or where erosion has kept pace with soil formation, or removed the top of the soil profile.

Figure 5-7. *Skeletic Colluvic Regosol to the NE of Fisiha Genet; profile PPS21-021.*

Figure 5-8. *Lithic Leptosol to the NE of Fisiha Genet; profile PPS21-021.*

The World Reference Base definition of Leptosols refers specifically to shallow soils with continuous hard rock within 25 cm of the soil surface. However, the definition also includes deeper, extremely gravelly and/or stony soils, provided they have less than 20 percent of fine earth over a depth of at least 75 cm.

Leptosols have a resource potential for grazing and as forest land or alternatively agroforestry. The rock exposure is frequent in the environments where Leptosols occur. Leptosols on hill slopes are generally more fertile than their counterparts on more level land. One or a few good crops could perhaps be grown on such slopes but at the price

of severe erosion. Steep slopes with shallow and stony soils can be transformed into cultivable land through terracing, the removal of stones by hand and their use as terrace fronts.

5.2 Soil properties

Indicators of soil properties can be categorized into four general groups: *morphological, physical, chemical, and biological*. Morphological indicators are observable attributes in the field of the soil within the various soil horizons and the description of the kind and arrangement of the horizons. Physical indicators are related to the arrangement of solid particles and pores (texture, bulk density, porosity etc.). Chemical indicators include measurements of pH, organic matter, cation-exchange capacity, nutrient status and concentrations of elements that may be potential contaminants. Biological indicators include the measurements of micro- and macroorganisms, their activity, and products.

The most identifiable properties of soils are texture, structure, and color, which provide the basis for distinguishing soil horizons and for grouping soils according to the soil classification system.

Soil texture, structure and color are intrinsic functions of the parent material of the soil modified by organic material. The advanced weathering of rocks in the (sub-) humid tropics produces typical tropical soils: red or yellow in color and strongly leached. Additional features: they are deep, finely textured, contain no more than traces of weatherable minerals, have low-activity clays, less than 5 percent of recognisable rock structure and gradual soil boundaries. Differences between soils in the (sub-) humid tropics can often be attributed to differences in lithology and/or (past) moisture regime (Driessen et al., 2001).

Soil **color** is also the property of soil that most reflects its pedogenic environment and history (age, and the temperature and moisture characteristics of the climate). These processes include the weathering of geologic material, the chemistry of oxidation-reduction actions upon the various minerals of soil, especially iron and manganese, and the biochemistry of the decomposition of organic matter. As the rocks containing iron or manganese weather, the elements oxidize: iron forms small crystals with a yellow or red color, organic matter decomposes into black humus, and manganese forms black mineral deposits (Lynn and Pearson, 2000). The darker the topsoil color, the more organic matter it usually contains, grey colors and mixed colors in subsurface horizons are often indicative of seasonally wet conditions when the water table is high, degree of redness in subsurface horizons can be correlated with soil age and landscape stability.

Soil **structure** refers to the way in which the sand, silt and clay particles are arranged into discrete soil units (aggregates or peds). Soil structure results from pedogenic processes. Aggregation is influenced by soil organic carbon, soil biology/microbiology, chemical reactivity, and the presence of clay. The basic types of aggregate arrangements are granular, blocky, prismatic, and massive structures. Soil structural properties tend to be more difficult to measure than other soil properties and reliable data are often lacking.

Soil texture refers to the proportions (by weight) of three particle-size classes: sand, silt, and clay-sized particles that make up the mineral fraction of the soil. Particles larger than clay and silt consist of unmodified parental rock material, clay particles are chemically and structurally transformed minerals, bearing little resemblance to the parental material.

This evaluation uses the 2000–63–2-µm system for particle-size fractions. Soil texture is one of the most important characteristics, which helps to classify Luvisols, Nitisols, Vertisols and Cambisols. Soil texture is also the basic characteristic for abrupt textural change and litological discontinuity (Hristov, 2013).

The following table (Tab. 5-1) shows soil texture, structure and color of surface and subsurface horizons in selected profiles of the most extensive Reference Soil Groups, which were sampled within a soil survey of the Gedeo Zone.

Table 5-1. Color, structure and soil particle distribution of the soils sampled in the Gedeo Zone

Sample	Color*	Structure	Clay [%]	Silt [%]	Sand [%]	Silt/ Clay	Texture
SG040 H-A	7.5YR3/4	Blocky subangular	40.8	50.2	9.0		Silty Clay
SG040 H-B	5YR2/4	Blocky angular	54.4	39.0	6.6	0.7	Clay
SG047 H-A	7.5YR3/4	Subangular	50.6	45.0	4.4		Silty Clay
SG047 H-B	7.5YR3/4	Subangular	53.4	40.2	6.4	0.8	Silty Clay
SG052 H-A	5YR2/4	Subangular	69.9	26.1	4.0		Clay
SG052 B	5YR2/4	Blocky subangular	75.0	21.5	3.5	0.3	Clay
UCS21-01-24-13-1	5YR2/3	Subangular	30.9	60.1	9.0		Silty Clay
UCS21-01-24-13-2	5YR2/4	Subangular	56.4	43.5	<1.0		Silty Clay
UCS21-01-24-13-3	5YR2/4	Subangular	76.1	22.6	1.3	0.3	Clay
UCS21-01-24-14-1	5YR2/4	Subangular	56.5	33.5	10.0		Clay
UCS21-01-24-14-2	5YR2/4	Subangular	67.6	23.4	9.0	0.3	Clay
DKS21-01-24-14a-01	2.5YR2/4	Subangular	63.5	32.9	3.6		Clay
DKS21-01-24-14a-02	2.5YR2/4	Subangular	80.5	17.8	1.7	0.2	Clay

*Munsell Color of moist matrix

The color of the soil matrix of each horizon was recorded under moist conditions using the notations for hue, value and chroma as given in the Munsell Soil Color Charts (Munsell, 2003). Soil color meets the criteria for the Chromic or Rhodic principal qualifiers in most of the sampled profiles.

Silt/clay ratio is an important criterion used in the classification of tropical soils. It is also used in the evaluation of clay migration, stage of weathering and age of parent material and soils. The more highly weathered a soil is, the lower the silt fraction. Therefore, soils with silt/clay ratio of less than 0.15 are regarded as highly weathered (Van Wambeke, 1962).

The silt to clay ratio < 0.4, clay content ≥ 30%, and blocky structure breaking into polyhedral or flat-edged or nut-shaped elements with shiny soil aggregate faces are important diagnostic criteria of a *nitic* horizon, which is the diagnostic horizon for Nitisols.

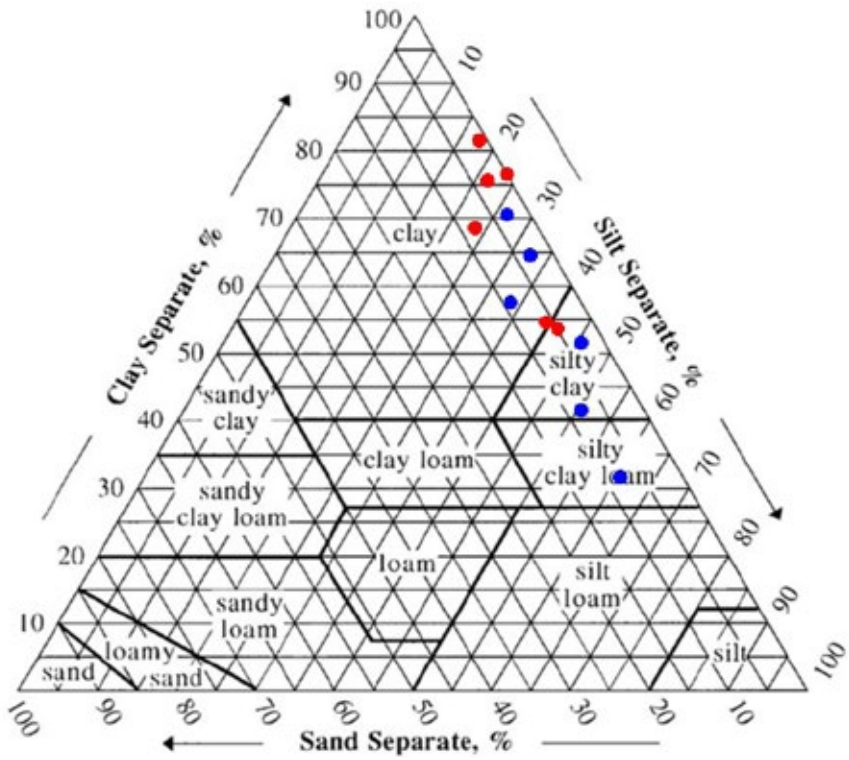

Figure 5-9. *Soil texture in topsoil (red) and subsoil (blue) of the sampled soils.*

The soil textural triangle was used to determine soil textural classes based on sand, silt and clay percentages (Fig. 5-9).

The textural triangle and table above show textures ranging from silty clay to clay, which meets criteria for clayic qualifier. Clay content is higher in subsoil horizons of the sampled profiles as a consequence of the geological conditions and pedogenic processes which form predominant soils in the area of interest (clay illuviation and nitidization).

5.3 Geochemistry of soil environment

Soil chemistry deals with the chemical properties and reactions of soils. Chemical soil parameters are measurable properties of soil that provide information about how the soil can function within natural or managed ecosystems. The understanding of the spatial variation of soil chemical properties is critical in agriculture and the environment.

The selection of the analyses that provide you with the most useful information is very important, since the soil tests are relatively expensive. The soil mapping at a scale of 1:100,000 uses analytical methods to obtain the essential characteristic of soil properties and for classification purposes.

The soil analyses required for the soil-environmental mapping at a scale of 1:100,000 were limited to the following soil quality indicators: pH in H_2O and CaCl2, cation exchange capacity (CEC), sum of base cations and base saturation (BS) and soil organic carbon (SOC).

Soil pH is the single most important aspect of soil chemistry because it affects the soil's physical, chemical, and biological properties and processes as well as plant growth.

Cation Exchange Capacity is a measure of the cations that a soil can retain on its negatively charged surfaces, which are found on clay particles and in soil organic matter. Therefore, clay soils generally have higher CEC values due to their clay content and generally hold more organic matter. Soils with high CEC values may also hold more water.

Base saturation represents the percentage of soil exchange sites (CEC) occupied by basic cations Ca^{2+}, K^{+}, Mg^{2+}, and Na+ (calcium, potassium, magnesium, sodium ions) in soil. The percentage base saturation is expressed as: % BS = $[(Ca^{2+} + Mg^{2+} + K^{+} + Na^{+}) / CEC] \times 100$.

Cation exchange capacity and base saturation are used as criteria in the definition of diagnostic horizons or properties as well as in the key to the reference soil groups. CEC of clay and BS (Tab. 5-2) in argic horizons help to distinguish Luvisols, Alisols, Lixisols, and Acrisols (Schad, 2005).

Table 5-2. Distinguishing of Luvisol, Alisol, Lixisol, and Acrisol

	BS ≥ 50% in 25–100 cm in the major part	**BS < 50%, no alic prop. in 25–100 cm in the major part**	**Alic properties in 25–100 cm in the major part**
CEC ≥ 24 $cmol_c\ kg^{-1}$ clay in the argic throughout	**Luvisols**		**Alisols**
CEC < 24 $cmol_c\ kg^{-1}$ clay in the argic in some part	**Lixisols**	**Acrisols**	

Soil Organic Carbon is a measureable component of soil organic matter (SOM). Soil organic matter (SOM) plays an important role in the physical, chemical and biological function of soils. SOM contributes to nutrient turnover and cation exchange capacity, soil structure, moisture retention and availability, degradation of pollutants, greenhouse gas emissions and soil buffering.

The values of mentioned characteristics in selected soil profiles of the Gedeo Zone are shown in Tab. 5-3.

The soil reaction (pH $CaCl_2$) of the sampled soils ranges from very strongly to slightly acidic soils. Acidic soils are predominant in the mapped area. Soil pH is important for cation exchange capacity because the CEC of soil organic matter and some clay minerals varies with pH.

The cation exchange capacity of the sampled soils mostly varies between medium to high values. Because organic matter and clay are major sources of negative electrostatic sites. There is a strong correlation between CEC values and the amount of clay and organic matter present in the soil. Soils with a higher clay fraction tend to have a higher CEC as well as the soils with a high content of organic matter. Clay has a great capacity to attract and hold cations because of its chemical structure. However, CEC varies according to the type of clay. It is highest in montmorillonite clay, and lowest in heavily weathered kaolinite clay. Low CEC values can be improved by adding organic matter, because organic matter colloids have large quantities of negative charges. Humus has a CEC two

Table 5-3. Selected chemical characteristics of the sampled profiles. CEC – Cation Exchange Capacity, BS – Base Saturation, SOC – Soil Organic Carbon

Sample	pH H_2O	pH $CaCl_2$	CEC [$cmol_c^+/kg$]	BS [%]	SOC [%]
SG040 H-A	5.65	5.14	29.78	46	1.50
SG040 H-B	6.06	5.18	30.12	43	1.31
SG047 H-A	4.82	4.10	36.63	18	2.04
SG047 H-B	5.14	4.07	34.55	14	1.42
SG052 H-A	6.42	5.78	28.68	57	1.24
SG052 B	6.54	5.78	25.68	51	1.02
UCS21-01-24-13-1	6.70	6.20	42.03	77	3.25
UCS21-01-24-13-2	6.81	6.15	37.93	70	1.81
UCS21-01-24-13-3	5.81	5.04	31.86	49	0.91
UCS21-01-24-14-1	6.93	6.09	33.05	71	1.80
UCS21-01-24-14-2	6.62	5.62	30.87	61	0.92
DKS21-01-24-14a-01	6.16	5.36	32.82	56	1.47
DKS21-01-24-14a-02	5.31	4.40	29.66	33	0.88

to five times greater than montmorillonite clay and up to 30 times greater than kaolinite clay.

Base saturation of sampled soils varies from extremely unsaturated (SG 47) to saturated soils.

The organic carbon concentrations in sampled soil profiles range from low to high values, but most soils only have a low content of organic carbon.

The key drivers influencing the variability of soil organic carbon in the tropics are texture, climate, topography, and land use management. The clay mineralogy and content of Al and Fe (hydro-) oxides have a significant influence on the stability of soil organic carbon in tropical soils (Bech Bruun et al., 2010). The role of SOC is especially important in tropical farming systems, where soil productivity often relies on limited external inputs so that the maintenance of SOC reservoir plays a key role in sustainable management of these soils.

Most indicators of soil chemical quality measure dynamic soil properties, i.e. properties that change over time and with management.

5.4 Land degradation and soil erosion

Soil erosion is a major threat to the soil resource, soil fertility and productivity in Ethiopia (Fig. 5-10). Soil erosion has a great effect on the change in soil properties due to the removal of the top fertile soil rich in organic matter and the deterioration of soil structure or aggregation. Erosion by water can occur as splash, sheet, rill, stream bank and gully erosion.

Figure 5-10. *Deforestation is a major cause of accelerated soil erosion. Eroded landscape in the Gedeo Zone.*

Recently, a large number of process-based soil erosion models have been used to assess the sheet and rill erosion (Ali and Hagos, 2016). The sheet, rill and inter-rill erosion has been estimated using the widely applied Universal Soil Loss Equation (USLE) (Wischmeier and Smith, 1978) modified by Hurni (1985) for the Ethiopian Highlands. Despite the disadvantages and uncertainties of the USLE are very well known, the USLE and its revised versions are widely used in the scientific and engineering world because of its relatively easy application.

Erosion rates are very sensitive to soil texture and moisture, vegetation cover, land use, slope, and climate as well as to soil conservation practices at the field level. USLE allows the prediction of annual soil loss based on the product of six factors. It is represented by $A = R * \mathrm{K} * \mathrm{L} * \mathrm{S} * \mathrm{C} * \mathrm{P}$; where A is the calculated spatial average soil loss and temporal average soil loss per unit area, usually expressed in t ha^{-1} $year^{-1}$, R is the rainfall erosivity index, K is soil erodibility. S and L are the topographical factors (length and gradient of the slope), C is the plant cover factor and P is the factor of specific erosion control practices.

The intensity of soil erosion is mainly influenced by three factors: erosivity of water, erodibility of soils, and human activities. Erodibility of tropical soils (K-factor) is highly dependent on grain size distribution, clay content and organic carbon content, which influence the stability of soil aggregates. Also, infiltration rates of soils are influenced by the morphometric characteristics of the land surface. Soils with a high percentage of silt and clay particles have a greater erodibility than a sandy soil under the same conditions. The initial K-factors can be derived from the study of Hurni (1985), showing a relationship between soil colour and the K-factor (Tab. 5-4).

Table 5-4. Soil erodibility estimation based on color for Ethiopia (Hurni, 1985)

Color	Soil reference group	K value (t ha h)·(ha MJ mm)$^{-1}$
Black	Andosols, Vertisols, etc.	0.020
Brown	Cambisols, Phaeozem, Regosols, Luvisols, etc.	0.026
Red	Lixisols, Nitisols, Alisols, etc	0.033
Yellow	Fluvisols, Xerosols, etc	0.040

The USLE parameters measure only sheet, rill and inter-rill erosion; therefore, the overall soil erosion rate, especially in areas where deep gullies exist, as found in the mapped area, could be much higher than predicted by the USLE. However, other similar studies have calibrated the USLE model parameter for Ethiopian conditions (Gebremichael et al., 2005; Nyssen et al., 2009; Haregeweyn et al., 2013).

In Ethiopia, extensive areas of agricultural land are eroded every year and most of this land (cultivated and grazing) is changed into gullies. Gully erosion produces channels larger than rills. As the volume of concentrated water increases and attains greater velocity on slopes, it enlarges the rills into gullies. Gullies can also originate from any depression such as cattle trails, footpaths, cart tracks, and traditional furrows and indicate neglect of land over a long period of time. In the Ethiopian Highlands, gullies are particularly severe and widespread, covering large tracts of areas. Gully erosion is more difficult and expensive to control than sheet and rill erosion. It is also more striking than other forms of erosion.

On steep slopes, soils are generally shallower and their nutrient and water storage capacities are limited. Thus, soils in these areas, when exposed to soil eroding agents, face greater degradation consequences compared to soils in flat areas. Since most of the terrain is undulating and hilly, most agricultural land is situated on sloping ground. Increasing population has resulted in a greater demand for cultivable land and pasture which have increasingly moved on to steeper slopes previously covered by forests. If soil depth is inadequate, the water holding capacity and rooting anchorage of the soil may decrease below the critical level. As soil depth decreases, croplands revert to grasslands and ultimately degrade to bare rock (Bezuayehu et al., 2002).

Various measures have been taken by the Ethiopian government to tackle the problem of low agricultural productivity due to high erosion and poor soil fertility. The measures include agricultural extension services focusing on the utilization of agricultural inputs such as chemical fertilizer and improved seed, and promotion of soil and water conservation (SWC). An example of such measures is the contour terracing shown in Fig. 5-11.

The susceptibility to land degradation differs within the main agricultural soils of the study area according to Stocking and Murnaghan (2001) (Tab. 5-5).

Figure 5-11. *Among the different soil and water conservation interventions, contour terracing has been implemented on farmlands.*

Table 5-5. Major Reference Soil Groups (RSG) of the map sheet and their susceptibility to land degradation

RSG	Main properties and susceptibility to land degradation
Luvisols	The tropical soil most used by small farmers because of its ease of cultivation and no great impediments. Base saturation > 50%. However, they are greatly affected by water erosion and loss in fertility. Nutrients are concentrated in topsoil and they have low levels of organic matter. Luvisols have moderate resilience to degradation and moderate to low sensitivity to yield decline.
Nitisols	One of the best and most fertile soils of the tropics. They can suffer acidity and P-fixation, and when organic carbon decreases, they become very erodible. But erosion has only a slight effect on crops. Nitosols have moderate resilience and moderate to low sensitivity.
Cambisols	They have a relatively good structure and chemical properties, thus not being greatly affected by degradation processes until these become larger. Because of increasing clay with depth, they tend not to be greatly impacted by degradation. Cambisols have high resilience to degradation, and moderate sensitivity to yield decline.
Fluvisols	Formed from unconsolidated water-borne materials. Highly variable, but much prized for intensive agriculture. Under most conditions, they have high resilience and low sensitivity. The big tropical exception concerns acid sulphate soils, which have massive chemical degradation impacts when drained for agriculture.
Leptosols	Characterised by extreme shallowness. Degradation serious with severe limitations imposed by depth and high permeability.

6) HYDROGEOLOGY

6.1 Hydrography and hydrology

The majority of the study area is found within the Rift Valley Lakes Basin (RVLB), the principal catchment of the area is the Lake Abaya Basin, where the Gelana and Gidabo rivers flow into Lake Abaya. The eastern part of the Gedeo Zone is found within the Genale catchment.

The Rift Valley Lakes Basin is a closed basin and surface water is drained by small rivers into its lakes and marshes which form the drainage for collected water. Lake Abaya is terminal, with no permanent outflow. Lake Chamo (Halcrow, 2008) has been suggested to be a groundwater outflow from the Rift Valley Lakes Basin but there is no real evidence for this, and little data to support a hypothesis either way. The Abaya – Chamo – Chew Bahir sub-basins are grouped into one because these lake complexes and river systems are spatially and temporally strongly interlinked. Significant inflow into Lake Abaya is formed by the Bilate, Gidabo and Gelana rivers, which have an estimated inflow of 650 Mm^3/year, 200 Mm^3/year and 140 Mm^3/year.

The Genale – Dawa Basin is one of the biggest basins of Ethiopia. The catchment area is 171,050 km^2, with an annual runoff of 5.8 Bm^3. The Genale River rises in the mountains east of Aleta Wendo in the Sidama Highlands, the river flows south and east to join with the Dawa River at the border with Somalia to become the Jubba River. The Sidama Highlands with their high annual rainfall are the main source of water for the Genale River, e.g. the river gauge in Girja monitoring the river flow in its upper reach has a flow of 2,350 Mm^3/year.

River flow regime

There is a large number of river gauging stations within the Rift Valley Lakes Basin and the Genale–Dawa Basin. Some of them are operational but many of the stations have no sufficient data. In the study area, there are 3 gauging stations registered. Other river gauging stations, including the lake level monitoring stations are within the neighboring areas and data from these stations were also used to calculate the assessment of surface as well as baseflow values and used for the comparison and correction of data from the study area (see Tab. 6-1).

Records from all stations reflect the fact that the river discharge is directly proportional to the intensity of rainfall within the basin. There is a high discharge fluctuation between the wet and dry seasons of the year. The first high flow period is usually from April to May, the highest flow period is from June to October and the peak flow for all rivers is usually recorded in August. The period from December to March is characterized by low flow when most of the smaller rivers are completely dry.

Measured discharge of the Bedesa River at the Dila College river gauge in the period from 1982 to 2006 is shown in Fig. 6-1. The figure shows that the flow is relatively regular; however, the total value of annual flow and particularly maximal monthly

flow can vary substantially from year to year. The highest daily discharge of 48.3 m^3/s (25^{th} of July, 1989) was recorded at the river gauge. The calculated mean annual flow of 1.9 m^3/s (see Fig. 6-2), for the station represents the flow generated mainly in the eastern escarpment and highlands.

Gauging stations with existing and reliable flow data were studied in detail and runoff data are summarized in Tab. 6-2.

Table 6-1. Basic data about river gauging stations of the study area.

Station number	River	Station	X UTM	Y UTM	Elevation [m a.s.l.]	Area [km^2]	Basin/ Sub-basin
82029	Upper Gelana	Yirga Chefe	409602	679526	1,826	285	Gelana
82044	Sala	Dila College	424474	709391	1,587	79	Gidabo
82034	Bedesa	Dila	422585	705263	1,527	149	Gidabo
82035	Gelana*	Tore	391079	642945	1,297	1,523	Gelana

Remark: * out of the study area but large catchment provides more averaged values

Table 6-2. Runoff data

River	Station	Mean flow [m^3/s]	Annual flow [mm]	Annual precip. [mm]	Area [km^2]	Specific runoff [$l/s.km^2$]	Dominant aquifer
Upper Gelana	Yirga Chefe	0.25	83.0	1,140	95	2.63	Volcanic/plat
Sala	Dila College	4.2	1,963.6	1,244	67.5	62.2	Volcanic/esc
Bedesa	Dila	1.9	740.2	1,244	81	23.5	Volcanic/esc
Gelana	Tore	4.44	92.0	1,181	1,523	2.9	Alluvium/ floor

The assessment of specific runoff is based on the data from flow measurements at the gauging stations and the appropriate area of the pertinent river basins. The specific runoff is assessed for the study area as follows:

- *8.0–16.0 $l/s.km^2$ for the eastern highlands,*
- *12.0–16.0 $l/s.km^2$ for the Rift Valley Lakes Basin escarpment areas,*
- *1.5–4.0 $l/s.km^2$ for the Rift Valley Lakes Basin, excluding the escarpment areas.*

The adopted value of specific surface flow for the study area is 8.6 $l/s.km^2$.

Lake Abaya

Lake Abaya is located to the west of the study area. Primary information on the lake is given in Tab. 6-3. Monthly measurements of lake levels are conducted at the stations in Lante and "Old gauge" stations near Arba Minch and a station at the Gidicho Odola Island

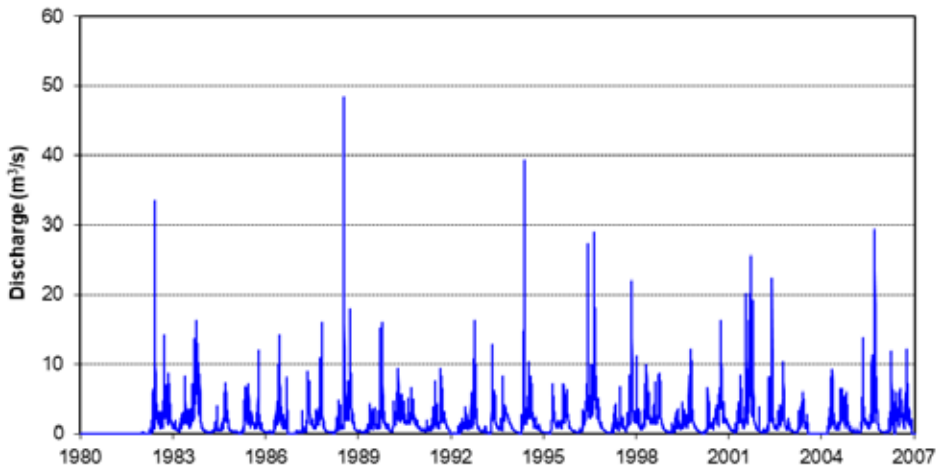

Figure 6-1. *Flow diagram of the Bedesa River at the Dila river gauge.*

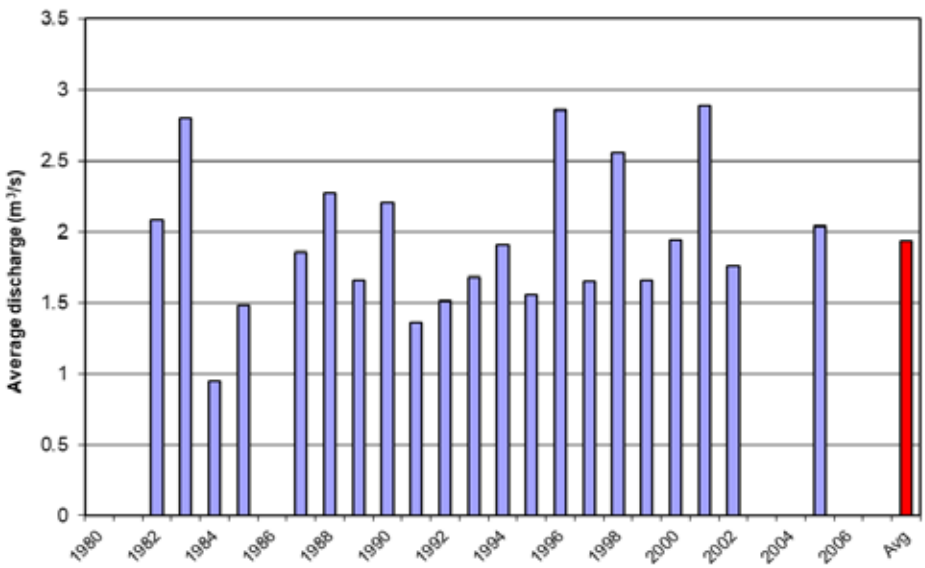

Figure 6-2. *Annual variability of the mean annual flow of the Bedesa River at the Dila river gauge.*

for Lake Abaya. The Abaya, Chamo and Chew Bahir (Ist Efanos) lakes form large basins at the southern end of the Rift Valley Lakes Basin.

Lake Abaya, together with Lake Chamo, has a basin area of 18,118 km^2. The basin consists of a relatively large sub-basin of the Bilate (5,900 km^2) to the north, and the Gidabo (3,447 km^2) and Gelana (3,463 km^2) rivers to the east. Their flow contributes significantly to the water level in Lake Abaya. Rivers flowing from the western escarpment contribute less water, but they bring a large amount of sediments into Lake Abaya. When the level of Lake Abaya is high, there is an outflow from the lake to the Kulfo River, and other rivers such as the Sile and Sego and an ephemeral stream, which flows to the south and contributes to Lake Chamo. Halcrow (2008) mentioned that water can flow from Lake Chamo to the Segen River, towards Lake Chew Bahir, when the lake level is extremely high.

Table 6-3. Basic characteristics of Lake Abaya

Elevation [m a.s.l.]	Max. depth [m]	Mean depth [m]	Surface area [km^2]	Storage volume [Mm^3]	Level fluctuation [m]	Salinity [g/l]
1,171	12	7	1,121	9,818	Lante 3.05 Old gauge 4.19	1.0

Currently, three large-scale irrigation schemes are planned by the MoWRI for rivers contributing to Lake Abaya. On the Gelana River, there are plans for a net irrigation command area of 5,356 ha. The command area currently being considered for the Gidabo River has a net area of 9,215 ha, and there are plans for a rehabilitation scheme for the existing state farms on the Lower Bilate River, providing a net command area of 7,715 ha.

Bed load to Lake Abaya is assumed to be 8% of the suspended sediment load, given an average total sediment load of approximately 27,000 tons/year, Water Works Design and Supervision Enterprise (WWDSE, 2004).

Baseflow

Baseflow represents one of the most important types of information on groundwater resources in the basin. The methods were analyzed by Bogena et al. (2005) and it was found by means of a correlation analysis that the appropriate baseflow values can be determined on the basis of daily river discharge data.

The Kille method (Kille, 1970) for calculation of baseflow was used in the study together with the separation of hydrographs where baseflow data are deduced from the discharge record of a stream by separating the baseflow component from the total discharge. The Kille method was used, even though the data series of the Upper Genale River is relatively short for this method. Data on baseflow assessed by the Kille method are listed in Tab. 6-4 together with baseflow data assessed by the hydrograph separation method.

Table 6-4. Baseflow data

River	Area [km^2]	Specific runoff [l/s.km^2]	Kille method [m^3/s]	Hydrograph separation [m^3/s]	Specific baseflow [l/s.km^2]	Aquifer
Upper Gelana	95.0	2.63	0.22	0.23	2.3/2.4	Volcanic/ floor
Sala	67.5	62.22	1.74	1.81	25.8/26.8	Volcanic/esc
Bedesa	81.0	23.46	0.60	1.15	7.4/14.2	Volcanic/esc
Gelana Tore	Tore	2.90	1.63	2.34	1.0/1.54	Alluvium/ floor

The examples of assessment of baseflow by the Kille method and by the separation of hydrograph are shown in Figs 6-3 and 6-4. A comparison of the assessment of baseflow using the Kille method and the hydrograph separation shows a small difference.

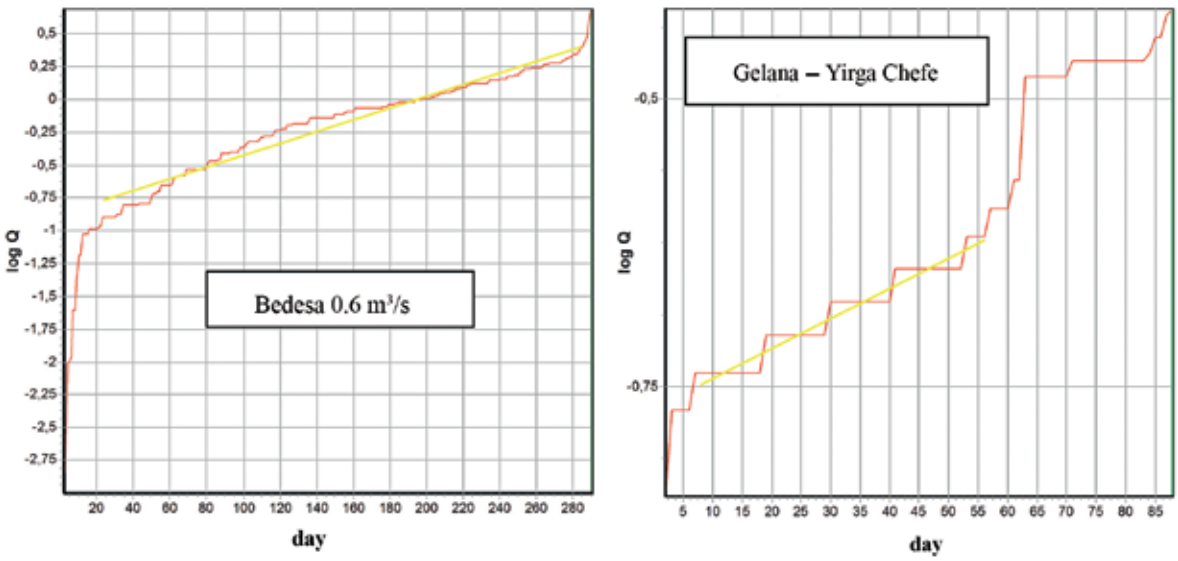

Figure 6-3. *Examples of baseflow assessment by the Kille method.*

> Figure 6-4. *Examples of baseflow assessment by the separation of hydrograph.*

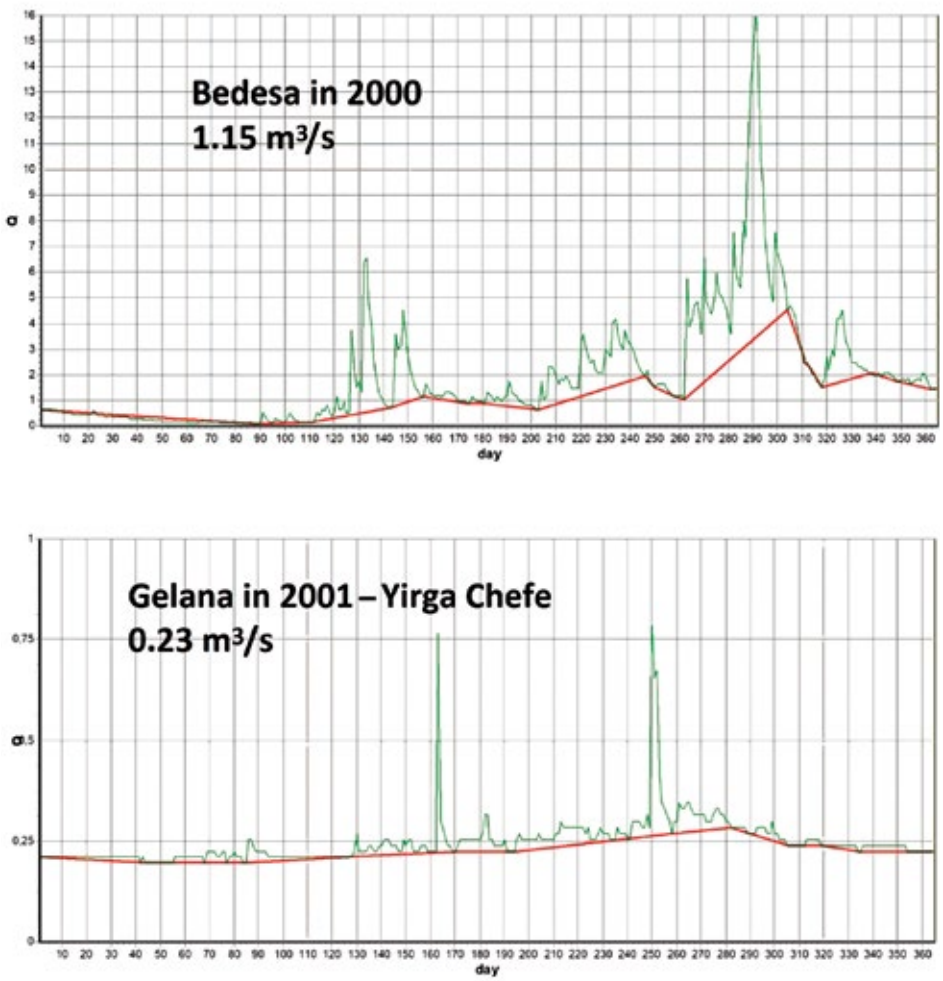

The assessment of specific baseflow is based on the data from hydrograph separation and using the Kille method. The specific baseflow is assessed for the study area based on the data from river gauges, and is shown in Tab. 6-4 below:

- *2.6–7.0 l/s.km^2 for the eastern highlands,*
- *6.0–8.0 l/s.km^2 for the Rift Valley Lakes Basin escarpment areas,*
- *1.0–2.0 l/s.km^2 for the Rift Valley Lakes Basin, excluding the escarpment areas (rift floor).*

The adopted value of specific baseflow for the study area is 3.9 l/s.km^2.

6.2 Hydrogeological conditions

Hydrogeological interpretations are based on the hydrogeological and hydrochemical map for the whole of Ethiopia at a scale of 1:250,000 (mapping completed in November 2019), and part of the project area is covered by a map at a scale of 1:50,000. The Gedeo area is a part of the hydrogeological and hydrochemical maps of Dila and Hagere Mariam at a scale of 1:250,000 and the map sheet of Dila at a scale of 1:50,000. Various archive data sets and information were supplemented by field hydrogeological and hydrochemical data collected during the field work of the project in May 2020. The methodology of the project is based on field mapping at a scale of 1:50,000.

The hydrogeological map of Ethiopia at a scale of 1:2,000,000 was published by Tesfaye (1993). He classified the geological units of Ethiopia into four major groups depending on the type of permeability and the extent of the aquifer. The latest assessment of groundwater resources in the Rift Valley Lakes Basin was done by Halcrow (2008) and by JICA (2012). The Master Plan Study by Halcrow (2008) compiled studies of both the geology and the hydrogeological conditions of the Rift Valley Lakes Basin. The Genale–Dawa Basin and its regional hydrogeological conditions were described by Lahmeyer International (2005) in the Genale–Dawa River Basin integrated resource development master plan study. Representative aquifer parameters from the existing studies are shown in Tab. 6-5.

Table 6-5. Representative parameters of aquifers of the Rift Valley Lakes Basin (partly by Halcrow, 2008 and JICA, 2012)

Formation	Transmissivity [m^2/day]	Yield [l/s]
Ignimbrite	1–1,300	0.1–8.0
Basalt	39–130	0.2–7.7
Lacustrine deposits	10–2,800	1.0–6.6
Alluvium	40–345	1.0–6.0
Rhyolite / Trachy-rhyolite	0.1–24	0.6–19.6
Pyroclastic and sedimentary rocks	0.2–84	1.5–13.25

The data set consists of an inventory of a total of 161 water points, from which 17 water samples were collected (field inventory in May 2020) and 30 referred (archival data) from previous works (see Tab. 6-6). Springs with records of both yield and temperature were evaluated. A relatively low number of dug wells is due to the fact that

priority was given to boreholes and springs, representing groundwater with longer and deeper circulation in aquifers of the study area. The static water level of open wells was measured using electrical sounding instruments wherever possible. Data assessment was mainly dedicated to the organization, processing, and interpretation of data in the form of maps and the text of the presented explanatory notes. The geographic information system (GIS) ArcGIS was used for compilation of the map. The density of water points in some parts of the study area was high and only representative points (measured and validate yield) were portrayed in the final hydrogeological map.

Table 6-6. Summary of water points used for map compilation from archive and field inventory. Remarks: + field inventory – May 2020, samples – May 2020, * a sample of Lake Abaya was taken in Arba Minch

Water point type	Archive data	Field inventory+	Sampled+	Total inventoried
Borehole (BH)	118	5	5	123
Dug well (DW)	8	2	2	10
Spring (CS, SP)	15	10	10	25
Surface water (RW)	2 (1*)	0	0	1
Total	**144**	**17**	**17**	**161**

Hydrogeological classification and characterization

Hydrogeological interpretation and standardized legend use the methodology described by ČGS–GSE (Hanžl and Verner eds, 2018) and Struckmeier and Margat (1995). Compilation of the hydrogeological map at a scale of 1:1,000,000 is based on the hydrogeological characteristics of lithological units shown in the geological map of the same scale. The main hydrogeological system is defined based on the combination of two basic types of data and information: (a) type of permeability – qualitative characteristic (e.g. porous, fissured aquifers) and (b) value of transmissivity (T= m^2/d), specific yield of wells (q = l/s.m) and yield (Q = l/s) for wells and/or springs – quantitative characteristics. The type of permeability is expressed by a specific color and quantitative characteristics are expressed by intensity of the color where a higher value has a more intensive color. This hydrogeological system and its characteristics are defined and described in the following text.

The qualitative division of lithological units is based on the hydrogeological characteristics of various rock types using the water point inventory data. The lithological units were grouped based on dominant permeability. Since quantitative data such as aquifer hydraulics, aquifer thickness and yield of wells are not adequate or evenly distributed enough to make a detailed quantitative potential classification, analogies were made to characterize the rocks which did not have the adequate number of water points. The geological description and qualitative division of various geological units together with their topographical position within the area led to a definition of elements of the hydrogeological system and its conceptual hydrogeological model. The system consists of the following elements:

- Porous aquifers developed in fluvial, alluvia, colluvial fans and lacustrine sediments and volcano-sedimentary (polygenetic) type of rocks along the rivers, lakes, at the foot of the eastern escarpment and as an infill of depressions on the rift floor.
- Fissured and mixed (porous and fissured) aquifers developed in Tertiary and Quaternary basalts, trachyte, ignimbrite and rhyolite in the highlands, escarpment and rift floor areas.
- Aquifers with shallow groundwater where groundwater accumulates in regolith derived from the underlying volcanic rocks in the highlands and on the rift floor.

Elements of the hydrogeological system of the area (aquifers/aquitards)

The hydrogeological system of the Gedeo area consists of the following elements:

1. Extensive (243 km^2) and moderately productive or locally developed and highly productive porous aquifers (T = 1.1–10 m^2/d, q = 0.011–0.1 l/s.m, with a spring and well yield of Q = 0.51–5 l/s). The aquifers consist of fluvial, alluvial colluvial, lacustrine and polygenetic sediments. The aquifers are shown in light blue.
2. Extensive (1395 km^2) and moderately productive fissured aquifers (T = 1.1–10 m^2/d, q = 0.011–0.1 l/s.m, with Q = 0.51–5 l/s). The aquifers consist of basalts, ignimbrite, trachyte and rhyolite. The aquifers are shown in light green.
3. Locally (3 km^2) developed and moderately productive mixed porous and fissured aquifers (T = 1.1–10 m^2/d, q = 0.011–0.1 l/s.m, with a spring and well yield of Q = 0.51–5 l/s). The aquifers consist of pyroclastic fall deposits with subordinate ignimbrite. The aquifers are shown in light green with light blue horizontal hatching.
4. Extensive (104 km^2) and low productive (with dug wells yielding Q = 0.25–0.6 l/s) aquifers with shallow groundwater for local use. Aquifers are developed in regolith and highly weathered volcanic rocks forming plains. The aquifers are shown on the map in diagonal yellow stripes.

Extensive and moderately productive porous aquifers

The porous aquifers make up 243 km^2 altogether, accounting for about 15% of the area (the largest outcrops of the aquifers are located in the southern part of the study area) and consist of fluvial, alluvial colluvial, lacustrine and polygenetic sediments.

Sedimentary (fluvial, alluvial and colluvial sediment with subordinate lacustrine deposits) and volcano-sedimentary rocks (polygenetic sediments resedimented pyroclastics and alluvial sediments) of Quaternary age in the study area are characterized by variable thickness and texture characteristics. The texture of sedimentary rocks ranges from clay to sand and gravel. These porous aquifers with moderate and locally high productivity are often developed in the Rift Valley Lakes Basin. River flow and high runoff from the escarpment transports material (alluvial fan deposits along the eastern escarpment) and carries sediment that is deposited in large lakes at the bottom of the rift. These aquifers are a very good source of groundwater depending on the thickness, sorting and recharge conditions. Unconsolidated sediments are mainly recharged from direct infiltration by vertically percolating rainwater but can also be horizontally recharged by bank infiltration during floods with high levels of water in river channels.

The variability of yield in wells is high, ranging from 5 to 18.8 l/s for wells. The very high yield was registered for the wells with a chance that a significant volume of groundwater is flowing into the wells from the underlying volcanic aquifers.

Extensive and moderately productive fissured aquifers

Fissured aquifers of moderate productivity make up 1,395 km^2, accounting for 85% of the area and mainly consist of basalts, ignimbrite, trachyte and rhyolite with some tuffs where they are not mapped separately. These aquifers mostly occur on the rift floor, but they also outcrop on the eastern escarpments, pediment slopes and adjacent eastern highlands. Their age, tectonic and geomorphological settings dictate their hydrogeological characteristics, but fissure flow is dominant.

Trachytic and rhyolitic are more viscous lavas, and flows are often thicker than basalts and less widespread, while located closer to the source of the volcano or extrusion. Jointing, fissures and regional faulting represent the major sources of secondary porosity. Where these flows are extensive, springs may occur, and aquifers have potentially high yields, but storage may be relatively limited because of the limited extent of flows and/or domes.

Basalts usually form less viscous, thinner lava flows and may be significantly affected by weathering, brecciation and may be interbedded with lacustrine or fluviatile deposits. Groundwater flows through joints, fractures, scoria intercalations and horizons as well as interbedded sediments. The continuity of fractures in both horizontal and vertical planes provides the aquifers with their hydraulic continuity with adjacent units and aquifers.

The yields of 85 water points (springs and wells) were measured and validated. The variability of yield is high, ranging from 0.1 to 19.6 l/s for springs and wells. The highest yield was registered for the wells drilled in ignimbrite (0.06–10.0 l/s) and basalts (6–12.5 l/s). A relatively low yield is shown by water points from trachyte (0.05–3.0 l/s). An average yield of fissured aquifers is 3.3 and median is 2 l/s (see Tab. 6-7). The frequency of yield of water points from fissured aquifers of the study area is shown in Fig. 6-5.

A relatively low median of yield values is given by a fact that there is a large number of small springs in the eastern escarpment and in the Sidama Highlands. The majority of

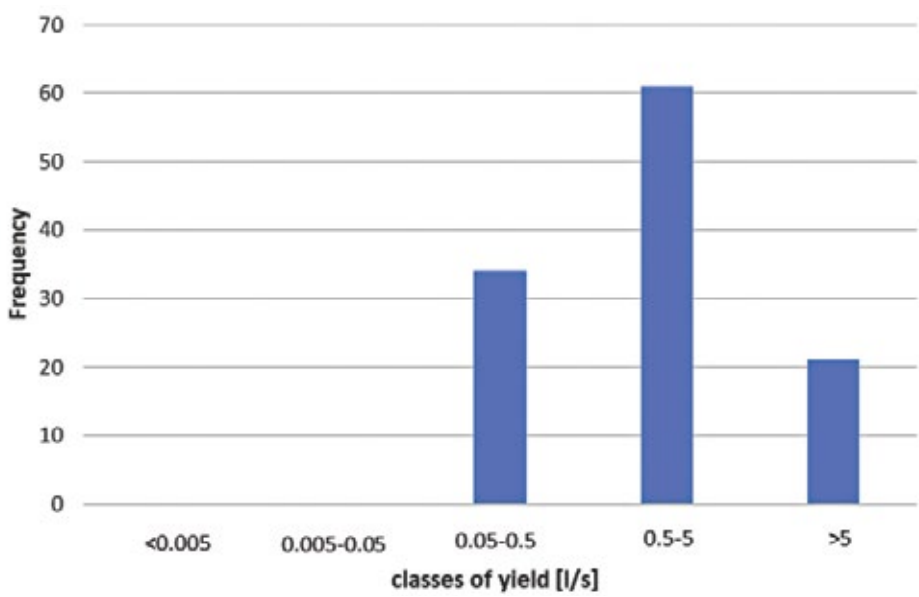

Figure 6-5. *Frequency of yield of water points from fissured aquifers of the study area.*

Table 6-7. Basic statistics of yield of water points from fissured aquifers in l/s. * water points with measured and validated yield

Number of data*	Max	Min	Median	Average
85	19.6	0.06	2	3.3

wells have a moderate yield, although some wells drilled at the foot of escarpment have a high yield because of fractured zones and concentrated groundwater flow from highlands through the escarpment area to the rift valley floor.

Extensive and low minimally productive porous aquifers developed in regolith

Extensive and low minimally productive aquifers developed in regolith covering volcanic cover 104 km^2. Regolith forms large (more than 100 ha) and small plains on the rift floor and in the eastern highlands. The yield of dug wells is 0.25–0.6 l/s and shallow groundwater levels vary from 10 to 30 m. The thickness of the saturated part of the aquifer is about 10 to 25 m when fully saturated after the rainy season. Groundwater can be reached by hand digging (common practice) and manual drilling. Casing and lining of wells is not usually required because groundwater is under water table conditions. Groundwater has an excellent quality for irrigation; however, it is not safe for drinking purposes. It can be contaminated by bacteria and human and animal waste. Dynamic shallow groundwater resources of aquifers can be assessed based on an average recharge of 80 mm and an aquifer area of 104 km^2. The porosity of the aquifers is approximately 15%. The sustainability of the shallow groundwater resources must be carefully balanced and monitored to prevent overpumping.

Locally moderately productive mixed porous and fissured aquifers

The mixed porous and fissured aquifers of moderate productivity cover only 3 km^2 of the area, but they cover large parts of the rift floor and escarpment in the other areas. The aquifers consist of pyroclastic fall deposits with subordinate ignimbrite. In general, volcanic rocks are often mixed with sediments accumulated in between lava flows and or volcanic episodes in rivers and lakes and/or relatively thick layers of unwelded tuffs, ash flows and pumiceous pyroclastic material. These intercalated porous materials do not act as independent aquifers, but they form a mixed fissured and porous multilayered aquifer together with the volcanic rocks. Porous materials can significantly contribute to the safe yield of wells when developed together with volcanic rocks. These porous materials are recharged indirectly by groundwater from the overlying volcanic rocks. Groundwater is under water table or semi-confined conditions. There is no water point in the aquifer outcrop in the study area, but it is characterized using analogy with other areas.

Hydrogeological conceptual scheme

The study area is characterized by four groundwater circulation regimes:
- In the eastern plateau
- In the eastern escarpment
- On the rift floor
- In the aquifers with shallow groundwater in regolith

In general, groundwater flow is parallel to the surface water flow system, flowing from the highlands through the escarpment to the rift floor.

Most of the springs emerging from the volcanic rocks of the plateau are topographically controlled and others emerge along structures indicating that the groundwater flow is controlled by both factors. Infiltration is particularly good in the areas where aquifers are covered by thick regolith. Aquifers outcropping in the plateau area also feed deeper fissured aquifers developed in the underlying volcanic and sedimentary rocks. Springs are relatively small in mountain areas and represent shallow local groundwater flow. The springs with greater discharge represent deep local groundwater flow and the existence of the Wora Kora hot spring in the basement of the Dodola sheet indicates the possibility for the development of deep regional groundwater flow. Springs at the foot of the escarpment are large (there are also hot springs at Yirga Alem – along the Gidabo River, located north of the study area) representing deep local/regional groundwater flow from the plateau area. Deep groundwater from the highlands flows westward to the rift valley and to the southeast to the adjacent eastern lowlands following the general dip of the whole Ogaden Basin to the east (southeast). This deep regional groundwater flow is drained by the major perennial rivers (Genale, Wabe, Bedesa and Gelana rivers) and their main tributaries. Similar situation is in the western plateau where deep regional groundwater flow in the western direction is drained by the Omo River.

The escarpment area is relatively steep for infiltration; however, in some parts there are local grabens providing a good opportunity for water to percolate underground and feed the aquifers. This area has a mainly transition hydrogeological structure between hydrogeological systems in the highlands and the rift floor. Groundwater from the escarpment area recharges aquifers on the rift floor in addition to the direct recharge from precipitation, and ultimately discharges into the main rivers of the Rift Valley Lakes Basin and through lacustrine sediments into Lake Abaya. A conceptual hydrogeological model of the eastern part of the study area is shown in Fig. 6-6.

Local ridges on the rift floor forming relative elevations between the individual sub-basins generate shallow local groundwater flow. This shallow local as well as deep groundwater flow appears in rivers as baseflow and recharges the lacustrine and alluvial sediments of lakes, which forms the regional drainage of the Rift Valley Lakes Basin. Groundwater is under water table conditions; however, artesian conditions are also known from the mixed volcanic-sedimentary aquifers of the rift floor. The existence of deep regional groundwater flow is confirmed by the existence of hot springs and hot water on the rift floor, for example the Abaya geothermal area. A conceptual hydrogeological model of the Rift Valley floor with adjacent eastern and western escarpment and plateaus is shown in Fig. 6-7.

The main principles of the general conceptual model of the study are based on the mechanisms of recharge and discharge, as follows:

- direct recharge to outcropping aquifers
- vertical recharge from overlying aquifers into underlying aquifers
- horizontal recharge from neighboring aquifers, rivers (bank infiltration) and Lake Abaya
- direct discharge by wells and springs from outcropping aquifers (springs at the foot of the escarpment, the rift floor and valleys of the eastern and western highlands)
- direct discharge to perennial rivers and Lake Abaya
- indirect discharge from one aquifer to another (vertical as well as horizontal)

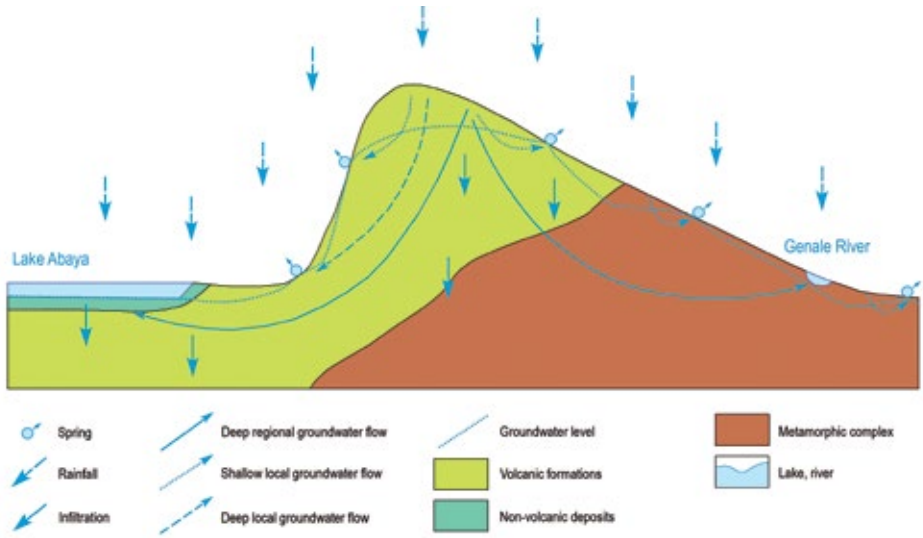

Figure 6-6. *Conceptual hydrogeological model of the eastern part of the study area.*

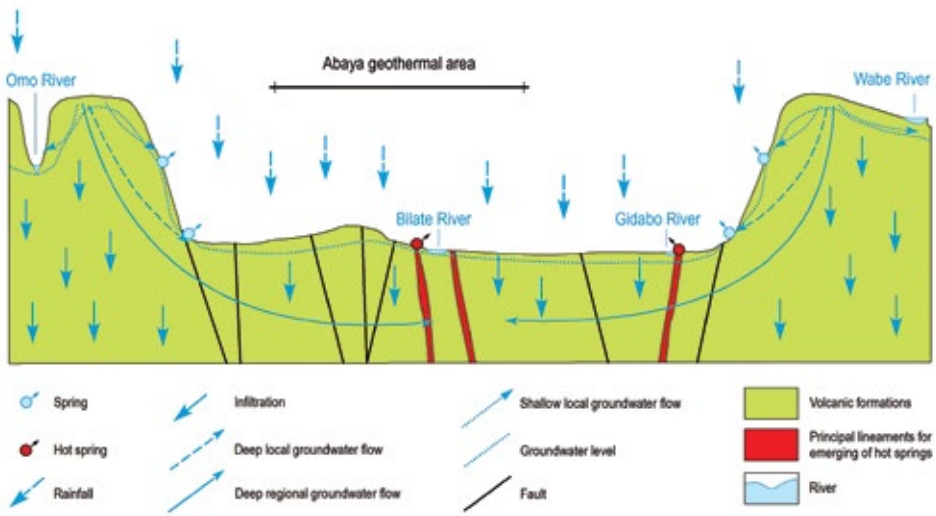

Figure 6-7. *Conceptual hydrogeological model of the rift floor.*

Recharge

There is a large amount of information from different reports about the assessment of recharge; however, the data vary significantly. The regional mechanism of recharge of aquifers in the area has been described above. As is the case in other areas, a substantial part the groundwater is recharged directly from precipitation depending on its intensity and annual distribution, the topographical gradient of the area as well as the lithological composition (particularly in the vertical profile) of outcropping rocks and their tectonic disturbance. The recharge area of outcrops of lithological units was considered only if the slope of the terrain is less than 20%. A less significant amount of bank recharge to aquifers is from the permanent as well as intermittent streams and Lake Abaya after rains when surface water levels are above the groundwater level in the surrounding aquifers. This type of recharge is important on the rift floor where evapotranspiration is much higher, and precipitation is lower than in the highlands.

Recharge assessment was performed based on rainfall infiltration (recharge from rainfall) according to the rainfall infiltration factor (RIF) defined by WWDST (2003) and shown in Tab. 6-8.

Table 6-8. Rainfall infiltration factor for the Wabe Shebelle Basin

Lithostratigraphical unit	Rainfall infiltration factor [%]
Alluvium	6
Basement rocks	5
Basaltic rocks	6
Sandstone and siltstone	5
Limestone	6
Gypsum beds	3
Shale/siltstone	2

Tesfaye (1993) characterized recharge as being between 150 and 250 mm in the highlands and between 50 and 150 mm in the rift basin. Zenaw and Tadesse (2003) assessed recharge for the Hawassa Basin as being approximately 5% of the rainfall (67 Mm^3/year). WABCO (1990) in Water Resources Development Master Plan for Ethiopia refers to 5% recharge to the aquifers in the Rift Valley Lakes Basin, representing approximately 57 mm of the annual recharge.

When applying an adopted average baseflow value for the rivers in the highlands and the rift floor, the recharge is about 200 mm and 50 mm, respectively. Compared to the adopted depth of precipitation of 1,200 mm, the calculated average infiltration (recharge) in the study area can be assessed as being 10% of the precipitation depth (i.e. 120 mm).

Thermal groundwater

Ethiopia is rich in thermal and mineral water resources and interest in their development has recently increased. A systematic investigation of geothermal resources started in 1969. The first integrated project was carried out by the United Nations Development Programme (UNDP) in 1969 and its results were presented in 1971 in the comprehensive report entitled "Investigation of Geothermal Resources for Power Development, Geology, Geochemistry and Hydrology of Hot Springs of the Eastern African Rift System in Ethiopia" (UN-UNDP, 1971).

Of the approximately 120 localities within the rift system that are believed to have independent circulation systems, about two dozen are judged to have potential for high enthalpy resource development, including generation of electricity. There is the Lake Abaya high enthalpy geothermal area, which is located west of the border of the study area and the Yirga Alem hot springs – along the Gidabo River, located north of the study area.

6.3 Hydrochemistry

One of the important tasks was to study the surface water and groundwater chemistry and to assess the groundwater quality for its use within the mapped area. Therefore, a study of the groundwater quality was carried out on the different aquifers (geological formations)

of the area as well as various parts of the water circulation system (rainwater, surface water, and groundwater). The results of the hydrochemical study can help to understand the groundwater circulation within the aquifers in addition to comparing the water quality with various standards.

An assessment done by Tesfaye (1993), which is shown in the hydrogeological map, identified the cold groundwater with total dissolved solids (TDS) below 1,000 mg/l and hot water with total dissolved solids above 1,000 mg/l in the Rift Valley. The groundwater chemistry is characterized as being dominantly sodium-bicarbonate for hot water; however, some cold water is of the calcium-bicarbonate type. Part of the groundwater in the Rift Valley has a high fluoride content. The chemistry of the groundwater in the eastern highlands was characterized as calcium-bicarbonate water with total dissolved solids below 1000 mg/l in the study area.

Hydrochemical characterization prepared by Tesfaye (1982), Zenaw et al. (2003), Halcrow (2008), JICA (2012), and other authors provides similar results to the previous characterization. Detailed characterization of thermal groundwater was performed in the UN-UNDP study (1971).

Archival data, sampling and analysis

There are large sets of analyses from previous reports and mapping projects. In addition to the existing archival data (29 analyses), a total of 17 water samples were collected from boreholes (5), dug wells (2) and springs (10) during a field season in May 2020. Samples were analyzed in the laboratory of the Ethiopian Construction Design and Supervision Works Corporation. The chemistry of the water obtained from the samples is shown in Tab. 6.10. Chemical analysis of the major constituents (Mg, Ca, Na, HCO_3, SO_4, Cl) and secondary constituents (K, NO_3, F, Fe, Mn, CO_2, SiO_2), and measurements of electrical conductivity (EC) and pH at room temperature were performed in the laboratory. Field measurements of pH, temperature and electrical conductivity were made at the time of sampling. Reliability of the new analyses was assessed using the cation-anion balance and showed that none of the samples exceeded the minimum reliability level of 10%. The analytical results were presented graphically on a hydrochemical scheme to facilitate visualization of the water type and their relationships. Suitability of groundwater for drinking, industrial and agricultural purposes is assessed based on the pertinent quality standards.

Classification of natural waters

Classification of natural water was used to express the groundwater chemistry on the hydrochemical scheme in the hydrogeological map. Hydrochemical types are classified based on the Meq% representation of the main cations and anions by implementing the following scheme:

- Basic hydrochemical type, where the content of the main cation and anion is higher than 50 Meq%. This chemical type is expressed on the hydrochemical scheme by a solid color.
- Transitional hydrochemical type, where the content of the main cation and anion lies between 35 and 50 Meq%, or exceeds 50% for one ion only. A dominant ion combination is expressed on the hydrogeological scheme by the relevant colored horizontal hatching.
- Mixed hydrochemical type, where the content of cations and anions is not above

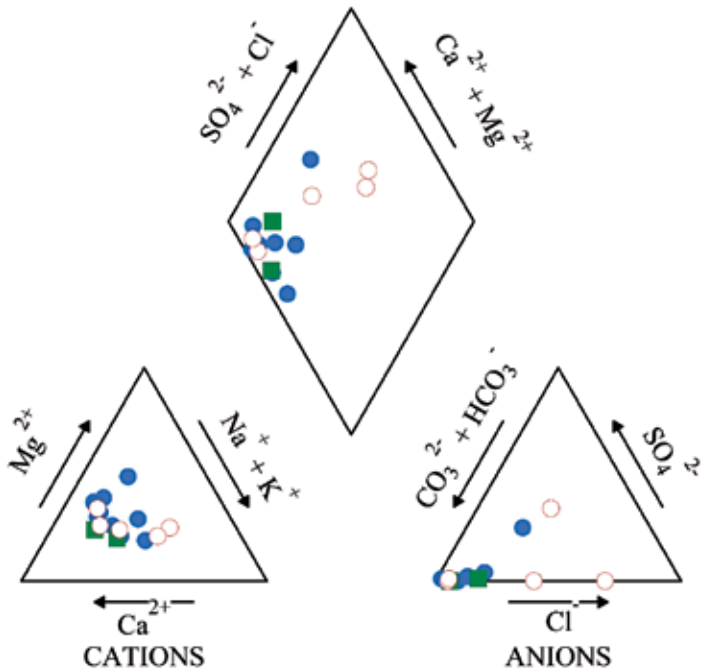

Figure 6-8. *Piper diagram for the classification of natural water (drilled wells – red circles, dug wells – green squares, springs – blue circles).*

50 Meq% and only one ion has a concentration over 35 Meq%. This type is expressed on the hydrogeological scheme by the relevant colored vertical hatching.

The results of new samples assessed in the form of water types are in agreement with previous regional hydrochemical maps at a scale of 1:250,000. The dominant hydrochemical type of groundwater in the study area is calcium bicarbonate.

To facilitate the visualization of the classification of water types, the percentage of the major cations and anions of the newly analyzed samples is plotted on the Piper diagram as shown in Fig. 6-8.

Groundwater residence time along flow paths, time length of water-rock interaction, lithology, ionic exchange, and evaporation may play a significant role in the groundwater composition. Major changes in the chemical composition of groundwater firstly occur in the soil zone during the concentration of salts by evaporation and evapotranspiration. The second most important correlation of water chemistry is the contact of water with hot rocks, including groundwater enrichment by carbon dioxide. This mechanism is believed to form the sodium bicarbonate groundwater chemistry in the northwestern part of the study area and the rest of the rift valley bottom. The third most important interaction is leaching of fluoride from acid volcanic rocks (rhyolitic pumice), mainly from their vitric component.

The low total dissolved solids (100 to 800 mg/l) and dominant calcium-bicarbonate type of groundwater indicate the hydrogeological regime with fast groundwater circulation within the area receiving a relatively high volume of rainfall where groundwater flows through fractured volcanic rocks of the study area.

The gradual development in total dissolved solids in the highlands and escarpment areas changes when the groundwater flow reaches the rift valley floor. Total dissolved solids increase rapidly together with a change of groundwater type from the calcium-bicarbonate into sodium-bicarbonate.

Chemistry of natural waters

Hydrochemistry of rainwater in the area is not known in detail; however, the chemical composition of a sample taken from the town of Dila is shown in Tab. 6-9. A difference in the ion (cation and anion) balance of 10% shows that the reliability of the analysis is relatively good for water with a very low content of dissolved solids. The water chemistry can be classified as a transient Ca-SO_4 type.

Table 6-9. Chemical composition of rainwater [mg/l]

HCO_3	Cl	SO_4	F	NO_3	Na	K	Ca	Mg	SiO_2	pH	TDS
4.0	0.21	6.1	0.05	0.05	0.3	1.9	1.6	0.3	0.1	5.16	15.0

A surface water sample from the Bedesa River is of the sodium-bicarbonate type with TDS of ca 520 mg/l. The sample from Lake Abaya represents the chemistry of the main rift valley lakes. The composition of lake water in rift valley lakes and total dissolved solids varies based on the character of the lake and the main source of water in the lake. Water chemistry of Lake Abaya is of the basic sodium-bicarbonate type, TDS value is approximately 840 mg/l. A relatively low TDS value in the lake shows a substantial inflow of surface water as well as groundwater with low TDS from the eastern and western escarpments.

Groundwater chemistry in the study area reflects the geological character of aquifers as well as the morphological position of aquifers. The type of groundwater depends on the morphological position of the aquifer on the plateau, escarpment and/or rift floor.

Groundwater in Dila and the adjacent rift valley floor is characterized by the basic sodium-bicarbonate type with TDS from 200 to 600 mg/l (the trend in TDS is increasing westwards). The area south of Dila (between Wenago and Yirga Chefe) and the area on the southeastern margin of the Gedeo Zone is characterized by the basic calcium-bicarbonate type with a TDS value of 200 mg/l. The central part of the Gedeo Zone is characterized by the transitional calcium-bicarbonate type with a TDS value of ca 200 mg/l. The low TDS and dominant calcium-bicarbonate type of groundwater indicate the hydrogeological regime with fast groundwater circulation in the area receiving a relatively high volume of precipitation where groundwater flows in fractured volcanic rocks of the plateau.

Water quality

The water quality in the mapped area was assessed from the point of view of drinking, agriculture and industrial use.

Domestic use

To assess the suitability of water for drinking purposes, the results of the new chemical analyses were compared with the Ethiopian standards for drinking water (see Tab. 6-10) published in the Negarit Gazeta No. 12/1990 and Drinking water – Specification Code of Ethiopian Standard (CES) 58, (ICS: 13.060.20, Published by Ethiopian Standards Agency, © ESA, 2013)

Table 6-10. Groundwater chemistry of new samples compared to drinking water standards and specifications. Remark: ND – not defined

Substance or characteristic	Range (min–max) [mg/l]	Ethiopian standards (1) and ESA CES 58 (2) [mg/l]		Number of exceeding values	
		Highest desirable level	Maximum permissible level	Highest desirable level	Maximum permissible level
Na (2)	0.3–206	ND	200	ND	1
K (2)	0.5–14.5	ND	1.5		33
Ca (1)	1.6–78	75	200	1	0
Ca (2)	1.6–78	ND	75	ND	1
Cl (1)	0.14–102	200	600	0	0
Cl (2)	0.14–102	ND	250	ND	0
HBO_2	0.03–2.15	ND	0.3	ND	5
Fe (1)	0.04–1.22	0.1	1	8	1
Fe (2)	0.04–1.22	ND	0.3	ND	3
Mg (1)	0.3–25	50	150	0	0
Mn (1)	T–0.16	0.05	0.5	1	0
Mn (2)	T–0.16	ND	0.5	ND	0
SO_4 (1)	0.05–86	200	400	0	0
SO_4 (2)	0.05–86	ND	250	ND	0
TDS (1)	15–824	500	1,500	2	0
TDS (2)	15–824	ND	1,000	ND	0
pH (1)	5.5–8.3	7.0–8.5	6.5–9.2	28	16
pH (2)	5.5–8.3	ND	6.5–8.5	ND	16
Total alkalinity $CaCO_3$	6–371	ND	200	ND	5
NO_3 (1)	0.03–133	10	45	11	9
NO_3 (2)	0.03–133	ND	50	ND	5
NO_2 (2)	0.01–4.13	ND	3	ND	1
F (1)	0.4–1.14	1	1.5	1	0
F (2)	0.4–1.14	ND	1.5	ND	0

Groundwater of the mapped area is suitable for drinking; however, in one water point the concentration of fluoride exceeds the drinking water standards and, in several water points, the concentrations exceed standard values for nitrate. This situation shows pollution by human and animal waste and reflects a lack of sanitation.

The content of nitrates is not related to the rock composition (type) but high concentrations of nitrates as well as elevated concentrations of chlorides due to the direct pollution by human and most probably also animal waste (urine), reflecting a lack of sanitation. The background content of nitrates in the groundwater is about 5 to 10 mg/l,

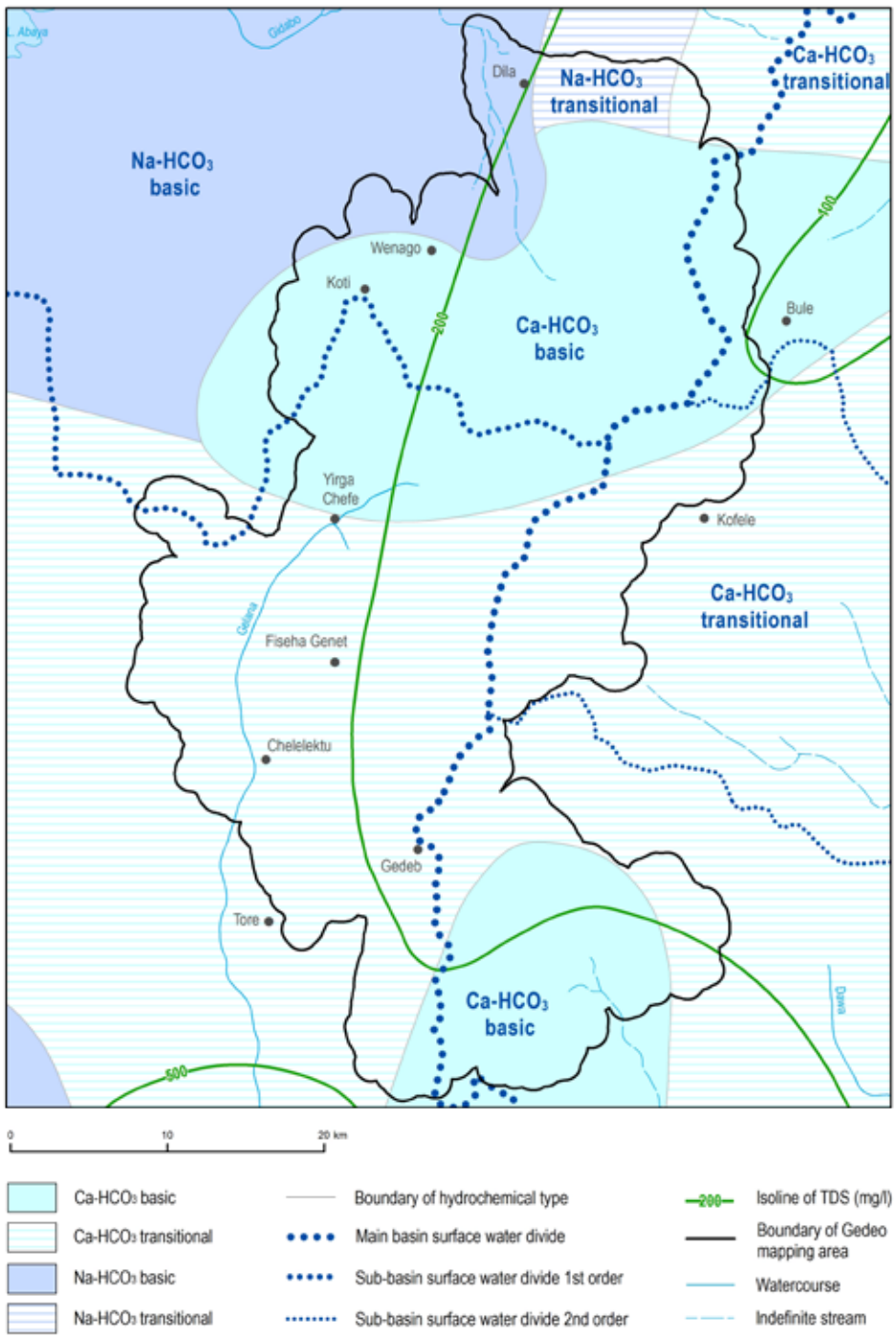

Figure 6-9.
Hydrochemical scheme of the Gedeo Zone.

depending on the relevant land cover. In forest areas, it can be even higher because of the decomposition of various plants and other organic material. In some circumstances, nitrates have been shown to present a health hazard to infants, and possibly older children, if they are present in drinking water at concentrations greater than 50 mg/l (expressed as NO_3) because after reduction of nitrate to nitrite they may give rise to methemoglobinemia.

Recently, concern has been expressed over the possibility of nitrosamine pollution in vivo. Nitrosamines may arise as the product of the reaction between ingested nitrates, some of which may also be formed by the action of gut bacteria on ingested nitrates from various sources including water. Because of their carcinogenic potential, nitrosamines are a possible human health hazard. From a toxicological point of view, the considerations applicable to nitrates also apply to any nitrites present in drinking water.

Out of 46 samples, 11 (24%) exceed 10 mg/l of NO_3 and 5 (11%) samples exceed 50 mg/l of NO_3. The highest concentration of NO_3 is 133 mg/l. An alarming fact is that the percentage of values of nitrates exceeding 50 mg/l in new samples taken in May 2020 (24%) is an order of magnitude higher than in 2013/14 (3%).

Nitrate pollution is an important factor particularly in vulnerable groundwater resources (shallow aquifers). This fact must also be considered when planning the future development and protection of groundwater resources in the area. Proper location of water points and suitable protective measures should be applied to boreholes, springs and wells dug for human water supply.

The majority of the water samples from the study area were found to be suitable for irrigation since the sodium adsorption ratio value lies within the water quality class of excellent and/or good for agricultural purposes. Water from the Bilate, Gelana and Gidabo rivers is widely used for irrigation.

Groundwater from the mapped area (Fig. 6-9) can be used for industry in general, but some specific techniques require water treatment before the water is used in the process (particularly pH adjustment for brewing). There is a threat of incrustation or corrosion when such groundwater is used in pipes for public water supply or for delivery of water for industry or agriculture in some areas.

6.4 Water resources

Water resources of the area depend mainly on rainfall and other climatic characteristics as well as the hydrological, geological and topographical settings of the study area. As part of an integrated water resource and development program, the use of surface water and groundwater must be looked at with keen interest in order to address the acute problems of adequate and safe water supply in the study area. The ultimate source of potable water is rain. There are many meteorological stations operated by the Meteorological Institute in the mapped area. Selected meteostations with long-term measurements were used to assess precipitation depth. The long-term mean annual rainfall in the area has been assessed to be approximately at 1,200 mm/year. The study area (including buffer zone) was calculated from a 1:100,000 hydrogeological map and its area of 1,642 km^2 is used for further calculation. The areas of active aquifers with the ability to store and transmit water were calculated based on the hydrogeological map. The active aquifers (see Tab. 6-11) with porous and fissured permeability cover an area of 1,642 km^2.

The hydrological characteristics vary widely because of the variability in climatic conditions and hydrogeological and hydrological (catchment area) characteristics between different monitoring points. For further calculations of water resources, the amount of rainfall at 1,200 mm, the value of specific surface runoff of 8.6 l/s.km^2 and specific baseflow of 3.9 l/s.km^2 are assumed for the study area. The assessed water resources of the study area are shown in Tab. 6-12. Dynamic shallow groundwater resources of aquifers in regolith can be assessed based on an average recharge of 80 mm and an aquifer

Table 6-11. Aquifers of the area

Aquifers	Area [km^2]
Porous aquifers (alluvial)	243
Fissured and mixed aquifers in volcanic rocks (deeper aquifers)	1,395
Total of the area	1,642
Porous aquifers with shallow groundwater (regolith)	104

area of 104 km^2. Porosity of the porous and fissured aquifers is approximately 5 and 15%, respectively, and the average saturated thickness is approximately 100 and 30 m, respectively.

Water resources in the area are huge; however, future utilization of water resources within the closed basin of the Rift Valley depends on changes in the climate, human demands for water, and water resource management practices. The hydrogeological system of the rift has been in equilibrium between inflow and outflow – evaporation from lakes.

Table 6-12. Assessment of water resources in the study area

	Input	Area [km^2]	Resources total [Mm^3]	Remark
Rainfall	1,200 mm	1,642	1,970	
Total water resources – map	8.6 l/s/km^2	1,642	446	23% of rainfall
Renewable groundwater resources of deeper active aquifers	3.9 l/s/km^2	1,642	202	10% rainfall
Static groundwater resources of fissured and mixed aquifers	5% porosity and 100 m of saturated thickness	1,395	6,957	Not proved
Static groundwater resources porous aquifers	15% porosity and 30 m of saturated thickness	243	1,094	Not proved
Renewable groundwater resources of porous aquifers with shallow groundwater	80 mm	104	8	

The development of new irrigation schemes and the use of more surface water as well as groundwater will cause a significant decline in the level of Lake Abaya as well as the vanishing of marshy areas in the center of the Rift Valley. The open system of the eastern plateau is more flexible for water development.

Surface water resources development

Based on data of the total runoff from the area, there are good water resources to be used for irrigation as well as for the drinking water supply of people living within the area. The total water resources of the area have been assessed to be 446 Mm^3/year.

The surface water of the area should be primarily used for irrigation. The irrigation plans and an assessment of potential and environmental impacts are discussed in detail by Halcrow (2008) for the Rift Valley Lakes Basin, by WWDST (2003) in the "Gelana and Gidabo Irrigation Project" and by various other specific studies.

Groundwater resources development

The river gauge measurements show that approximately 10% of precipitation infiltrates and appears as baseflow. There are good groundwater resources to be used for the supply of drinking water to people living within the area. The total volume of renewable groundwater resources of active of deeper aquifers in the area has been assessed to be 202 Mm^3/year. From an agricultural point of view, very important are the porous aquifers developed in regolith with a high water table, which have groundwater resources of 8 Mm^3. This represents a good irrigation potential, particularly for household irrigation from shallow groundwater resources developed in the regolith.

Most of the people within the area live in small towns and villages, which are supplied mainly by springs, and drilled and dug wells. Halcrow (2008) estimates that groundwater makes up 92% of the water supply. In addition to further development of springs and dug wells, water supply based on drilled wells represents the most sanitary secure water and should be used for small towns as well as for rural inhabitants. The strategy chosen in siting the hydrogeological wells for the public water supply follows three basic principles:

- Basalts, trachyte and ignimbrites contain groundwater, the quality of which mostly corresponds to the standards for potable water.
- Avoid drilling of shallow wells in areas covered by acid volcanic rocks (white rhyolitic pumice fall), where high contents of fluoride can be found.
- The yields of the wells, which penetrate volcanic rocks and thick sediments, usually fluctuate between 2 and 10 l/s, and they are sufficient for the supply of as many as 8,000 to 40,000 inhabitants, the consumption per person being 20 l/day.

Some of the existing water points do not represent a safe water supply as they show an increasing content of nitrates in shallow water supply systems. Deeper wells currently represent a safe type of water supply; however, they must be protected against pollution from the local pollution sources like human and animal waste (sources of pathogens and nitrates) as well as from potential industrial activities (wastewater from tanneries, textile industry, flower plantations, etc.). A minimum required distance of water supply wells and potential pollution sources should be maintained in the plans for groundwater resource development in towns and villages. The same level of interest should also be applied to the development and protection of groundwater resources for rural communities. Safe water supplies, with appropriate safety measures taken into account, should be set up in relatively concentrated communities where the feasibility and impact of developed schemes will be most significant.

Development and protection of water resources in the area and the environment as a whole are most important in the development of infrastructure with the aim of eradicating poverty (development of irrigated agriculture, provision for livestock during drought). Access to safe drinking water improves the health of the population (statistics show that 40% of child death rates are related to water-borne diseases). Approximately 15% of the rural population has access to safe drinking water. This is a serious problem for the creation of strong farming and pastoral as well as industrial communities capable of full-time engagement in working activity. Therefore, it is important to provide safe

drinking water to communities. Protection of the environment, particularly prevention of soil erosion and degradation causing food and water scarcity, is an important development aspect within the area. This aspect is based on the importance of water retention in the landscape, which is of primary importance regarding the increase in population, bringing with it an increased demand on soil use.

Despite some local and regional environmental problems, the study area has the potential for feasible and environmentally sound natural and human resource management.

6.5 Recommendations

The Gedeo area receives an average of 1,200 mm of rainfall which is a relatively good volume for direct infiltration into aquifers. The majority of the area is composed of fissured aquifers that occur in various volcanic rocks that provide a large volume of groundwater resource. A small area is covered by alluvial sediments forming porous aquifers. Relatively large shallow groundwater resources also accumulate in regolith and can be used particularly for household irrigation.

Groundwater is of good quality for drinking water; however, pollution by nitrates has been found in several water points, showing a lack of protection from human and animal waste.

It is recommended to develop groundwater in deeper fissured aquifers by drilled wells and use them particularly for drinking purposes. Shallow groundwater in regolith can be developed by cheap dug wells. All water points (deep and shallow) used for drinking purposes must be appropriately protected against pollution from industrial, human, and animal waste.

7) GEOLOGICAL HAZARDS

The geomorphological nature of the area, with its large differences in altitude, the high degree of weathering of the rocks, active tectonism, the presence of torrential rainfall together with significant deforestation creates conditions in which there is a frequent occurrence of geological processes such as erosion and land degradation, landslides, and floods. In turn, these have a negative effect on infrastructure, settlements, agriculture and food security and sometimes directly threaten human lives.

6.1 Geological hazards description

The analysis of geological hazards was carried out from a synthesis and interpretation of acquired geological, geomorphological, and remote-sensing data, while also being based on the field surveys focused on geological and geomorphological phenomena such as geomorphological features (landform origin, slope deformation, impact of head-ward erosion) as well as the geological setting (lithology, degree and character of weathering, hydrogeological properties of rocks, structural setting), land use and human interventions in the landscape. The most important and frequent geodynamical processes identified in the mapped area (Fig. 7-1) are slope processes and mass movement, surface erosion, land degradation and flooding (Figs 7-2 to 7-7). The areas prone to respective geohazards are shown in Fig. 7-1.

Slope processes and mass-movement processes include creep, landslides, earthflows, toppling, and rock-falls. The sites prone to slope processes are on the fault scarps and erosional relief between the eastern highland plateau and the rift floor in the west of the mapped area.

Falls and toppling are abrupt movements of material such as rocks and boulders that become detached from steep slopes or cliffs. Their separation occurs along discontinuities. Falls are strongly influenced by mechanical weathering and by the presence of interstitial water. The occurrence of toppling and rockfall areas is associated with outcrops of competent volcanic rocks such as basalts, trachytes and welded ignimbrites with a high density of columnar and tectonic jointing and mechanical weathering in the steep fault scarps, at the tops of fossil landslides or on the vertical slopes of the erosional canyons. Several minor rockfall collapses were observed at roadcuts, particularly in the places where joints and fractures in competent rocks were more abundant.

Landslides are one of the most common hazardous geological phenomena in the Gedeo Zone, currently threatening homes and infrastructure (Fig. 7-1). The fossil landslides are concentrated on fault scarps and erosional slopes east of Dila in the northern part of the region and around Werka Chelbesa in the southeast of the zone. These landslides represent a deep-seated complex of fossil slope deformations on a scale of tens of meters to kilometers, where competent high strength rocks with permeable fissures overlie a more weathered succession. The accumulation areas of landslides are often affected and modelled by subsequent processes like erosion and denudation, but

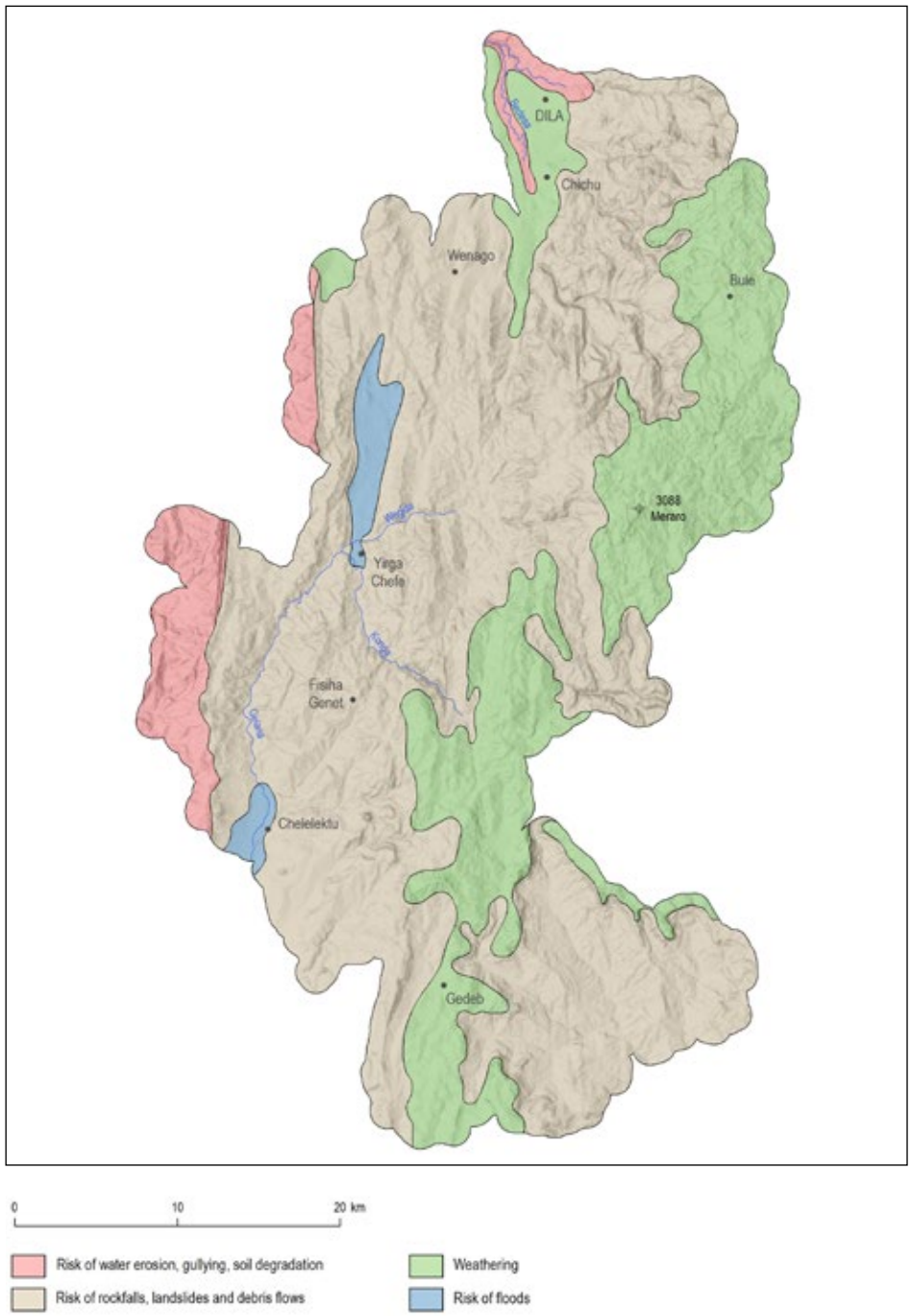

Figure 7-1. *Schematic map of areas prone to geological hazards.*

they can be distinguished by careful observations in the field, for example by partially undrained depressions with wetlands, tilted blocks, and hummocky surfaces with large colluvial accumulations. These slope failures appear to be currently more or less stable; their reactivation may occur during infrastructure installation, such as road construction and housing developments.

Many active shallow landslides on the scale of tens to a few hundred meters have been identified in the area. These slumps, rotational or transitional landslides and flows were created mainly in highly weathered rocks and residual sandy and clayey soils. Most are triggered by heavy rainfall. Tens of landslides were documented along the main road between Yirga Chefe and Gedeb where the slopes are made up of a highly weathered basalt. The inappropriately designed steep road cuts in the weak rocks do not respect the reduced stability and lead to a series of failures that threaten the road itself and the adjacent houses and farmland. An inadequate or unmaintained drainage system also often contributes to slope instability.

Surface water erosion is a result of intensive runoff in the areas with poor vegetation (see Fig. 7-3). Active tectonism causes the stream gradient to become out of equilibrium, while high gradient relief, strongly weathered volcanic or volcaniclastic rocks, climatic characteristics with torrential rains and intensive deforestation are the main factors controlling intensive surface runoff. Inappropriate land use with extensive deforestation and reduced infiltration lead to the concentration of surface runoff and formation of large zones with soil degradation, creation of erosion rills and gullies. Badland landscape is developing locally, with up to 10-meter-deep gullies. The most affected area is in the western margin of the region, where vegetation cover is significantly reduced and the area is completely deforested.

Floods are associated with alluvial processes that occur in the river channels, flood plains, and alluvial fans. The landforms mentioned above are for the most part subjected to flooding during heavy rainfall and high discharge. Although there are no major river systems within the Gedeo Zone, only emphemeral streams or minor alluvial systems, floods and associated hazardous events are among the most common geological hazards. Floods are usually accompanied by intense lateral erosion of the banks of braided or meandering channels. Clastic material transported by braided streams can be accumulated in the form of lateral and in-channel gravel bars and this leads to a decrease in channel capacity. A reduction in channel capacity often amplifies the negative impact of floods, leading to a higher water column rise and an increase in erosive capacity of the stream. Emphemeral streams in erosion valleys are often subject to flash floods with very rapid increases in discharge. These streams often transport large quantities of clastic material in the form of earth and debris flows from other parts of the catchment area. Accumulation of sediment is usually connected with floods as well as with mass movement processes. It occurs in the areas where the topographic gradient decreases and the transport medium is reduced. The most vulnerable areas are the surfaces of alluvial cones and the mouths of gullies as well as erosional valleys, where thick accumulations of a few meters can be deposited during a single event.

6.2 Prevention and mitigation

Prevention and mitigation strategies are vital for maintaining an emergency preparedness and response plan based on the vulnerability of the area. This will ensure that the population is safeguarded from the main hazards. Prevention of the negative impacts of geological hazards should take place at two levels.

1) Long-term strategy using studies to predict the areas that are vulnerable and mitigate the impact of natural hazards on humans.

Figure 7-2. *Shallow landslide in the roadcut formed by completely weathered basalts.*

Figure 7-3. *Area affected by surface erosion and soil degradation with poor vegetation, W of Wenago.*

2) Addressing and solving current problems, including proposing remedial and security measures to reduce damage caused by existing hazardous natural processes.

The geological hazards are a result of geodynamic processes that have taken place throughout the history of the Earth, so the application of measures to prevent or mitigate geological dangers should take this into consideration. Human intervention in natural systems or an inappropriate mitigation strategy could amplify the negative impacts of the geodynamic processes mapped in the Gedeo Zone. Inappropriate land use and deforestation increase water erosion and threaten farmland and infrastructure which is not designed for intensive surface runoff. The bridges and culverts are constructed with an insufficient flow capacity which leads to an increased impact by flood events and destruction of infrastructure. Moreover, landslides (Figs 7-4 and 7-5) such as those along the main road between Yirga Chefe and Gedeb, are often addressed by inappropriate means, such as by removing the landslide accumulation from the base of the slope, thereby removing support and increasing slope instability. Also, landslides are sometimes stabilized with gabion baskets (Fig. 7-6), which are inappropriate given the size of the landslides and the potential volume of material that could move. The gabions are tilted by the movement of the slope and subsequently collapse.

Long-term preventive and rehabilitation measures that aim to address some aspects of the common problems caused by surface processes, and potential remedial measures, are discussed in the following text. The infrastructure is commonly affected by a range of dangerous superficial processes mentioned briefly above. Obviously, there is a considerable movement of material. Construction design often does not respect local geological and geomorphological conditions. The roadcuts have been created regardless of geological structure at the site and regardless of short-term and long-term issues. Rock faces and shallow landslides might appear stable but could be reactivated during the rainy season. The recommendation is to drain the unstable area to enhance slope stabilization and to build a retaining wall along that stretch of the road. The retaining wall would need to be adequately designed.

Reforestation is necessary to decrease the negative impact of erosion (Fig. 7-7). Planting of trees and diversified agriculture production could help slow down erosional rates. To decelerate the runoff of water and sediment load, it is recommended to plant

Figure 7-4. *Tension crack of active landslide close to main road between Yirga Chefe and Gedeb.*

Figure 7-5. *Building destroyed by an active landslide, Widesa.*

rows of trees as well as to construct small dams and polders in the drainage system. Trees and deep-rooted bushes should also be planted around the boundary of plots of land to prevent soil erosion. Alluvial erosion threatens farmland as well as infrastructure that is not designed for intensive surface runoff. The bridges and culverts are constructed with an insufficient flow capacity which leads to an increased impact of flood events and destruction of the infrastructure.

Preventive and mitigation measures for rehabilitation of natural disasters

- Dangers that strongly affect infrastructure development and land use in the Gedeo Zone are represented mainly by exogenous processes associated with high precipitation during the rainy season.
- The main prerequisite for eliminating the negative impacts of natural hazards is to incorporate the natural processes that cause the danger. It is important to note that intervention in any natural system will induce a response, often with adverse effects. Prior to each technical intervention concerning the development of the area, it is therefore important to carry out a study of possible impacts on both the planned project and the further decentralization of the concerned natural system.
- All structures closely associated with fluvial channels (buildings, bridges, culverts) must be designed to resist 100% of the maximum discharges. Simple reduction of flow capacity with regard to its natural rate is only a short-term solution of the problem. Line constructions (roads, power lines, etc.), culverts and bridges should respect the topography of the area so that they will not create a barrier to the natural runoff during high discharge and rainy seasons.
- It is necessary to permanently maintain the same stream channel capacity by cleaning and removing the deposited material, particularly in the vicinity of bridges or other constructions, where the reduction of channel capacity may cause damage or even lead to the destruction of the whole structure.
- Reforestation is the best option for a natural way to tackle the issue in areas susceptible to erosion. Planting rows of trees, construction of small dams and polders in the drainage pattern and gullies are recommended to decelerate the runoff and to reduce the transport of sediment.

Figure 7-6. *Tilted gabions in an active landslide in the main road, south of Yirga Chefe.*

Figure 7-7. *Culvert with insufficient width and limiting run-off capacity of the stream.*

- Sites affected by active and fossil slope failure represent areas unsuitable for urban development. Also, it is advisable to avoid these places for road construction. Before construction of any type, it is recommended to carry out a detailed geomorphological and engineering geological survey to check stability and to ensure an appropriate design with the implementation of useful drainage.
- If the construction is damaged by any natural processes, it is necessary to analyze the causes of the damage before embarking on mitigation procedures, to make a detailed survey of the affected sites and investigate what the natural mechanisms and human interventions were that caused the damage. This information should be gathered before reconstruction in order to prevent a recurrence of natural hazards.

REFERENCES

Abbate, E., Bruni, P., Sagri, M. (2015): Geology of Ethiopia: a review and geomorphological perspectives. In: Billi, P. (ed.): *Landscapes and Landforms of Ethiopia*, pp. 33–64. Springer, Dordrecht.

Acocella, V. (2010): Coupling volcanism and tectoncs along divegent plate boundarie: collapsed rifts from central Afar, Etiopia. *Geological Society of America Bulletin*, 122, 1717–1728.

Agezew, T., Regassa, T., Šíma, J. (2014): *Hydrogeological and hydrochemical maps of Dila NB 37-2*. Explanatory notes. Aquatest a.s., Prague.

Agostini, A., Bonini, M., Corti, G., Sani, F., Manetti, P. (2011): Distribution of Quaternary deformation in the central Main Ethiopian Rift, East Africa. *Tectonics*, 30, TC4010. DOI 10.1029/2010TC002833

Ali, S. A., Hagos, H. (2016): Estimation of soil erosion using USLE and GIS in Awassa Catchment, Rift valley, Central Ethiopia. *Geoderma Regional*, 7(2), 159–166.

Asfaw, B., Beyene, Y., Semaw, S., Suwa, G., White, T., Woldegabriel, G. (1991): Fejej: a new paleoanthropological research area in Ethiopia. *Journal of Human Evolution*, 21(2), 137–143.

Ayalew, D., Yirgu, G., Pik, R. (1999): Geochemical and isotopic (Sr, Nd and Pb) characteristics of volcanic rocks from southwestern Ethiopia. *Journal of African Earth Sciences*, 29(2), 381–391.

Ayalew, D., Barbey, P., Marty, B., Reisberg, L., Yirgu, G., Pik, R. (2002): Source, genesis, and timing of giant ignimbrite deposits associated with Ethiopian continental flood basalts. *Geochimica et Cosmochimica Acta*, 66(8), 1429–1448.

Ayalew, D., Marty, B., Barbey, P., Yirgu, G., Ketefo, E. (2006): Sub-lithospheric source for Quaternary alkaline Tepi shield, southwest Ethiopia. *Geochemical Journal*, 40(1), 47–56.

Bech Bruun, T., Elberling, B., Christensen, B. T. (2010): Lability of soil organic carbon in tropical soils with different clay minerals. *Soil Biology and Biochemistry*, 42(6), 888–895.

Bezuayehu, T., Gezahegn, A., Yigezu, A., Jabbar, M. A., Paulos, D. (2002): *Nature and causes of land degradation in the Oromiya Region: A review*. Socio-economics and Policy Research Working Paper 36, International Livestock Research Institute, Nairobi.

Bloomer, S. H., Curtis, P. C., Karson, J. A. (1989): Geochemical variation of Quaternary basaltic volcanics in the Turkana Rift, northern Kenya. *Journal of African Earth Sciences*, 8(2–4), 511–532.

Bogena, H., Kunkel, R., Schrobel, T., Schrey, H. P., Wendland, F. (2005): Distributed modeling of groundwater recharge at the macroscale. *Ecological Modelling*, 187(1), 15–26.

Bonini, M., Corti, G., Innocenti, F., Manetti, P., Mazzarini, F., Abebe, T., Pecskay, Z. (2005): Evolution of the Main Ethiopian Rift in the frame of Afar and Kenya rifts propagation. *Tectonics*, 24(1), 1–21.

Boynton, W. V. (1984): Chapter 3 – Cosmochemistry of the rare earth elements: meteorite studies. *Developments in Geochemistry*, 2, 63–114.

Brown, F. H., Carmichael, I. S. E. (1969): Quaternary volcanoes of the Lake Rudolf region: The basanite-tephrite series of the Korea range. *Lithos*, 2(3), 239–260.

Brown, F. H., Carmichael, I. S. E. (1971): Quaternary volcanoes of the Lake Rudolf region: II. The lavas of North Island, South Island and the Barrier. *Lithos*, 4(3), 305–323.

Buriánek, D. (ed.), Hroch, T., Verner, K., Megerssa, L., Martínek, K., Yakob, M., Haregot, A., Janderková, J., Šíma, J., Kryštofová, E., Valenta, J., Tadesse, E., Mosisa, A., Dalke, G., Legesse, F., Assefa, G., Pécskay, Z., Hejtmánková, P., Krejčí, Z. (2018): *Explanatory notes to the thematic geoscientific maps of Ethiopia at a scale of 1 : 50 000, Map Sheet 0638-C2 Dila*. 103 pp., 7 annexes, 4 maps. Czech Geological Survey, Prague.

Corti, G. (2009): Continental rift evolution: from rift initiation to incipient break-up in the Main Ethiopian Rift, East Africa. *Earth-Science Reviews*, 96, 1–53.

Corti, G., Molin, P., Sembroni, A., Bastow, I. D., Keir, D. (2018): Control of pre-rift lithospheric structure on the architecture and evolution of continental rifts: Insights from the Main Ethiopian Rift, East Africa. *Tectonics*, 37, 477– 496. DOI 10.1002/2017TC004799

Davidson, A. (1983): The Omo river project, reconnaissance geology and geochemistry of parts of Ilubabor, Kefa, Gemu Gofa and Sidamo, Ethiopia. *Bulletin (Ethiopian Institute of Geological Surveys)*, 2, 1–89.

Debeko, D., Angassa, A., Abebe, A., Burka, A., Tolera, A. (2018): Human-climate induced drivers of mountain grassland over the last 40 years in Sidama, Ethiopia: perceptions versus empirical evidence. *Ecological Processes*, 7(1), 34. DOI 10.1186/s13717-018-0145-5

De Wispelaere, L., Marcelino, V., Regassa, A., De Grave, E., Dumon, M., Mees, F., Van Ranst, E. (2015): Revisiting nitic horizon properties of Nitisols in SW Ethiopia. *Geoderma*, 243, 69–79.

Dhont, D., Chorowicz, J. (2006): Review of the neotectonics of the Eastern Turkish–Armenian Plateau by geomorphic analysis of digital elevation model imagery. *International Journal of Earth Sciences*, 95(1), 34–49.

Di Paola, G. M. (1971): Geology of the Corbetti Caldera area (Main Ethiopian Rift Valley). *Bulletin volcanologique*, 35(2), 497–506.

Di Paola, G. M. (1972): The Ethiopian Rift Valley (between 7°00′ and 8°40′ lat. north). *Bulletin volcanologique*, 36(4), 517–560.

Driessen, P., Deckers, J., Spaargaren, O., Nachtergaele, F. (2001): *Lecture notes on the major soils of the world.* World Soil Resources Reports No. 94, FAO, Rome.

Droop, G. T. R. (1987): A general equation for estimating Fe^{3+} concentrations in ferromagnesian silicates using stoichiometric criteria. *Mineralogical Magazine*, 51(361), 431–435.

Ebinger, C. J., Yemane, T., Woldegabriel, G., Aronson, J. L., Walter, R. C. (1993): Late Eocene-Recent volcanism and faulting in the southern main Ethiopian rift. *Journal of the Geological Society*, 150(1), 99–108.

Ebinger, C. J., Yemane, T., Harding, D. J., Tesfaye, S., Kelley, S., Rex, D. C. (2000): Rift deflection, migration, and propagation: Linkage of the Ethiopian and Eastern rifts, Africa. *Geological Society of America Bulletin*, 112(2), 163–176.

Ethiopian Standards Agency (ESA) (2013): *Compulsory Ethiopian standard: Drinking water Specification*. ESA; ICS: 13.060.20.

Furman, T., Bryce, J. G., Karson, J., Iotti, A. (2004): East African Rift System (EARS) plume structure: Insights from quaternary mafic lavas of Turkana, Kenya. *Journal of Petrology*, 45(5), 1069–1088.

Gebremichael, D., Nyssen, J., Poesen, J., Deckers, J., Haile, M., Govers, G., Moeyersons, J. (2005): Effectiveness of stone bunds on controlling soil erosion on cropland in the Tigray highlands, Northern Ethiopia. *Soil Use and Management*, 21(3), 287–297.

Gedeo Cultural Landscape (2021), updated 1. 9. 2019 [ref. 18. 10. 2021], from: https://whc.unesco.org/en/tentativelists/6448/.

George, R. M., Rogers, N. W. (1999): The petrogenesis of Plio-Pleistocene alkaline volcanic rocks from the Tosa Sucha region, Arba Minch, southern Main Ethiopian Rift. *Acta vulcanologica*, 11, 121–130.

George, R. M., Rogers, N. W., Kelley, S. (1998): Earliest magmatism in Ethiopia: Evidence for two mantle plumes in one flood basalt province. *Geology*, 26(10), 923–926.

Haileab, B., Brown, F. H., McDougall, I., Gathogo, P. N. (2004): Gombe Group basalts and initiation of Pliocene deposition in the Turkana depression, northern Kenya and southern Ethiopia. *Geological Magazine*, 141(1), 41–53.

Halcrow (2008): *Rift Valley Lakes Basin Integrated Resources Development Master Plan Study Project, Draft Phase 2, Report Part II, Prefeasibility Studies*. Unpublished report, Halcrow Group Limited and Generation Integrated Rural Development (GIRD) consultants, Ministry of Water Resources, Addis Ababa.

Hanžl, P., Verner, K. (eds), Buriánek, D., Šíma, J., Janderková, J., Kryštofová, E., Paleček, M., Hroch, T., Martínek, K., Megerssa, L., Hrdličková, K., Metelka, V. (2018): *Basic principles of geological and thematic mapping*. 107 pp. Czech Geological Survey, Prague.

Haregeweyn, N., Poesen, J., Govers, G., Verstraeten, G., de Vente, J., Nyssen, J., Deckers, S., Moeyersons, J. (2013): Evaluation and adaptation of a spatially-distributed erosion and sediment yield model in Northern Ethiopia. *Land Degradation and Development*, 24, 188–204.

Hart, W. K., Woldegabriel, G., Walter, R. C., Mertzman, S. A. jr. (1989): Basaltic volcanism in Ethiopia: Constraints on continental rifting and mantle interactions. *Journal of Geophysical Research*, 94(B6), 7731–7748.

Hassen, N., Yemane, T., Genzebu, W. (1997): *Geology of the Agere Maryam Area*. 86 pp. Geological Survey of Ethiopia, Addis Ababa.

Hayward, N. J., Ebinger, C. J. (1996): Variations in the along-axis segmentation of the Afar Rift system. *Tectonics*, 15(2), 244–257.

Hristov, B. (2013): The importance of soil texture in soil classification systems. *Journal of Balkan Ecology*, 16(2), 137–39.

Hurni, H. (1985): *Soil conservation manual for Ethiopia: a field manual for conservation implementation*. 86 pp. Soil Conservation Research Project, Addis Ababa.

ICS:13.060.20 (2013): *Drinking water – Specifications*. Ethiopian Standards Agency, ESA.

IUSS Working Group WRB (2015): *World Reference Base for Soil Resources 2014, update 2015 International soil classification system for naming soils and creating legends for soil maps*. World Soil Resources Reports No. 106. FAO, Rome.

Jahn, R., Blume, H. P., Asio, V. B., Spaargaren, O., Schad, P. (2006): *Guidelines for soil description, 4th edition*. 97 pp. FAO, Rome.

Janoušek, V., Farrow, C. M., Erban, V. (2006): Interpretation of whole-rock geochemical

data in igneous geochemistry: introducing Geochemical Data Toolkit (GCDkit). *Journal of Petrology*, 47(6), 1255–1259.

JICA (2012): *The Study on Groundwater Resources Assessment in the Rift Valley Lakes Basin in the Federal Democratic Republic of Ethiopia, Main Report*. 60 pp., 2 annexes. Japan International Cooperation Agency, Kokusai Kogyo Co., Ltd., Ministry of Water and Energy, Addis Ababa.

Juch, D. (1975): Geology of the south-eastern escarpment of Ethiopia between 39° and 42° long. East. In: Pilger, A., Roesler, A. (eds): *Afar Depression of Ethiopia*, pp. 310–316. Schweizerbart, Stuttgart.

Kassa, M., Alemu, A., Muluneh, A. (2021): Determination of gravity and isostatic Moho: Implications for the evolution of rifting in the central Main Ethiopian Rift. *Journal of African Earth Sciences*, 184, 104350. DOI 10.1016/j.jafrearsci.2021.104350

Katoh, S., Nagaoka, S., Woldegabriel, G., Renne, P. R., Snow, M. G., Beyene, Y., Suwa, G. (2000): Chronostratigraphy and correlation of the Plio-Pleistocene tephra layers of the Konso Formation, southern Main Ethiopian Rift, Ethiopia. *Quaternary Science Reviews*, 19(13), 1305–1317.

Kibret, K. S., Marohn, C., Cadisch, G. (2016): Assessment of land use and land cover change in South Central Ethiopia during four decades based on integrated analysis of multi-temporal images and geospatial vector data. *Remote Sensing Application: Society and Environment*, 3, 1–19.

Kifle, S., Teferi, B., Kebedom, A., Abiyot, L. (2016): Factors influencing farmers decision on the use of introduced soil and water conservation practices in the lowland's of Wenago Woreda, Gedeo Zone, Ethiopia. *American Journal of Rural Development*, 4(1), 24–30.

Kille, K. (1970): Das Verfahren MoMNQ, ein Beitrag zur Berechnung der mittleren langjährigen Grundwasserneubildung mit Hilfe der monatlichen Niedrigwasserabflüsse. *Zeitschrift der Deutschen Gesellschaft für Geowissenschaften*, 120(2), 89–95.

Kunz, K., Kreuzer, H., Müller, P. (1975): Potassium-Argon age determinations of the Trap basalt of the south-eastern part of the Afar Rift. In: Pilger, A., Roesler, E. A. (eds): *Afar Depression of Ethiopia*, pp. 370–374. Schweizerbart, Stuttgart.

Lahmeyer International (2005): *Genale-Dawa River Basin Integrated Resource Development Master Plan Study*. Ministry of Water Resources, Addis Ababa.

Land Cover & Land Use (online), updated 2. 10. 2019 [ref. 17. 10. 2021], from: https://www.nrcan.gc.ca/maps-tools-and-publications/satellite-imagery-and-air-photos/tutorial-fundamentals-remote-sensing/educational-resources-applications/land-cover-biomass-mapping/land-cover-land-use/9373.

Leake, B. E., Wooley, A. R., Arps, C. E. S., Birch, W. D., Gilbert, M. C., Grice, J. D., Hawthorne, F. C., Kato, A., Kisch, H. J., Krivovichev, V. G., Linthout, K., Laird, J., Mandarino, J., Maresch, W. V., Nickel, E. H., Rock, N. M. S., Schumacher, J. C., Smith, J. C., Stephenson, N. C. N., Whittaker, E. J. W., Youzhi, G. (1997): Nomenclature of amphiboles; report of the Subcommittee on Amphiboles of the International Mineralogical Association Commission on New Minerals and Mineral Names. *Canadian Mineralogist*, 35, 219–246.

Le Bas, M. J., Le Maitre, R. W., Streckeisen, A., Zanettin, B. (1986): A chemical classification of volcanic rocks based on the total alkali-silica diagram. *Journal of Petrology*, 27(3), 745–750.

Le Turdu, C., Tiercelin, J.-J., Gibert, E., Travi, Y., Lezzar, K.-E., Richert, J.-P., Mas-

sault, M., Gasse, F., Bonnefille, R., Decobert, M., Gensous, B., Jeudy, V., Tamrat, E., Mohammed, M. U., Martens, K., Atnafu, B., Chernet, T., Williamson, D., Taieb, M. (1999): The Ziway–Shala lake basin system, Main Ethiopian Rift: Influence of volcanism, tectonics, and climatic forcing on basin formation and sedimentation. *Palaeogeography, Palaeoclimatology, Palaeoecology*, 150(3), 135–177. DOI 10.1016/S0031-0182(98)00220-X

Lynn, W. C., Pearson, M. J. (2000): The color of soil. *The Science Teacher*, 67(5), 20.

MacDonald, R., Gibson, I. L. (1969): Pantelleritic obsidians from the volcano Chabbi (Ethiopia). *Contributions to Mineralogy and Petrology*, 24(3), 239–244.

Mahatsente, R., Jentzsch, G., Jahr, T. (1999): Crustal structure of the Main Ethiopian Rift from gravity data: 3-dimensional modeling. *Tectonophysics*, 313(4), 363–382. DOI 10.1016/S0040-1951(99)00213-9

Mahatsente, R., Jentzsch, G., Jahr, T. (2000): Three-dimensional inversion of gravity data from the Main Ethiopian Rift. *Journal of African Earth Sciences*, 31(2), 451–466. DOI 10.1016/S0899-5362(00)00099-3

McDonough, W. F., Sun, S. S. (1995): The composition of the Earth. *Chemical Geology*, 120(3–4), 223–253.

Merla, G., Abbate, E., Azzaroli, A., Bruni, P., Canuti, P., Fazzuoli, M., Tacconi, P. (1979): *A Geological Map of Ethiopia & Somalia (1973) 1 : 2,000,000: And Comment with a Map of Major Landforms*. University of Florence, Florence.

Morbidelli, L., Nicoletti, M., Petrucciani, C., Piccirillo, E. M. (1975): Ethiopian South-Eastern Plateau and related escarpment: K/Ar ages of the main volcanic events (Main Ethiopian Rift from 8° 10′ to 9° 00′ lat. North). In: Pilger, A., Roesler, E. A. (eds): *Afar Depression of Ethiopia*, pp. 362–369. Schweizerbart, Stuttgart.

Morimoto, N., Fabries, J., Ferguson, A. K., Ginzburg, I. V., Ross, M., Seifert, F. A., Zussman, J., Aoki, K., Gottardi, G. (1988): Nomenclature of pyroxenes. *American Mineralogist*, 73, 1123–1133.

Muluneh, A. A., Cuffaro, M., Doglioni, C. (2014): Left-lateral transtension along the Ethiopian Rift and constrains on the mantle-reference plate motions. *Tectonophysics*, 632, 21–31.

Munsell Soil Color Charts (2003): *Revised Washable Edition. Munsell Color*. 13 pp. Research Council for Agriculture, Forestry and Fisheries, Ministry of Agriculture and Forestry, Japan.

Nyssen, J., Poesen, J., Haile, M., Moeyersons, J., Deckers, J., Hurni, H. (2009): Effects of land use and land cover on sheet and rill erosion rates in the Tigray highlands, Ethiopia. *Zeitschrift für Geomorphologie*, 53(2), 171–197.

Pearce, J. A. (1996): A user's guide to basalt discrimination diagrams. In: Wyman, D. A. (ed.): *Trace element geochemistry of volcanic rocks: applications for massive sulphide exploration*. Geological Association of Canada, Short Course Notes, 12, 79–113.

Pouchou, J. L., Pichoir, F. (1985): "PAP" ((ΦρZ) procedure for improved quantitative microanalysis. In: Armstrong, J. T. (ed.): *Microbeam Analysis*, pp. 104–106. San Francisco Press, San Francisco.

Rapprich, V., Habtamu, E., Kycl, P., Hroch T., Verner, K., Kopačková, V., Mišurec, J., Šíma, J., Málek, J., Malík, J., Tesema, T., Bekele, Y., Megerssa, L., Filfilu, E., Legesse, F., Tadesse, E., Bewketu, H., Demewoz, A., Negash, T., Pecskay, Z., Freymuth, H. (2014): *Explanation Booklet to the Geological Hazards and Engineering Geology Maps of Dila, NB 37-6*. Czech Geological Survey, Prague; Aquatest a.s., Prague; Geological Survey of Ethiopia, Addis Ababa.

Rapprich, V., Žáček, V., Verner, K., Erban, V., Goslar, T., Bekele, Y., Legesa, F., Hroch, T., Hejtmánková, P. (2016): Wendo Koshe pumice: the latest Holocene silicic explosive eruption product of the Corbetti volcanic system (southern Ethiopia). *Journal of Volcanology and Geothermal Research*, 310, 159–171.

Rogers, N. W., Macdonald, R., Fitton, J. G., George, R. M. M., Smith, M., Barreiro, B. (2000): Two mantle plumes beneath the East African rift system: Sr, Nd and Pb isotope evidence from Kenya Rift basalts. *Earth and Planetary Science Letters*, 176(3–4), 387–400.

Rooney, T. O. (2010): Geochemical evidence of lithospheric thinning in the southern Main Ethiopian Rift. *Lithos*, 117(1–4), 33–48.

Rooney, T. O., Hart, W. K., Hall, C. M., Ayalew, D., Ghioprso, M. S., Hidalgo, P. J., Yirgu, G. (2012): Peralkaline magma evolution and the tephra record in the Ethiopian Rift. *Contributions to Mineralogy and Petrology*, 164(3), 407–426.

Saria, E., Calais, E., Stamps, D. S., Delvaux, D., Hartnady, C. J. H. (2014): Present-day kinematics of the East African Rift. *Journal of Geophysical Research*, 119(4), 3584–3600.

Schad, P. (2005): Mineral soils conditioned by wet tropical climate: Plinthisols, Ferralsols, Nitisols, Alisols, Acrisols, Lixisols. In: Jones, A. R., Panagos, P., Michéli, E., Montanarella, L. (eds): *3rd European Summer School on Soil Survey*. Joint Research Centre – Szent István University, 18–22 July 2005. Presentation.

Shinjo, R., Chekol, T., Meshesha, D., Tatsumi, Y., Itaya, T. (2011): Geochemistry and geochronology of the mafic lavas from the southeastern Ethiopian rift (the East African Rift System): assessment of models on magma sources, plume-lithosphere interaction and plume evolution. *Contributions to Mineralogy and Petrology*, 162(1), 209–230.

Singh, B., Gilkes, R. J. (1992): Properties and distribution of iron oxides and their association with minor elements in the soils of south-western Australia. *European Journal of Soil Science*, 43(1), 77–98.

Steiner, R. A., Rooney, T. O., Girard, G., Rogers, N., Ebinger, C., Peterson, L., Phillips, R. (2021): Initial Cenozoic magmatic activity in East Africa: New geochemical constraints on magma distribution within the Eocene continental flood basalt province. *Special Publications (Geological Society of London)*, 518, 435–465.

Stewart, K., Rogers, N. (1996): Mantle plume and lithosphere contributions to basalts from southern Ethiopia. *Earth and Planetary Science Letters*, 139(1–2), 195–211.

Stocking, M., Murnaghan, N. (2001): *Handbook for the Field Assessment of Land Degradation*. 169 pp. Earthscan, London.

Struckmeier, W. F., Margat, J. (1995): *The Proposal for the International Legend to the Hydrogeological Maps.* 177 pp. International Association of Hydrogeologists, 17, Heise, Hannover.

Tefera, S., Snyman, H. A., Smit, G. N. (2007): Rangeland dynamics of southern Ethiopia: (2). Assessment of woody vegetation structure in relation to land use and distance from water in semi-arid Borana rangelands. *Journal of Environmental Management*, 85(2), 443–452.

Tesfaye, C. (1982): *Hydrogeology of the Lakes region, Ethiopia*. Ministry of Mines and Energy, Addis Ababa.

Tesfaye, C. (1993): *Hydrogeology of Ethiopia and Water Resources Development – MS EIGS*. Ministry of Mines and Energy, Addis Ababa.

Trua, T., Deniel, C., Mazzuoli, R. (1999): Crustal control in the genesis of Plio-Quaternary

bimodal magmatism of the Main Ethiopian Rift (MER): geochemical and isotopic (Sr, Nd, Pb) evidence. *Chemical Geology*, 155(3–4), 201–231.

UNDP (1971): Ethiopia: Investigation of Geothermal Resources for Power Development (ETH 26). Geology, Geochemistry and Hydrology of Hot Springs of the Eastern African Rift System in Ethiopia.

Van Wambeke, A. R. (1962): Criteria for classifying tropical soils by age. *European Journal of Soil Science*, 13(1), 124–132.

Verner, K., Megerssa, L. (eds), Hroch, T., Buriánek, D., Martínek, K., Mihret, Y., Janderková, J., Šíma, J., Kryštofová, E., Abadi, H., Gete, B., Aberash, M., Ezra, T., Valenta, J., Pécskay, Z., Hejtmánková, P. (2018): *Explanatory notes to the thematic geoscientific maps of Ethiopia at a scale of 1 : 50 000, Map Sheet 0638-D2 Mejo*. 97 pp., 7 annexes, 4 maps. Czech Geological Survey, Prague.

WABCO (1990): Water Resources Development Master Plan for Ethiopia.

Wischmeier, W. H., Smith, D. D. (1978): *Predicting rainfall erosion losses-a guide to conservation planning*. US Department of Agriculture Handbook, No. 537, Washington DC.

Wolde, B., Widenfalk, L. (1994): Petrochemical and geochemical constraints on Cenozoic magmatism in Ethiopia. *Africa Geoscience Review*, 1, 475–494.

Woldegabriel, G., Aronson, J. L. (1987): Chow Bahir: a 'failed' rift, in Southern Ethiopia. *Geology*, 15, 430–433.

Woldegabriel, G., Yemane, T., Suwa, G., White, T., Asfaw, B. (1991): Age of volcanism and rifting in the Burji-Soyoma area, Amaro Horst, southern Main Ethiopian Rift: geo- and biochronologic data. *Journal of African Earth Sciences*, 13(3–4), 437–447.

Woldegabriel, G., Hart, W. K., Katoh, S., Beyene, Y., Suwa, G. (2005): Correlation of Plio-Pleistocene tephra in Ethiopian and Kenyan rift basins: Temporal calibration of geological features and hominid fossil records. *Journal of Volcanology and Geothermal Research*, 147(1–2), 81–108.

Wolela, A. (2014): Volcanism, sedimentation, K/Ar and palynology studies, Yayu and Delbi-Moye Basins, Southwestern Plateau of Ethiopia. *Journal of African Earth Sciences*, 93, 1–13.

WWDSE (2004): *Study and Design of Gelana, Gidabo and Bilate Irrigation Project*. Water Works Design and Supervision Enterprise, Addis Ababa.

WWDST (2003): *Wabe Shebelle River Basin Integrated Development Master Plan Study*. Ministry of Water Resources, Addis Ababa.

Yemane, T., Woldegabriel, G., Tesfaye, S., Berhe, S. M., Durary, S., Ebinger, C. J., Kelley, S. P. (1999): Temporal and geochemical characteristics of Tertiary volcanic rocks and tectonic history in the southern Main Ethiopian Rift and the adjacent volcanic fields. *Acta vulcanologica*, 11, 99–119.

Yismaw, A., Mitiku, B., Gebretsadik, T., Beyene, B., Dure, T., Edris, M., Burusa, G., Wenduante, M., Yehualashet, E., Abdulahid, T., Alemu, T., Ashenafi, S. (2015): *Geology, geochemistry and gravity survey of Dila map sheet.* Geological Survey of Ethiopia, Memoir 37, Addis Ababa.

Zanettin, B., Justin-Visentin, E., Nicoletti, M., Petrucciani, C. (1978a): The evolution of the Chencha escarpment and the Ganjiuli graben (Lake Abaya) in the southern Ethiopian rift. *Neues Jahrbuch für Geologie und Paläontologie*, 9, 567–574.

Zanettin, B., Justin-Visentin, E., Piccirillo, E. M. (1978b): Volcanic succession, tectonics and magmatology in central Ethiopia. *Atti e memorie dell'Accademia patavina di scienze, lettere ed arti*, 90, 5–19.

Zanettin, B., Justin-Visentin, E., Nicoletti, M., Piccirillo, E. M. (1980): Correlations among Ethiopian volcanic formations with special references to the chronological and stratigraphical problems of the "Trap Series", Rome, Italy. *Atti dei Convegni Lincei*, 47, 231–252.

Zenaw, T., Tadesse, D. (2003): *Hydrology and engineering geology of Awassa Lake catchment*. 67 pp., 2 maps. Geological Survey of Ethiopia, Addis Ababa.

www.esri.com

http://www.levoyageur.net/weather-city-YIRGA-CHEFE/DILLA.html

ANNEXES

Annex 1: Whole-rock chemical composition of rocks

Tab. 1. Whole-rock compositions of volcanic rocks (oxide wt. % for major elements and ppm for trace elements)

Sample	DE551	DE550
Rock	basalt	trachybasalt
wt. %		
SiO_2	46.14	51.04
Al_2O_3	16.74	17.14
Fe_2O_3	13.46	11.41
MgO	6.33	3.13
CaO	8.32	5.45
Na_2O	3.31	4.7
K_2O	0.87	2.3
TiO_2	2.31	1.75
P_2O_5	0.37	0.77
MnO	0.22	0.21
Cr_2O_3	0.005	0.005
LOI	1.6	1.7
Sum	99.72	99.72
ppm		
Mo	1.1	1.6
Cu	24.6	18.9
Pb	1.0	3.5
Zn	102	80
Ni	24.3	16.2
As	< 0.5	< 0.5
Cd	< 0.1	< 0.1
Sb	< 0.1	< 0.1
Bi	< 0.1	< 0.1
Ag	< 0.1	< 0.1
Au	< 0.5	2.5
Hg	< 0.01	< 0.01
Tl	< 0.1	< 0.1
Se	< 0.5	< 0.5
Ba	369	818
Sc	21	8

Sample	DE551	DE550
Rock	basalt	trachybasalt
wt. %		
Be	< 1	< 1
Co	44.3	21.3
Cs	0.1	0.5
Ga	17.8	15.1
Hf	3.7	4.8
Nb	28.0	78.2
Rb	13.9	59.1
Sn	< 1	1
Sr	581.1	1076.1
Ta	1.6	4.0
Th	2.5	7.1
U	0.6	1.4
V	257	70
W	3.3	1.9
Zr	160.2	223.3
Y	25.2	28.5
La	25.2	55
Ce	51.8	97.1
Pr	6.34	11.28
Nd	26.1	42.8
Sm	5.40	7.15
Eu	1.93	2.32
Gd	5.57	6.70
Tb	0.86	0.93
Dy	5.15	5.34
Ho	1.0	1.1
Er	2.52	3.06
Tm	0.35	0.43
Yb	2.29	2.71
Lu	0.38	0.44

Annex 2: Representative chemical composition of rock-forming minerals

Tab. 2. Representative chemical composition of pyroxenes

Sample	DE 094B	DE 112	DE 112	DE362	DE 094 A	TD 102	TD 102	TD 082
Rock	basalt	trachyte	trachyte	trachyte	ignimbrite	basalt	basalt	basalt
Age	Oligocene	Oligocene	Oligocene	Oligocene	Oligocene	Pliocene	Pliocene	Pliocene
SiO_2	47.91	50.68	51.42	49.77	50.24	50.17	50.71	51.26
TiO_2	2.20	0.70	0.54	0.46	0.87	1.69	1.46	1.56
Al_2O_3	3.68	1.83	1.34	1.56	1.71	3.10	2.67	2.63
Cr_2O_3	0.05	0.00	0.00	0.01	0.00	0.01	0.03	0.03
Fe_2O_3	3.47	2.21	1.01	2.13	2.84	1.10	1.86	1.23
FeO	9.78	12.43	14.12	16.83	10.72	7.91	7.29	7.11
MnO	0.33	0.57	0.68	0.79	0.65	0.27	0.29	0.21
MgO	12.67	13.51	13.41	6.94	11.35	12.86	13.30	13.90
CaO	19.08	17.18	16.77	20.93	20.97	22.17	22.21	22.25
Na_2O	0.44	0.46	0.38	0.64	0.51	0.43	0.48	0.44
K_2O	0.03	0.00	0.00	0.04	0.01	0.00	0.00	0.01
Total	99.64	99.57	99.68	100.11	99.86	99.72	100.28	100.63
Si	1.821	1.924	1.954	1.945	1.915	1.884	1.891	1.898
Al	0.165	0.082	0.060	0.072	0.077	0.137	0.117	0.115
Fe^{2+}	0.099	0.063	0.029	0.063	0.082	0.031	0.052	0.034
Fe^{3+}	0.002	0.000	0.000	0.000	0.000	0.000	0.001	0.001
Cr	0.063	0.020	0.015	0.013	0.025	0.048	0.041	0.043
Ti	0.311	0.395	0.449	0.550	0.342	0.248	0.227	0.220
Mn	0.011	0.018	0.022	0.026	0.021	0.009	0.009	0.006
Mg	0.718	0.765	0.760	0.404	0.645	0.720	0.739	0.767
Ca	0.777	0.699	0.683	0.876	0.856	0.892	0.888	0.883
Na	0.032	0.034	0.028	0.049	0.038	0.032	0.034	0.032
K	0.001	0.000	0.000	0.002	0.000	0.000	0.000	0.000
Total	4.000	4.000	4.000	4.000	4.000	4.000	4.000	4.000

Tab. 3. Representative chemical composition of feldspar

Sample	DE 094B	DE 094B	DE362	DE362	TD102	TD102	TD082	TD082
Rock	basalt	basalt	trachyte	trachyte	basalt	basalt	basalt	basalt
Age	Oligocene	Oligocene	Oligocene	Oligocene	Pliocene	Pliocene	Pliocene	Pliocene
SiO_2	52.55	53.27	67.00	67.01	52.50	55.60	58.76	54.21
P_2O_5	0.02	0.02	0.00	0.01	0.00	0.04	0.00	0.02
Al_2O_3	27.62	28.10	18.86	19.63	29.11	27.52	24.82	27.94
FeO	1.81	0.93	0.39	0.26	0.54	0.33	0.74	0.69
CaO	11.92	12.12	0.23	0.38	12.84	10.57	7.78	11.40
Na_2O	4.27	4.36	6.95	7.81	5.09	5.45	7.24	4.99
K_2O	0.29	0.32	6.56	5.25	0.27	0.43	0.75	0.30
BaO	0.00	0.01	0.09	0.72	0.08	0.04	0.11	0.04
Total	98.48	99.11	99.98	100.34	100.35	99.93	100.09	99.54
Si	2.430	2.440	3.000	2.970	2.360	2.510	2.620	2.460
Al	1.510	1.520	1.000	1.020	1.540	1.460	1.310	1.500
Fe	0.070	0.040	0.010	0.010	0.020	0.010	0.030	0.030
P	0.000	0.000	0.000	0.000	0.000	0.000	0.000	0.000
T-site	4.010	4.000	4.010	4.000	3.920	3.990	3.960	3.990
K	0.020	0.020	0.370	0.300	0.020	0.020	0.040	0.020
Na	0.380	0.390	0.600	0.670	0.440	0.480	0.630	0.440
Ca	0.590	0.600	0.010	0.020	0.620	0.510	0.370	0.560
Ba	0.000	0.000	0.000	0.010	0.000	0.000	0.000	0.000
Rb	0.000	0.000	0.000	0.000	0.000	0.000	0.000	0.000
O-site	0.990	1.000	0.990	1.000	1.080	1.010	1.040	1.010
K+Na+Ca	0.990	1.000	0.990	0.980	1.080	1.010	1.040	1.010
Mol. %								
An	59.6	59.4	1.1	1.8	57.4	50.5	35.7	54.9
Ab	38.6	38.7	61.0	68.1	41.2	47.1	60.2	43.4
Or	1.8	1.9	37.9	30.1	1.4	2.4	4.1	1.7

Tab. 4. Representative chemical composition of olivine

Sample	TD102	TD102	TD102	TD082	TD082	TD082	TD082	TD082
Rock	basalt	basalt	basalt	basalt	basalt	basalt	basalt	basalt
Age	Pliocene	Pliocene	Pliocene	Pliocene	Pliocene	Pliocene	Pliocene	Pliocene
SiO_2	36.26	36.01	36.28	36.47	36.06	36.56	37.11	36.79
TiO_2	0.05	0.06	0.17	0.13	0.05	0.06	0.04	0.09
Al_2O_3	0.11	0.00	0.03	0.05	0.13	0.00	0.07	0.05
Cr_2O_3	0.00	0.01	0.00	0.00	0.01	0.00	0.01	0.00
FeO	35.60	35.58	35.88	34.24	34.22	33.57	33.42	34.04
MnO	0.90	0.96	0.99	0.78	0.88	0.81	0.74	0.82
MgO	26.85	26.89	26.04	28.63	28.46	28.73	28.92	28.22
NiO	0.01	0.01	0.03	0.01	0.00	0.00	0.02	0.06
CaO	0.39	0.39	0.40	0.38	0.39	0.38	0.37	0.37
Total	100.16	99.91	99.82	100.69	100.21	100.10	100.69	100.43
Si	1.009	1.006	1.015	1.002	0.997	1.007	1.013	1.012
Ti	0.001	0.001	0.004	0.003	0.001	0.001	0.001	0.002
Al	0.003	0.000	0.001	0.001	0.004	0.000	0.002	0.002
Cr	0.000	0.000	0.000	0.000	0.000	0.000	0.000	0.000
Fe(ii)	0.828	0.831	0.839	0.787	0.791	0.773	0.763	0.783
Mn	0.021	0.023	0.023	0.018	0.021	0.019	0.017	0.019
Mg	1.114	1.120	1.086	1.173	1.173	1.180	1.177	1.157
Ni	0.000	0.000	0.001	0.000	0.000	0.000	0.001	0.001
Ca	0.012	0.012	0.012	0.011	0.012	0.011	0.011	0.011
Mol. %								
Fo	56.7	56.7	55.7	59.3	59.1	59.8	60.1	59.1
Fa	42.2	42.1	43.1	39.8	39.9	39.2	39.0	40.0
Tp	1.1	1.2	1.2	0.9	1.0	1.0	0.9	1.0